

# Carbon-Chain Chemistry in the Interstellar Medium

Kotomi Taniguchi<sup>1\*†</sup>, Prasanta Gorai<sup>2,3,4†</sup> and Jonathan C. Tan<sup>2,5</sup>

<sup>1\*</sup>Division of Science, National Astronomical Observatory of Japan,  
2-21-1 Osawa, Mitaka, Tokyo, 181-8588, Japan.

<sup>2</sup>Department of Space, Earth and Environment, Chalmers University of  
Technology, SE-412 96, Gothenburg, Sweden.

<sup>3</sup>Rosseland Centre for Solar Physics, University of Oslo, PO Box 1029  
Blindern, 0315, Oslo, Norway.

<sup>4</sup>Institute of Theoretical Astrophysics, University of Oslo, PO Box 1029  
Blindern, 0315, Oslo, Norway.

<sup>5</sup>Department of Astronomy, University of Virginia, Charlottesville,  
22904-4325, Virginia, USA.

\*Corresponding author(s). E-mail(s): [kotomi.taniguchi@nao.ac.jp](mailto:kotomi.taniguchi@nao.ac.jp);

Contributing authors: [prasanta.astro@gmail.com](mailto:prasanta.astro@gmail.com);

†These authors contributed equally to this work.

## Abstract

The presence of carbon-chain molecules in the interstellar medium (ISM) has been known since the early 1970s and  $> 130$  such species have been identified to date, making up  $\sim 43\%$  of the total of detected ISM molecules. They are prevalent not only in star-forming regions in our Galaxy but also in other galaxies. These molecules provide important information on physical conditions, gas dynamics, and evolutionary stages of star-forming regions. Larger species of polycyclic aromatic hydrocarbons (PAHs) and fullerenes ( $C_{60}$  and  $C_{70}$ ), which may be related to the formation of the carbon-chain molecules, have been detected in circumstellar envelopes around carbon-rich Asymptotic Giant Branch (AGB) stars and planetary nebulae, while PAHs are also known to be a widespread component of the ISM in most galaxies. Recently, two line survey projects toward Taurus Molecular Cloud-1 with large single-dish telescopes have detected many new carbon-chain species, including molecules containing benzene rings. These new findings raise fresh questions about carbon-bearing species in the Universe. This article reviews various aspects of carbon-chain molecules, including observational

studies, chemical simulations, quantum calculations, and laboratory experiments, and discusses open questions and how future facilities may answer them.

**Keywords:** astrochemistry, ISM: molecules, ISM: abundances

# 1 General Introduction

## 1.1 Brief Overview of Astrochemistry

Astrochemistry is an interdisciplinary research field concerning “study of the formation, destruction, and excitation of molecules in astronomical environments and their influence on the structure, dynamics, and evolution of astronomical objects” (Dalgarno 2008). Astrochemical studies can involve various approaches: astronomical observations; laboratory experiments on reactions and diagnostic spectroscopy; chemical simulations; and quantum chemical calculations. Collaborative studies among these approaches have been crucial in revealing the great variety of chemical pathways that operate in space.

More than 300 molecules have been discovered in the interstellar medium (ISM) or circumstellar envelopes (CSEs) to date (the Cologne Database for Molecular Spectroscopy (CDMS)<sup>1</sup>; McGuire (2022)). Technical innovations and advances in observational facilities have boosted the detection of new, rarer interstellar molecules including isotopologues. These molecules have been detected in various physical conditions of the ISM; diffuse atomic H clouds ( $n_{\text{H}} \approx 100 \text{ cm}^{-3}$ ,  $T \approx 70 - 80 \text{ K}$ ), molecular clouds ( $n_{\text{H}} \approx 10^4 \text{ cm}^{-3}$ ,  $T \approx 10 \text{ K}$ ), prestellar cores<sup>2</sup> ( $n_{\text{H}} \approx 10^5 - 10^6 \text{ cm}^{-3}$ ,  $T \approx 10 \text{ K}$ ), protostellar cores ( $n_{\text{H}} \approx 10^7 \text{ cm}^{-3}$ ,  $T \approx 100 - 300 \text{ K}$ ), protoplanetary disks ( $n_{\text{H}} \approx 10^4 - 10^{10} \text{ cm}^{-3}$ ,  $T \approx 10 - 500 \text{ K}$ ), and envelopes of evolved stars ( $n_{\text{H}} \approx 10^{10} \text{ cm}^{-3}$ ,  $T \approx 2000 - 3500 \text{ K}$ ). Beyond our Galaxy, about 73 molecules have been detected in extragalactic sources.

Although 98% of the total mass of baryons consists of hydrogen (H) and helium (He), heavier trace elements such as carbon (C), oxygen (O), and nitrogen (N) are important constituent elements of interstellar molecules. These elements can make interstellar molecules complex and chemically rich. In particular, carbon composes the backbones of many molecules and is a prerequisite for organic chemistry.

Astrochemical studies of star-forming regions in our Galaxy have progressed rapidly in recent years, including in both nearby low-mass and more distant high-mass star-forming regions. The interstellar molecules in these regions provide information on both macroscopic aspects and microscopic processes that help us to understand physical conditions and star formation histories. In the Universe, including our Galaxy, most stars form from self-gravitating molecular clouds, i.e., where hydrogen exists predominantly in the form of  $\text{H}_2$ , mediated via formation on dust grain surfaces (Hollenbach & Salpeter 1971). In the gas phase, ion-molecule reactions, which can proceed

---

<sup>1</sup><https://cdms.astro.uni-koeln.de/classic/molecules>

<sup>2</sup>We use this term for gravitationally bound objects with central number densities above  $10^5 \text{ cm}^{-3}$  (Caselli et al. 2022).

even at cold temperatures as low as  $\sim 10$  K, synthesize many molecules (e.g., [Herbst 1983](#); [Herbst et al. 1983, 1984](#)). At the same time, complex organic molecules (COMs)<sup>3</sup> begin to form mainly by hydrogenation reactions on dust grain surfaces (e.g., CH<sub>3</sub>OH formation by successive hydrogenation reactions of CO; [Watanabe & Kouchi \(2002\)](#)). During the protostellar and protoplanetary disk stage, chemical processes and chemical composition become much more complex because of stellar feedbacks, such as protostellar radiative heating via dust reprocessed infrared radiation, direct impact of energetic UV and X-ray photons and relativistic cosmic ray particles, and shock heating produced by protostellar outflows and stellar winds.

In addition to chemical composition, isotopic fractionation in some molecules can be an indicator of chemical inheritance or *in situ* chemical changes and has been subject to a variety of astrochemical studies. Especially deuterium fractionation (D/H) and nitrogen fractionation (<sup>14</sup>N/<sup>15</sup>N) are essential for helping to trace the journey of materials during star and planet formation (for reviews [Caselli & Ceccarelli 2012](#); [Jørgensen et al. 2020](#); [Öberg & Bergin 2021](#)). These are particularly important for revealing the formation of our Solar System (e.g., [Jensen et al. 2019](#)), one of the most fundamental questions of astronomy.

This review focuses on “carbon-chain molecules”, one of the major groups of molecules in the Universe. They are abundant in the ISM and known to be useful tracers of current physical conditions and past evolutionary history. In particular, as we will see, they can be used to probe the kinematics of chemically young gas and of the early stage of molecular clouds (e.g., [Dobashi et al. 2018](#); [Pineda et al. 2020](#)). This means that line emission from rotational transitions of carbon-chain species is unique probes of gas kinematics related to star formation. Some carbon-chain species have been suggested to possess the potential to form COMs or more complex molecules that are related to biologically relevant molecules including amino acids. For example, cyanoacetylene (HC<sub>3</sub>N) has been suggested to be a candidate for the precursor of Cytosine, Uracil, and Thymine ([Choe 2021](#)). These aspects further motivate us to study their chemical characteristics in the Universe.

## 1.2 History of Studies of Carbon-Chain Molecules

Carbon-chain molecules are one of the major constituents of molecules detected in the Universe (see section 2.2). After the discovery of the first carbon-chain molecules in the ISM in the 1970s, many efforts to explain their formation routes were made by laboratory experiments and chemical simulations in the 1980s. In the beginning, the focus was on gas-phase chemical reactions of small species ([Prasad & Huntress 1980a,b](#); [Graedel et al. 1982](#)). [Herbst \(1983\)](#) was able to reproduce the observed abundance of a larger species, C<sub>4</sub>H, in Taurus Molecular Cloud-1 (TMC-1;  $d \approx 140$  pc), which is one of the most carbon-chain-rich sources. [Herbst \(1983\)](#) found that ion-molecule reactions with a large amount of atomic carbon (with its abundance of  $\sim 10^{-5}$ ) are necessary to explain the observed C<sub>4</sub>H abundance. [Suzuki \(1983\)](#) found that reactions including C<sup>+</sup> can also play essential roles in carbon-chain growth. These results suggested that carbon-chain species could efficiently form in young molecular clouds before carbon is locked into CO molecules.

---

<sup>3</sup>Molecules consisting of more than 6 atoms ([Herbst & van Dishoeck 2009](#)).



mechanism starting from CH<sub>4</sub> was proposed (see section 2.3). This was named Warm Carbon-Chain Chemistry (WCCC; for a review Sakai & Yamamoto 2013). More recently, carbon-chain chemistry around massive young stellar objects (MYSOs) has been explored (section 2.4), and Hot Carbon-Chain Chemistry (HCCC) has been proposed (Taniguchi et al. 2023).

Furthermore, very complex carbon-chain species, branched-chain molecules, and molecules including benzene rings have been discovered in the ISM in the last few years (section 3.1). These new findings bring fresh challenges and excite our curiosity for a deeper understanding of carbon-chain chemistry in the ISM.

### 1.3 Outline of This Review

In this review article, we summarize results from studies of carbon-chain molecules by astronomical observations, chemical simulations, quantum chemical calculations, and laboratory experiments. In section 2, we overview the current status of the detected carbon-chain species in the ISM and the main concepts of carbon-chain chemistry around protostars, which are different from the chemistry in cold starless cores (*i.e.*, Fig. 1). We review observational studies (section 3), chemical models (section 4), quantum chemical calculations (section 5), and laboratory experiments (section 6). Finally, we list current open and key questions regarding carbon-chain species and summarise points of this review in section 7.

Here, we set a definition of “carbon-chain molecules” for this review article, as recent detections of new interstellar species complicate this categorization. We include linear carbon-chain species with more than two carbon atoms and cyclic species with more than three carbon atoms containing at least one double (=) or triple (≡) bond as carbon-chain molecules. Even if molecules meet the above criteria, species containing functional groups related to organic chemistry (e.g., -OH, -NH<sub>2</sub>) are excluded from carbon-chain molecules because they are generally categorized as COMs. As an exception, *cyclic*-C<sub>2</sub>Si, which consists of a cyclic structure with two carbon atoms and one Si atom, is treated as a carbon-chain species.

In addition, we include molecules containing the structure of benzene, polycyclic aromatic hydrocarbons (PAHs), and fullerenes (C<sub>60</sub> or C<sub>70</sub>) in this review. Currently, it is unclear whether these species are directly or indirectly related to the above-defined “standard” carbon-chain species. However, for instance, PAHs are one of the larger carbon reservoirs in the ISM; they account for up to ~15% of the interstellar carbon and their IR luminosity is up to 20% of the total IR power emitted by the Milky Way and star-forming galaxies (e.g., Li 2020, and references therein). These species could be the origin of some carbon-chain species in early-stage star-forming regions via the top-down mechanism operating in harsh, diffuse ISM environments (e.g., Pety et al. 2005). Addressing the importance of the top-down scenario and connection of carbon-chain species with PAHs is a major topic of study, which can be addressed by sensitive mm, e.g., with the Atacama Large Millimeter/submillimeter Array (ALMA), and infrared, e.g., with the James Webb Space Telescope (JWST), observations.

In the following sections, we abbreviate *linear*- and *cyclic*- as *l*- and *c*-, if necessary to indicate the molecular structure (e.g., *l*-C<sub>3</sub>H<sub>2</sub> and *c*-C<sub>3</sub>H<sub>2</sub>). This review article summarizes literature results until the end of December 2023.

## 2 Development of Carbon-Chain Chemistry

### 2.1 Different carbon-chain families and their present status

All of the carbon-chain species belonging to the various groups,  $C_n$ ,  $C_nH$ ,  $C_nH^-$ ,  $C_nO$ ,  $C_nN$ ,  $C_nN^-$ ,  $C_nS$ ,  $C_nP$ ,  $HC_{2n+1}N$ ,  $HC_{2n}N$ ,  $HC_nO$ ,  $HC_nS$ ,  $H_2C_n$ ,  $HC_nH$ ,  $MgC_nH$ ,  $MgC_nN$ , are summarized in Table 1. Information is given on their electronic ground state, electric polarizability, electric dipole moment, and present astronomical status.

Regarding the present astronomical detection status provided in Table 1, we have organized the data into three columns. The first column contains information on carbon-chain species detected in the ISM or CSEs. The second column pertains to detections in TMC-1 and the third one is specific to detections in IRC+10216 only. We have made these distinctions because the majority of known carbon-chain species have been discovered in these two sources. Note that the absence of a check mark ( $\checkmark$ ) does not necessarily mean that a species does not exist in TMC-1 or IRC+10216 because some species have not yet been searched for in each source or may not have been detected due to low abundance. We will summarize each group in the following subsections.

**Table 1:** Ground state, polarizability ( $\alpha$ ), dipole moment ( $\mu$ ) and present astronomical status of different carbon chain species

Species	Ground State	$\alpha$ ( $\text{\AA}^3$ )	$\mu$ (D)	Detection Status		
				ISM or CSE	TMC-1	IRC+10216
$C_2$	singlet	5.07 <sup>a</sup>	0.0	<a href="#">Souza &amp; Lutz (1977)</a>		$\checkmark$
$C_3$	singlet	5.18 <sup>a</sup>	0.0	<a href="#">Hinkle et al. (1988)</a>		$\checkmark$
$C_4$	singlet	7.51 <sup>a</sup>	0.0			
$C_5$	singlet	11.16 <sup>a</sup>	0.0	<a href="#">Bernath et al. (1989)</a>		$\checkmark$
$C_6$	singlet	14.32 <sup>a</sup>	0.0	–		
$C_7$	singlet	20.50 <sup>a</sup>	0.0	–		
$C_8$	singlet	23.96 <sup>a</sup>	0.0	–		
$C_9$	singlet	33.36 <sup>a</sup>	0.0	–		
$C_{10}$	singlet	37.70 <sup>a</sup>	0.0	–		
$C_nH$						
$C_2H$	doublet	4.42 <sup>a</sup>	0.81 <sup>a</sup>	<a href="#">Tucker et al. (1974)</a>	$\checkmark$	$\checkmark$
<i>l</i> - $C_3H$	doublet	5.36 <sup>a</sup>	3.52 <sup>a</sup>	<a href="#">Thaddeus et al. (1985a)</a>	$\checkmark$	$\checkmark$
$C_3H^+$	singlet	3.69 <sup>*</sup>	3.00 <sup>b</sup>	<a href="#">Pety et al. (2012)</a>	$\checkmark$	
$C_4H$	doublet	7.15 <sup>a</sup>	2.40 <sup>c</sup>	<a href="#">Guelin et al. (1978)</a>	$\checkmark$	$\checkmark$
$C_4H^-$	singlet	9.57 <sup>*</sup>	5.9 <sup>d</sup>	<a href="#">Cernicharo et al. (2007)</a>	$\checkmark$	$\checkmark$
$C_5H$	doublet	10.50 <sup>a</sup>	4.84 <sup>a</sup>	<a href="#">Cernicharo et al. (1986)</a>	$\checkmark$	$\checkmark$
$C_5H^+$	singlet	8.44 <sup>*</sup>	2.88 <sup>e</sup>	<a href="#">Cernicharo et al. (2022a)</a>	$\checkmark$	
<i>c</i> - $C_5H$	doublet	8.77 <sup>*</sup>	3.39 <sup>f</sup>	<a href="#">Cabezas et al. (2022a)</a>	$\checkmark$	
$C_6H$	doublet	13.68 <sup>a</sup>	5.6 <sup>a</sup>	<a href="#">Suzuki et al. (1986)</a>	$\checkmark$	$\checkmark$
$C_6H^-$	singlet	15.74 <sup>*</sup>	8.2 <sup>d</sup>	<a href="#">McCarthy et al. (2006)</a>	$\checkmark$	$\checkmark$
$C_7H$	doublet	17.37 <sup>a</sup>	5.83 <sup>a</sup>	<a href="#">Guelin et al. (1997)</a>		$\checkmark$

Cont.						
C <sub>8</sub> H	doublet	21.85 <sup>a</sup>	6.43 <sup>a</sup>	Cernicharo & Guelin (1996)	✓	✓
C <sub>8</sub> H <sup>-</sup>	singlet	24.39*	11.9 <sup>5</sup>	Brünken et al. (2007); Remijan et al. (2007)	✓	✓
C <sub>9</sub> H	doublet	26.38 <sup>a</sup>	6.49 <sup>a</sup>	–		
C <sub>10</sub> H	doublet	31.05 <sup>a</sup>	7.13 <sup>a</sup>	Remijan et al. (2023)	✓	
C <sub>10</sub> H <sup>-</sup>	singlet	–	–	Remijan et al. (2023)	✓	✓
HC <sub>n</sub> H						
HC <sub>2</sub> H	singlet	3.38 <sup>a</sup>	0.0 <sup>a</sup>	Ridgway et al. (1976)		✓
HC <sub>3</sub> H	triplet	2.58 <sup>a</sup>	0.51 <sup>g</sup>	–		
HC <sub>4</sub> H	singlet	7.05 <sup>a</sup>	0.0 <sup>a</sup>	Cernicharo et al. (2001)		
HC <sub>5</sub> H	triplet	–	–	–		
HC <sub>6</sub> H	singlet	11.95 <sup>a</sup>	0.0 <sup>a</sup>	Cernicharo et al. (2001)		
HC <sub>7</sub> H	triplet	–	–	–		
HC <sub>8</sub> H	singlet	18.59 <sup>a</sup>	0.0	–		
H <sub>2</sub> C <sub>n</sub>						
<i>l</i> -H <sub>2</sub> C <sub>3</sub>	singlet	5.61 <sup>a</sup>	4.16 <sup>a</sup>	Cernicharo et al. (1991a)	✓	✓
<i>l</i> -H <sub>2</sub> C <sub>4</sub>	singlet	8.12 <sup>a</sup>	4.43 <sup>a</sup>	Cernicharo et al. (1991b)		✓
<i>l</i> -H <sub>2</sub> C <sub>5</sub>	singlet	11.32 <sup>a</sup>	5.89 <sup>a</sup>	Cabezas et al. (2021)	✓	
<i>l</i> -H <sub>2</sub> C <sub>6</sub>	singlet	15.15 <sup>a</sup>	6.15	Langer et al. (1997)	✓	
C <sub>n</sub> O						
C <sub>2</sub> O	triplet	4.09 <sup>a</sup>	1.43 <sup>a</sup>	Ohishi et al. (1991)	✓	✓
C <sub>3</sub> O	singlet	6.03 <sup>a</sup>	2.39 <sup>h</sup>	Matthews et al. (1984)	✓	✓
HC <sub>3</sub> O <sup>+</sup>	singlet	–	3.41 <sup>i</sup>	Cernicharo et al. (2020b)	✓	
C <sub>4</sub> O	triplet	9.21 <sup>a</sup>	3.01 <sup>j</sup>	–		
C <sub>5</sub> O	singlet	10.93*	4.06 <sup>k</sup>	Cernicharo et al. (2021a)	✓	✓
C <sub>6</sub> O	triplet	15.41*	4.88 <sup>j</sup>	–		
C <sub>7</sub> O	singlet	19.51*	4.67 <sup>l</sup>	–		
C <sub>8</sub> O	triplet	25.99*	4.80 <sup>l</sup>	–		
C <sub>n</sub> S						
C <sub>2</sub> S	triplet	6.87 <sup>a</sup>	3.12 <sup>a</sup>	Saito et al. (1987)	✓	✓
HC <sub>2</sub> S <sup>+</sup>	triplet	–	2.29 <sup>11</sup>	Cabezas et al. (2022b)	✓	
C <sub>3</sub> S	singlet	9.65 <sup>a</sup>	3.939 <sup>a</sup>	Kaifu et al. (1987)	✓	✓
HC <sub>3</sub> S <sup>+</sup>	singlet	–	1.73 <sup>d</sup>	Cernicharo et al. (2021f)	✓	
C <sub>4</sub> S	triplet	13.70 <sup>a</sup>	4.62 <sup>a</sup>	Cernicharo et al. (2021e)	✓	✓
C <sub>5</sub> S	singlet	15.79*	4.65 <sup>m</sup>	Agúndez et al. (2014)	✓	✓
C <sub>6</sub> S	triplet	21.53*	5.40 <sup>l</sup>	–		
C <sub>7</sub> S	singlet	26.44*	6.17 <sup>l</sup>	–		
C <sub>8</sub> S	triplet	34.54*	6.50 <sup>l</sup>	–		
C <sub>n</sub> N						
C <sub>2</sub> N	doublet	4.27 <sup>a</sup>	0.60 <sup>a</sup>	Anderson & Ziurys (2014)		✓
C <sub>3</sub> N	doublet	5.68 <sup>a</sup>	2.86 <sup>a</sup>	Guélin & Thaddeus (1977)	✓	✓
C <sub>3</sub> N <sup>-</sup>	singlet	7.58*	3.1 <sup>n</sup>	Thaddeus et al. (2008)	✓	✓
C <sub>4</sub> N	doublet	8.75 <sup>a</sup>	0.06 <sup>a</sup>	–		
C <sub>5</sub> N	doublet	9.43 <sup>a</sup>	3.33 <sup>a</sup>	Guélin et al. (1998)	✓	✓

Cont.						
C <sub>5</sub> N <sup>-</sup>	singlet	13.26*	5.20 <sup>o</sup>	Cernicharo et al. (2008)	✓	✓
C <sub>6</sub> N	doublet	14.91*	0.21 <sup>p</sup>	–		
C <sub>7</sub> N	doublet	18.95 <sup>a</sup>	0.87 <sup>a</sup>	–		
C <sub>7</sub> N <sup>-</sup>	singlet	–	7.5	Cernicharo et al. (2023b)	✓	✓
C <sub>8</sub> N	doublet	24.16*	–	–		
NC <sub>4</sub> NH <sup>+</sup>	singlet	–	9.1	Agúndez et al. (2023)	✓	
C <sub>n</sub> P						
C <sub>2</sub> P	doublet	7.52 <sup>a</sup>	3.24 <sup>a</sup>	Halfen et al. (2008)		✓
C <sub>3</sub> P	doublet	10.50 <sup>a</sup>	3.89 <sup>a</sup>	–		
C <sub>4</sub> P	doublet	12.76 <sup>a</sup>	4.19 <sup>a</sup>	–		
C <sub>5</sub> P	doublet	17.22*	–	–		
C <sub>6</sub> P	doublet	22.13*	–	–		
C <sub>7</sub> P	doublet	27.90*	–	–		
C <sub>8</sub> P	doublet	34.41*	–	–		
HC <sub>2n</sub> N						
HC <sub>2</sub> N	triplet		3.30 <sup>q</sup>	Guelin & Cernicharo (1991)		✓
HC <sub>4</sub> N	triplet	8.84 <sup>a</sup>	4.30 <sup>a</sup>	Cernicharo et al. (2004)		✓
HC <sub>6</sub> N	triplet	15.07 <sup>a</sup>	4.89 <sup>a</sup>	–		
HC <sub>8</sub> N	triplet	22.96 <sup>a</sup>	5.57 <sup>a</sup>	–		
H <sub>2</sub> CCCN	doublet		3.60	Cabezas et al. (2023b)	✓	
HC <sub>2n+1</sub> N						
HC <sub>3</sub> N	singlet	5.85 <sup>a</sup>	3.78 <sup>a</sup>	Turner (1971)	✓	✓
HNC <sub>3</sub>	singlet	6.41*	6.46 <sup>p</sup>	Kawaguchi et al. (1992)	✓	✓
HC <sub>3</sub> NH <sup>+</sup>	singlet	4.90*	1.87 <sup>r</sup>	Kawaguchi et al. (1994)	✓	
HC <sub>5</sub> N	singlet	10.42 <sup>a</sup>	4.41 <sup>a</sup>	Avery et al. (1976)	✓	✓
HC <sub>5</sub> NH <sup>+</sup>	singlet	10.67*	3.26 <sup>n1</sup>	Marcelino et al. (2020)	✓	
HC <sub>7</sub> N	singlet	16.69 <sup>a</sup>	4.90 <sup>a</sup>	Kroto et al. (1978)	✓	✓
HC <sub>7</sub> NH <sup>+</sup>	singlet	–	6.40 <sup>o1</sup>	Cabezas et al. (2022b)	✓	
HC <sub>9</sub> N	singlet	23.89 <sup>a</sup>	5.29 <sup>a</sup>	Brotten et al. (1978)	✓	✓
HC <sub>11</sub> N	singlet	–	5.47	Loomis et al. (2021)	✓	
HC <sub>n</sub> O						
HC <sub>2</sub> O	doublet	4.20 <sup>c</sup>	1.8 <sup>s</sup>	Agúndez et al. (2015)	✓	
HC <sub>3</sub> O	doublet	5.20 <sup>c</sup>	2.74 <sup>s</sup>	Cernicharo et al. (2020b)	✓	
HC <sub>4</sub> O	doublet	7.83*	2.64 <sup>m1</sup>	–		
HC <sub>5</sub> O	doublet	10.87*	2.16 <sup>m1</sup>	McGuire et al. (2017)	✓	
HC <sub>6</sub> O	doublet	14.46*	2.11 <sup>m1</sup>	–		
HC <sub>7</sub> O	doublet	–	2.17 <sup>m1</sup>	Cordiner et al. (2017)	✓	
HC <sub>8</sub> O	doublet	–	2.19 <sup>m1</sup>	–		
HC <sub>n</sub> S						
HC <sub>2</sub> S	doublet	6.92 <sup>s</sup>	1.36 <sup>s</sup>	Cernicharo et al. (2021f)	✓	
HC <sub>3</sub> S	doublet	9.62 <sup>s</sup>	1.28 <sup>s</sup>	–		
HC <sub>4</sub> S	doublet	11.60*	1.45 <sup>p1</sup>	Fuentetaja et al. (2022b)	✓	
HC <sub>5</sub> S	doublet	–	1.92 <sup>q1</sup>	–		
HC <sub>6</sub> S	doublet	19.86*	2.75 <sup>r1</sup>	–		



Cont.

HC <sub>7</sub> S	doublet	–	2.10 <sup>q1</sup>			
HC <sub>8</sub> S	doublet	–	3.21 <sup>r1</sup>			
Metal Containing						
MgC <sub>2</sub> H	doublet	10.44*	1.68 <sup>t</sup>	Agúndez et al. (2014)		✓
MgC <sub>4</sub> H	doublet	15.01*	2.12 <sup>u</sup>	Cernicharo et al. (2019)		✓
MgC <sub>3</sub> N	doublet	13.16*	6.30 <sup>u</sup>	Cernicharo et al. (2019)		✓
MgC <sub>5</sub> N	doublet	19.22	7.30 <sup>v</sup>	Pardo et al. (2021)	✓	✓
MgC <sub>6</sub> H	doublet	21.54*	2.50 <sup>v</sup>	Pardo et al. (2021)		✓
<i>c</i> -C <sub>2</sub> Si	doublet	6.79 <sup>a</sup>	2.4 <sup>a</sup>	Thaddeus et al. (1984)		✓
<i>c</i> -C <sub>3</sub> Si	singlet	11.90 <sup>a</sup>	4.1 <sup>a</sup>	Apponi et al. (1999)		✓
C <sub>4</sub> Si	singlet	–	6.3 <sup>w</sup>	Ohishi et al. (1989a)		✓
HMgCCN	singlet		4.5	Cabezas et al. (2023a)		✓
NaCCCN	singlet		12.9	Cabezas et al. (2023a)		✓
MgC <sub>4</sub> H <sup>+</sup>	singlet		13.5	Cernicharo et al. (2023a)		✓
MgC <sub>3</sub> N <sup>+</sup>	singlet		18.5	Cernicharo et al. (2023a)		✓
MgC <sub>6</sub> H <sup>+</sup>	singlet		18.2	Cernicharo et al. (2023a)		✓
MgC <sub>5</sub> N <sup>+</sup>	singlet		23.7	Cernicharo et al. (2023a)		✓
Cyclic carbon chains						
<i>c</i> -C <sub>3</sub> H	doublet	4.80 <sup>a</sup>	2.60 <sup>a</sup>	Yamamoto et al. (1987)	✓	
<i>c</i> -C <sub>3</sub> H <sub>2</sub>	singlet	4.58 <sup>a</sup>	3.41 <sup>a</sup>	Thaddeus et al. (1985b)	✓	✓
<i>c</i> -C <sub>3</sub> HCCCH	singlet	–	4.93 <sup>x</sup>	Cernicharo et al. (2021b)	✓	
<i>c</i> -H <sub>2</sub> C <sub>3</sub> O	singlet	5.20 <sup>s</sup>	4.39 <sup>s</sup>	Hollis et al. (2006)	✓	
PAHs and benzene ring related species						
C <sub>6</sub> H <sub>6</sub>	singlet	10.35 <sup>a</sup>	0.0	Cernicharo et al. (2001)		
C <sub>60</sub> <sup>+</sup>	doublet		0.0	Foing & Ehrenfreund (1994)		
C <sub>60</sub>	singlet	79.0 <sup>y</sup>	0.0	Cami et al. (2010)		
C <sub>70</sub>	singlet	10 <sup>z</sup>	0.0	Cami et al. (2010)		
<i>c</i> -C <sub>6</sub> H <sub>5</sub> CN	singlet	11.91 <sup>y</sup>	4.51 <sup>k1</sup>	McGuire et al. (2018)	✓	
<i>c</i> -C <sub>9</sub> H <sub>8</sub>	singlet	121.20 <sup>a1</sup>	0.87 <sup>b1</sup>	Cernicharo et al. (2021b)	✓	
<i>c</i> -C <sub>5</sub> H <sub>4</sub> CCH <sub>2</sub>	singlet	–	0.69 <sup>c1</sup>	Cernicharo et al. (2022b)	✓	
<i>c</i> -C <sub>5</sub> H <sub>6</sub>	singlet	–	0.42 <sup>d1</sup>	Cernicharo et al. (2021b)	✓	
1- <i>c</i> -C <sub>5</sub> H <sub>5</sub> CN	singlet	10.93*	4.42 <sup>e1</sup>	McCarthy et al. (2021)	✓	
2- <i>c</i> -C <sub>5</sub> H <sub>5</sub> CN	singlet	10.65*	5.13 <sup>e1</sup>	Lee et al. (2021a)	✓	
1-C <sub>10</sub> H <sub>7</sub> CN	singlet	19.83*	6.60 <sup>f1</sup>	McGuire et al. (2021)	✓	
2-C <sub>10</sub> H <sub>7</sub> CN	singlet	20.43*	6.10 <sup>f1</sup>	McGuire et al. (2021)	✓	
<i>o</i> -C <sub>6</sub> H <sub>4</sub>	singlet	–	1.38 <sup>h1</sup>	Cernicharo et al. (2021c)	✓	
1- <i>c</i> -C <sub>5</sub> H <sub>5</sub> CCH	singlet	12.36*	1.13 <sup>g1</sup>	Cernicharo et al. (2021d)	✓	
2- <i>c</i> -C <sub>5</sub> H <sub>5</sub> CCH	singlet	11.93*	1.48 <sup>g1</sup>	Cernicharo et al. (2021d)	✓	
C <sub>6</sub> H <sub>5</sub> CCH	singlet	–	0.66 <sup>i1</sup>	Loru et al. (2023)	✓	
C <sub>9</sub> H <sub>7</sub> CN	singlet	–	5.04 <sup>j1</sup>	Sita et al. (2022)	✓	
CH <sub>3</sub> C <sub>5</sub> N	singlet		5.75	Snyder et al. (2006)	✓	
CH <sub>3</sub> C <sub>6</sub> H	singlet		1.50	Remijan et al. (2006)	✓	
<i>E</i> -1-C <sub>4</sub> H <sub>5</sub> CN	singlet	11.18	4.81	Cooke et al. (2023)	✓	
(CH <sub>3</sub> ) <sub>2</sub> CCH <sub>2</sub>	singlet		0.50	Fatima et al. (2023)	✓	

The  $\checkmark$  mark in the last three rows means detection including tentative detection. References: <sup>a</sup>Woon & Herbst (2009), <sup>b</sup>Pety et al. (2012), <sup>c</sup>Oyama et al. (2020), <sup>d</sup>Blanksby et al. (2001), <sup>e</sup>Botschwina (1991), <sup>f</sup>Crawford et al. (1999), <sup>g</sup>Nguyen et al. (2001), <sup>h</sup>Brown et al. (1983), <sup>i</sup>Cernicharo et al. (2020b), <sup>j</sup>Ewing (1989), <sup>k</sup>Botschwina (1993), <sup>l</sup>Etim et al. (2020), <sup>m</sup>Pascoli & Lavendy (1998), <sup>n</sup>Thaddeus et al. (2008), <sup>o</sup>Cernicharo et al. (2008), <sup>p</sup>Kawaguchi et al. (1992), <sup>q</sup>Hirano et al. (1989), <sup>r</sup>Botschwina (1987), <sup>s</sup>KIDA (<https://kida.astrochem-tools.org/>), <sup>t</sup>Woon (1996), <sup>u</sup>Cernicharo et al. (2019), <sup>v</sup>Pardo et al. (2022), <sup>w</sup>Ohishi et al. (1989b), <sup>x</sup>Travers et al. (1997), <sup>y</sup><https://cccbdb.nist.gov/pollistx.asp>, <sup>z</sup>Compagnon et al. (2001), <sup>a1</sup>Ghiasi & Monnajemi (2006), <sup>b1</sup>Caminati (1993), <sup>c1</sup>Sakaizumi et al. (1993), <sup>d1</sup>Laurie (1956), <sup>e1</sup>Sakaizumi et al. (1987), <sup>f1</sup>McNaughton et al. (2018), <sup>g1</sup>Cernicharo et al. (2021d), <sup>h1</sup>Kraka & Cremer (1993), <sup>i1</sup>Cox et al. (1975), <sup>j1</sup>Sita et al. (2022), <sup>k1</sup>Wohlfart et al. (2008), <sup>l1</sup>Puzzarini (2008), <sup>m1</sup>Mohamed et al. (2005), <sup>n1</sup>Marcelino et al. (2020), <sup>o1</sup>Cabezas et al. (2022c), <sup>p1</sup>Fuentetaja et al. (2022a), <sup>q1</sup>Gordon et al. (2002), <sup>r1</sup>Wang et al. (2009) \*This work (estimated with B3LYP/6-311++G(d,p) level of theory using Gaussian software (Frisch et al. 2013))

### 2.1.1 Pure carbon chains - $C_n$

All pure linear carbon-chain species are indicated as  $C_n$  ( $n > 1$ ). The electronic ground state of all these species is singlet, and they do not have a permanent dipole moment (see Table 1). Hence, they do not show rotational transitions, and so are not detectable via rotational transitions using radio observations. Instead, they show emission in the infrared domain through their rotational-vibrational transitions, and so far three chains ( $n = 2, 3, 5$ ) are astronomically detected from this group (see Table 1). In diffuse and translucent environments,  $C_2$  formation starts with the reaction of  $C^+ + CH \rightarrow C_2^+ + H$  (see Fig. 1), followed by a series of hydrogen abstraction reactions and dissociative recombination reactions that yield  $C_2$  via several channels (Welty et al. 2013, and reference therein).  $C_3$  is formed via a dissociative recombination reaction of  $C_3H^+$  that can also produce CCH (Fig. 1), though neutral-neutral reactions (e.g.,  $C + C_2H_2$ ) may also contribute to the formation of  $C_3$  (Roueff et al. 2002).

### 2.1.2 Hydrocarbons - $C_nH$

The  $C_nH$  group represents the simplest hydrocarbons and carbon-chain radicals. All carbon chains from this group have permanent dipole moments and show strong rotational transitions. To date, seven neutral ( $n = 2 - 8$ ) carbon-chain species have been detected from this group. All of them have been identified towards both TMC-1 and IRC+10216. In starless cores, carbon-chain species are generally considered to form mainly by the electron recombination reactions of protonated ions such as  $C_2H_2^+$  and *c,l*- $C_3H_3^+$ , as shown Fig. 1.

Apart from neutrals, four anions ( $C_4H^-$ ,  $C_6H^-$ ,  $C_8H^-$ , and  $C_{10}H^-$ ) and two cations ( $C_3H^+$  and  $C_5H^+$ ) have also been identified in TMC-1. The anions could form by the electron attachment for the neutral species; the cases of  $C_4H^-$  and  $C_5H^-$  are shown in Fig. 1. The anions belong to the even series ( $n = 2, 4, 6$ ), while the cations

belong to the odd series ( $n = 3, 5$ ). In addition, two cyclic chains,  $c$ -C<sub>3</sub>H, and  $c$ -C<sub>5</sub>H, have been identified. All neutral species have a doublet ground state and show a trend of increasing dipole moment with the number of carbon atoms ( $n$ ), especially for neutrals and anions (see Table 1).

The C<sub>*n*</sub>H family is mainly formed through the atomic reactions in the following channel,  $C + C_{n-1}H_2 \rightarrow C_nH + H$  (Remijan et al. 2023). This reaction scheme is indicated in Fig. 1, from CH<sub>2</sub> to CCH. Another two channels, which involve atomic and their related anions, can also form C<sub>*n*</sub>H family species efficiently:  $C + C_{n-1}H^- \rightarrow C_nH + e^-$  and  $H + C_n^- \rightarrow C_nH + e^-$ .

### 2.1.3 Oxygen-bearing carbon chains - C<sub>*n*</sub>O

To date, three oxygen (O)-bearing carbon chains, C<sub>*n*</sub>O ( $n = 2, 3, 5$ ) have been detected in the ISM. In this series, C<sub>3</sub>O was the first, detected toward TMC-1 in 1984, while C<sub>2</sub>O was identified in the same source in 1991. It took around three decades to detect the higher-order chain, C<sub>5</sub>O, in TMC-1. C<sub>4</sub>O is yet to be detected. Carbon chains in this group have alternate ground states, i.e., triplet and singlet, and show a trend of increasing dipole moment with the number of carbon atoms (see Table 1). A protonated species, HC<sub>3</sub>O<sup>+</sup> with singlet ground state, has been detected in TMC-1 (Cernicharo et al. 2020b). The observed trend toward TMC-1 shows that C<sub>3</sub>O is the most abundant, followed by C<sub>2</sub>O and C<sub>5</sub>O, with C<sub>5</sub>O about 50 times less abundant than C<sub>2</sub>O and about 80 times less abundant than C<sub>3</sub>O (Cernicharo et al. 2021a). In addition, all these species have been identified towards the circumstellar envelope of IRC+10216. The formation of C<sub>*n*</sub>O and HC<sub>*n*</sub>O chains follows similar formation mechanisms as discussed above. The first step involves the radiative association of C<sub>*n-1*</sub>H<sup>+</sup>, C<sub>*n-1*</sub>H<sub>2</sub><sup>+</sup>, and C<sub>*n-1*</sub>H<sub>3</sub><sup>+</sup> ions with CO, which is then followed by dissociative electron recombination reactions (Adams et al. 1989; Cernicharo et al. 2021a).

### 2.1.4 Sulfur-bearing carbon chains - C<sub>*n*</sub>S

Similar to C<sub>*n*</sub>O, several sulfur (S)-bearing carbon chains, C<sub>*n*</sub>S ( $n = 2, 3, 4, 5$ ), have been identified in the ISM. Two protonated species, HCCS<sup>+</sup> and HC<sub>3</sub>S<sup>+</sup>, have only been detected towards TMC-1 so far. The discovery of HC<sub>3</sub>S<sup>+</sup> supports the formation route of CCS and C<sub>3</sub>S via the electron recombination reactions of HC<sub>3</sub>S<sup>+</sup> indicated in Fig. 1. Carbon chains in this group have alternative ground states, i.e., triplet and singlet, and show a trend of increasing dipole moment with the number of carbon atoms, similar to the C<sub>*n*</sub>O group (see Table 1). The abundances of C<sub>2</sub>S and C<sub>3</sub>S are almost three orders of magnitude higher than C<sub>4</sub>S and C<sub>5</sub>S toward TMC-1 (Cernicharo et al. 2021e). On the other hand, the C<sub>5</sub>S column density is slightly less than those of C<sub>2</sub>S and C<sub>3</sub>S, with differences less than one order of magnitude, toward IRC+10216 (Agúndez et al. 2014). C<sub>2</sub>S and C<sub>3</sub>S are mainly produced via several ion-neutral reactions followed by electron recombination reactions and via several neutral-neutral reactions (Sakai et al. 2007). Higher order chains of this family, such as C<sub>4</sub>S and C<sub>5</sub>S, are thought to be formed via reactions of S + C<sub>4</sub>H and C + HC<sub>3</sub>S, and C<sub>4</sub>H + CS and S + C<sub>5</sub>H, respectively. However, the kinetics and product distribution of these reactions are poorly known (Cernicharo et al. 2021e).

### 2.1.5 Nitrogen-bearing carbon chains - $C_nN$

In this group,  $C_3N$  was the first detected species, done so tentatively toward IRC+10216 in 1977 and more robustly toward TMC-1 in 1980. The next higher order chain in this series,  $C_5N$  was detected toward TMC-1 and tentatively detected toward IRC+10216 in 1998. The lower order chain, CCN, was found in 2014. Their anions,  $C_3N^-$  and  $C_5N^-$ , were discovered in the circumstellar envelope of the carbon-rich star IRC+10216 (Thaddeus et al. 2008; Cernicharo et al. 2008). They have also been identified toward TMC-1 by the QUIJOTE group, including their neutral analogs ( $C_3N$ ,  $C_5N$ ) (Cernicharo et al. 2020c). They measured similar abundance ratios of  $C_3N^-/C_3N = 140$  and  $194$ , and  $C_5N^-/C_5N = 2$  and  $2.3$  in TMC-1 and IRC+10216, respectively, even though physical conditions are completely different for TMC-1 and IRC+10216. It might be a coincidence that there are similar abundance ratios of anion and neutral forms of  $C_nN$  ( $n = 3, 5$ ). All carbon chains from this group have doublet ground state, and the two anionic forms have singlet state. Since the dipole moment of CCN is low compared to those of  $C_3N$ ,  $C_5N$ , and their anionic forms, the detection of CCN is more challenging, even though it is of lower order in the chain (see Table 1).  $C_4N$ ,  $C_6N$ , and  $C_7N$  show even smaller values of their dipole moments, which suggests that much high sensitivity observations are required for their identification.  $C_2N$  is produced through the reactions of  $N + C_2$  and  $C + CN$ . Similarly,  $C_3N$  is produced in reactions of  $N + C_3$  and  $C + CCN$ , and  $C_5N$  is produced through  $N + C_5$  on dust surfaces<sup>4</sup>. The production of  $C_3N^-$  mainly comes from the reaction between N atoms and bare carbon-chain anions  $C_n^-$  (Cernicharo et al. 2020c), whereas  $C_5N^-$  is produced via the electron radiative attachment to  $C_5N$  (Walsh et al. 2009).

### 2.1.6 Phosphorus-bearing carbon chains - $C_nP$

Although phosphorus (P) has a relatively small elemental abundance, it plays a crucial role in the development of life (Chantzos et al. 2020). Among the known eight phosphorus-bearing molecules,  $C_2P$  (or CCP) is the only P-bearing carbon-chain species and detected toward IRC+10216 (Halfen et al. 2008). All carbon chains in this group have doublet ground states (Table 1). Higher order chains,  $C_3P$  and  $C_4P$ , show a higher value of dipole moments, but they are yet to be detected in the ISM or circumstellar environments. Since the overall elemental abundance of phosphorous is small, higher-order phosphorous chains are expected to have very low abundances. CCP may be produced by radical-radical reactions, between CP and hydrocarbons (CCH and  $C_3H$ ), or ion-molecule chemistry involving  $P^+$  and HCCH followed by the dissociative electron recombination reaction (Halfen et al. 2008).

### 2.1.7 $HC_nO$ family

Four neutral  $HC_nO$  ( $n = 2, 3, 5, 7$ ) chains have been identified toward TMC-1 (Cernicharo et al. 2021a; McGuire et al. 2017; Cordiner et al. 2017). The detection summary of this group indicates odd  $n$  chains are more abundant compared to their even  $n$  counterparts. This trend is the same as in the  $C_nO$  family. All neutral chains have doublet ground states and dipole moment values are less than 3 Debye. The observed

---

<sup>4</sup><https://kida.astrochem-tools.org/>

cation  $\text{HC}_3\text{O}^+$  has a singlet ground state and a dipole moment of 3.41 Debye (see Table 1). As mentioned before,  $\text{C}_n\text{O}$  and  $\text{HC}_n\text{O}$  are linked through their formation routes (see Sec. 2.1.3).

### 2.1.8 $\text{HC}_n\text{S}$ family

This family is similar to  $\text{HC}_n\text{O}$  but contains sulfur instead of oxygen. Only two neutral species,  $\text{HCCS}$  and  $\text{HC}_4\text{S}$  have been identified toward TMC-1 (Cernicharo et al. 2021e; Fuentetaja et al. 2022a). Observed statistics suggest chains with even  $n$  have higher abundance than odd  $n$  species. All neutral chains of this group have doublet ground states (see Table 1). The dipole moments of neutral species are less than 2.2 Debye.  $\text{HCCS}$  is mainly formed through the reaction,  $\text{C} + \text{H}_2\text{CS}$  (Cernicharo et al. 2021e).  $\text{HC}_4\text{S}$  is produced through the reaction between  $\text{C}$  and  $\text{H}_2\text{C}_3\text{S}$  and by the dissociative recombination reaction of  $\text{H}_2\text{C}_4\text{S}^+$ , which is formed via reactions of  $\text{S} + \text{C}_4\text{H}_3^+$  and  $\text{S}^+ + \text{C}_4\text{H}_3$  (Fuentetaja et al. 2022b). This group has protonated ions, and  $\text{HC}_2\text{S}^+$  and  $\text{HC}_3\text{S}^+$  have been detected in TMC-1 (Cabezas et al. 2022b; Cernicharo et al. 2021f). For  $\text{HC}_3\text{S}^+$ , proton transfer to  $\text{C}_3\text{S}$  from  $\text{HCO}^+$  and  $\text{H}_3\text{O}^+$  is the main formation route. The reactions of  $\text{S}^+ + c, l - \text{C}_3\text{H}_2$  (see Fig. 1) and  $\text{S} + c, l - \text{C}_3\text{H}_3$  are also equally important and efficient (Cernicharo et al. 2021f).

### 2.1.9 Cyanopolyynes - $\text{HC}_{2n+1}\text{N}$

Cyanopolyynes are the most important, interesting, and ubiquitous organic carbon chains ( $n = 1 - 5$ ) detected in the ISM so far. As mentioned above,  $\text{HC}_3\text{N}$  was the first detected carbon-chain molecule in space. In this series, five species, starting from  $\text{HC}_3\text{N}$  to  $\text{HC}_{11}\text{N}$ , have been found in TMC-1. All these species have also been detected toward IRC+10216, except  $\text{HC}_{11}\text{N}$  (Morris et al. 1976; Winnewisser & Walmsley 1978; Matthews et al. 1985). In this series, especially  $\text{HC}_3\text{N}$  and  $\text{HC}_5\text{N}$ , have been identified in various star-forming environments (see section 3.4.2). Three cations,  $\text{HC}_3\text{NH}^+$ ,  $\text{HC}_5\text{NH}^+$ , and  $\text{HC}_7\text{NH}^+$ , have also been identified toward TMC-1 (Kawaguchi et al. 1994; Marcelino et al. 2020; Cabezas et al. 2022c). The detection of these protonated species in TMC-1 supports the formation route of the neutral species via electron recombination reactions (see Fig. 1). Their main formation pathways have been studied by observations of their  $^{13}\text{C}$  isotopic fractionation, as we discuss in section 3.5. All neutral cyanopolyynes have a singlet ground state and show a trend of increasing dipole moment with length of the chain (see Table 1). Unlike other carbon-chain species, the cyanopolyne family could form on dust surfaces through reactions  $\text{N} + \text{C}_{2n+1}\text{H}$  ( $n = 1 - 4$ ) and  $\text{H} + \text{C}_{2n+1}\text{N}$  ( $n = 1 - 4$ ) (see section 3.5 for more detail regarding the formation of cyanopolyynes in the gas phase). Protonated cyanopolyynes (e.g.,  $\text{HC}_3\text{NH}^+$ ,  $\text{HC}_5\text{NH}^+$ ) are mainly formed via a proton donor (e.g.,  $\text{HCO}^+$ ) to cyanopolyynes (e.g.,  $\text{HC}_3\text{N}$ ,  $\text{HC}_5\text{N}$ ). Protonated cyanopolyynes are destroyed by dissociative electron recombination reactions (Marcelino et al. 2020).

### 2.1.10 Allenic chain family - $\text{HC}_{2n}\text{N}$

$\text{HCCN}$  was the first member of the allenic chain family,  $\text{HC}_{2n}\text{N}$ , observed in space (Guelin & Cernicharo 1991), and  $\text{HC}_4\text{N}$  was the second. These species have been

identified toward IRC+10216. The allenic chain family has a triplet ground state and shows increasing dipole moment with size, similar to cyanopolyynes and other families (Table 1).  $\text{HC}_4\text{N}$  may form through the reactions of  $\text{C}_3\text{N} + \text{CH}_2$  and  $\text{C}_3\text{H} + \text{HCN}$ . For this family, ion-molecule paths are relatively slow (Cernicharo et al. 2004). However, HCCN is formed by the reactions between atomic nitrogen and  $\text{H}_n\text{CCH}^+$ .

## 2.2 Statistics of Detected Species

Fig. 2 shows the cumulative plot of carbon-chain detection together with the histogram plot in each year starting from 1971, the first carbon-chain detection year, until 2023. Following the definition mentioned earlier in section 1.3, 132 carbon-chain species have been discovered until the end of 2023. This accounts for approximately 43% of all the known 305 molecules. Carbon-chain species that have been detected so far and candidates for future detection are summarized in Table 1.

Following the discovery of  $\text{HC}_3\text{N}$  in 1971 (Turner 1971), new carbon-chain species continued to be found at a rate of just over one species per year for the next 50 years. A steep increase is seen after 2021 in Fig. 2, thanks to the two deep line survey projects toward TMC-1 CP (section 3.1). 29, 18, and 14 carbon-chain species have been discovered in 2021, 2022, and 2023, respectively. Before that, the maximum number was five in 1984. Hence, the number of discovered new carbon-chain species in the last three years is larger than those in the previous era by a factor of three to five.

Note that most of the achievements in the last three years are at TMC-1 CP. We cannot conclude that these new carbon-chain species are prevalent in other starless cores and star-forming regions. In addition, this also raises the question as to why TMC-1 appears to be particularly rich in carbon-chain species compared to other starless cores. Line survey observations toward a large sample of starless and star-forming cores in various environments are needed to answer this question.

## 2.3 Warm Carbon-Chain Chemistry (WCCC)

In section 1.2, we mentioned that carbon-chain molecules have been classically known as early-type species, because they are abundant in young starless cores and deficient in evolved star-forming cores. Against this classical picture, Sakai et al. (2008) detected various carbon-chain molecules toward IRAS 04368+2557 in the low-mass star-forming region L1527 in Taurus. The derived rotational temperature from the  $\text{C}_4\text{H}_2$  lines is  $12.3 \pm 0.8$  K, which is higher than excitation temperatures of carbon-chain species in the starless core TMC-1 ( $\approx 4 - 8$  K). They proposed that evaporation of  $\text{CH}_4$  from ice mantles could be the trigger of formation of carbon-chain molecules in the lukewarm envelopes around low-mass protostars, and named such a carbon-chain formation mechanism “Warm Carbon-Chain Chemistry (WCCC)”. A second WCCC source, IRAS 15398-3359 in the Lupus star-forming region, was discovered soon after (Sakai et al. 2009). This suggested that the WCCC mechanism may be a common feature around low-mass protostars, and WCCC has been widely accepted in the astrochemical field.

Later studies using chemical simulations support the formation mechanism of carbon-chain molecules starting from  $\text{CH}_4$  around temperatures of 25–30 K (Hassel

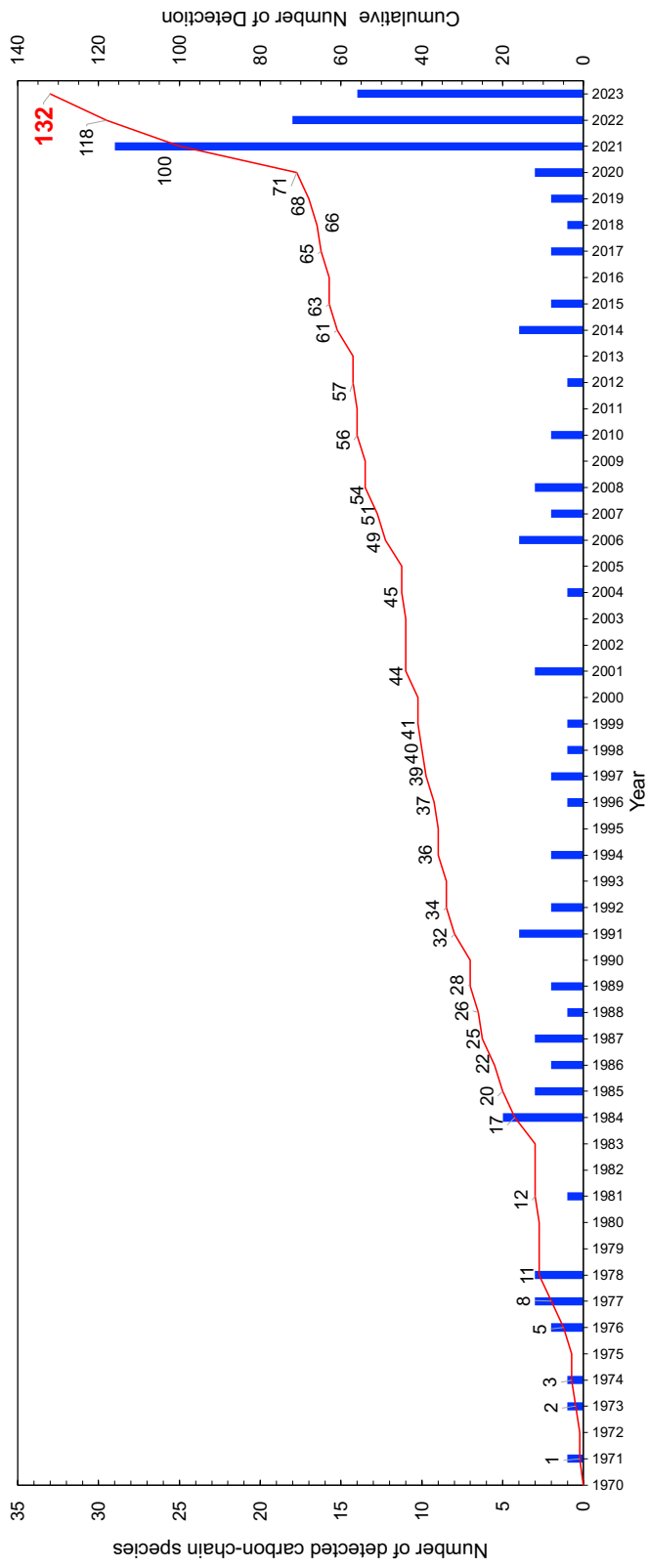


**Fig. 2** The number of detected carbon-chain species in each year (blue bars) and its cumulative plot (red curves and numbers).



et al. 2008). The  $\text{CH}_4$  molecules react with  $\text{C}^+$  in the gas phase to produce  $\text{C}_2\text{H}_3^+$  or  $\text{C}_2\text{H}_2^+$ . The  $\text{C}_2\text{H}_2^+$  ion reacts with  $\text{H}_2$  leading to  $\text{C}_2\text{H}_4^+$ . Then, electron recombination reactions of  $\text{C}_2\text{H}_3^+$  and  $\text{C}_2\text{H}_4^+$  produce  $\text{C}_2\text{H}_2$ . Regarding WCCC, the review article by Sakai & Yamamoto (2013) summarized related studies in detail. We thus avoid duplication here.

However, an important question has been raised since the review of Sakai & Yamamoto (2013), namely, the origin(s) of WCCC sources, which is still controversial. The focus is on how  $\text{CH}_4$ -rich ice is formed. This means that carbon atoms need to be adsorbed onto dust grains without being locked up in CO molecules. Sakai et al. (2008) proposed a possible solution involving short collapse times of prestellar cores in order to produce conditions needed for WCCC sources. However, there is limited evidence for such short collapse times, e.g., based on observed infall velocities (Keto & Caselli 2010), levels of deuteration (Kong et al. 2016) or demographics of prestellar versus protostellar cores (Könyves et al. 2015).

As an alternative scenario, Spezzano et al. (2016) suggested that variations in the far ultraviolet (FUV) interstellar radiation field (ISRF) could produce carbon-chain-rich or COM-rich conditions, based on their observational results toward the prestellar core L1544. They found a spatial distribution of *c*- $\text{C}_3\text{H}_2$  in a region relatively exposed to the ISRF, while  $\text{CH}_3\text{OH}$  was found in a relatively shielded region. In this scenario, the FUV ISRF destroys CO, a precursor of  $\text{CH}_3\text{OH}$ , leading to formation of C and/or  $\text{C}^+$ , precursors of carbon-chain species. Spezzano et al. (2020) also found similar trends with observations of *c*- $\text{C}_3\text{H}_2$  and  $\text{CH}_3\text{OH}$  toward six other starless cores. They concluded that the large-scale effects have a direct impact on the chemical segregation; *c*- $\text{C}_3\text{H}_2$  is enhanced in the region more illuminated by the ISRF, whereas  $\text{CH}_3\text{OH}$  tends to reside in the region shielded from the ISRF. Such chemical segregation observed in starless cores may be inherited to the protostellar stage and recognized as the different classes of WCCC protostars and COM-rich hot corinos. The feasibility of this scenario is boosted by its ability to explain the data of multiple independent cores.

In addition, several authors have since presented chemical simulations of the effects of these factors on the abundances of carbon-chain species and COMs (Aikawa et al. 2020; Kalvāns 2021). We discuss their modeling results in section 4.

## 2.4 Concept of Hot Carbon-Chain Chemistry

The discovery of the WCCC mechanism around low-mass protostars naturally raised a question: are carbon-chain molecules formed around high-mass ( $m_* > 8M_\odot$ ) protostars? With such a motivation, observations and chemical simulations focusing on carbon-chain species around massive young stellar objects (MYSOs) have proceeded since the late 2010s. Observational studies show that carbon-chain species are abundant around some MYSOs, but their abundances, especially cyanopolyynes, cannot be reproduced by WCCC. Then, a different carbon-chain chemistry has been proposed (Taniguchi et al. 2023). Here, we briefly explain the concept of “Hot Carbon-Chain Chemistry (HCCC)” proposed to reproduce the observational results around MYSOs. Details of these observational and simulation studies are summarized in sections 3.4 and 4, respectively.



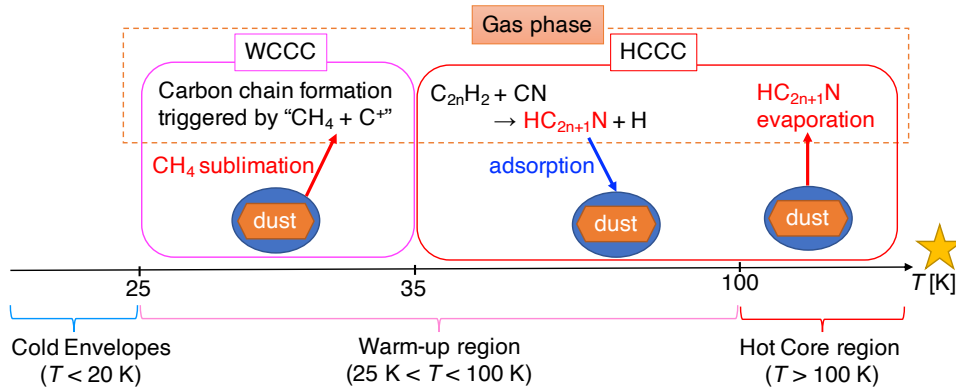


**Fig. 3** Temperature dependence of carbon-chain chemistry. WCCC occurs around 25–35 K, while HCCC occurs in higher-temperature regions.

Fig. 3 shows a schematic view of carbon-chain chemistry around MYSOs based on the result of the chemical simulation by Taniguchi et al. (2019a). We distinguish HCCC from WCCC depending on the temperature. The HCCC mechanism refers to carbon-chain formation in the gas phase, adsorption onto dust grains, and accumulation in ice mantles during the warm-up phase ( $25 \text{ K} < T < 100 \text{ K}$ ), followed by evaporation into the gas phase in the hot-core stage ( $T > 100 \text{ K}$ ).

This mechanism is particularly important for cyanopolyynes ( $\text{HC}_{2n+1}\text{N}$ ). Cyanopolyynes are relatively stable species because of no dangling bond, and they are not destroyed in the gas phase by reactions with O or  $\text{H}_2$ , which are major destroyers of other carbon-chain species with dangling bonds in the warm gas. Instead, cyanopolyynes are consumed by reactions with protonated ions such as  $\text{HCO}^+$  in the gas phase. Thus, the gas-phase destruction rates of cyanopolyynes are lower than those of the other carbon-chain species, which enables cyanopolyynes to be adsorbed onto dust grains. During the warm-up stage, cyanopolyynes are efficiently formed by the gas-phase reactions between  $\text{C}_{2n}\text{H}_2$  and CN. The formed cyanopolyynes are adsorbed onto dust grains and accumulated in ice mantles. When conditions reach their sublimation temperatures above 100 K, the species sublime into the gas phase and their gas-phase abundances show peaks.

Radical-type species, such as CCH and CCS, would not behave as cyanopolyynes do, because they are efficiently destroyed by the gas-phase reactions with O or  $\text{H}_2$  (Taniguchi et al. 2019a). Their gas-phase peak abundances are reached just after WCCC starts to form them around 25 K, and decrease as the temperature increases. Thus, we expect that radical-type carbon-chain species are abundant in the lukewarm regions and deficient in the hot-core regions, whereas the emission of cyanopolyynes is expected to show their peaks at the hot-core regions, similar to the emission of COMs.

Basically, HCCC can operate even around low-mass YSOs, because higher temperature is the only important factor to distinguish from WCCC and low-mass YSOs will have localized regions reaching the required temperatures of  $\sim 100 \text{ K}$ . However, these regions are much smaller than the equivalent ones around MYSOs, making it

more difficult to resolve the relevant temperature structures and detect the presence of HCCC around low-mass YSOs.

The main points of this section are summarized below:

1. Carbon-chain molecules account for around 44% of the interstellar molecules. These molecules have been detected in the ISM since the 1970s, and an increased number of reported detections made by recent Green Bank 100m telescope (GBT) and Yebes 40m telescope observations are astonishing.
2. WCCC refers to the carbon-chain formation mechanism in the lukewarm gas ( $T \approx 25\text{--}35$  K) starting from  $\text{CH}_4$  desorbing from dust grains around 25 K. The gas-phase reaction between  $\text{CH}_4$  and  $\text{C}^+$  is the trigger of the WCCC mechanism.
3. HCCC refers to the gas-phase carbon-chain formation and adsorption and accumulation in ice mantles during the warm-up phase ( $T < 100$  K), and their sublimation in the hot-core phase ( $T > 100$  K).

## 3 Observations

### 3.1 Carbon-Chain Species in TMC-1

Taurus Molecular Cloud-1 (TMC-1) is one of the best-studied filament (e.g., [Kaifu et al. 2004](#)). Its ‘‘Cyanopolyne Peak’’ (hereafter TMC-1 CP), which is located south-east of the filament, is the famous site where carbon-chain molecules are particularly abundant (Fig. 4). A number of deep-integration observations of carbon-chain species have been conducted toward this position.

[Dobashi et al. \(2018\)](#) identified four velocity components ( $v_{\text{LSR}} = 5.727, 5.901, 6.064,$  and  $6.160$  km s $^{-1}$ ) at TMC-1 CP with very high velocity resolution (0.0004 km s $^{-1}$ ) spectra of the CCS and  $\text{HC}_3\text{N}$  lines in the 45 GHz band obtained by the Z45 receiver ([Nakamura et al. 2015](#)) installed on the Nobeyama 45m radio telescope. They revealed the gas kinematics of the TMC-1 filament and found that these four velocity components indicate moving inward toward the center of the TMC-1 filament. [Dobashi et al. \(2019\)](#) identified 21 subfilaments in the TMC-1 filament using CCS ( $J_N = 4_3 - 3_2$ ; 45.379033 GHz) line data. They found that the subfilaments have line densities that are close to the critical line density for dynamical equilibrium ( $\sim 17M_{\odot} \text{pc}^{-1}$ ). These results indicate that self-gravity is important in the dynamics of the subfilaments.

The CCS ( $J_N = 4_3 - 3_2$ ) line was also used for measurement of the line-of-sight magnetic field strength by its Zeeman splitting ([Nakamura et al. 2019](#)). The derived magnetic field strength is  $\sim 117 \pm 21$   $\mu\text{G}$ , which implies that the TMC-1 filament is magnetically supercritical. As these studies show, rotational-transition lines of carbon-chain species are useful to investigate physical conditions of starless cores.

Two research groups have been carrying out line survey observations toward TMC-1 CP and have reported the detection of new interstellar molecules. Their research programs are still ongoing as of the writing of this review article. Here we highlight groundbreaking results done by each project. The sample of detected species from these projects is also summarized in section 2.1.

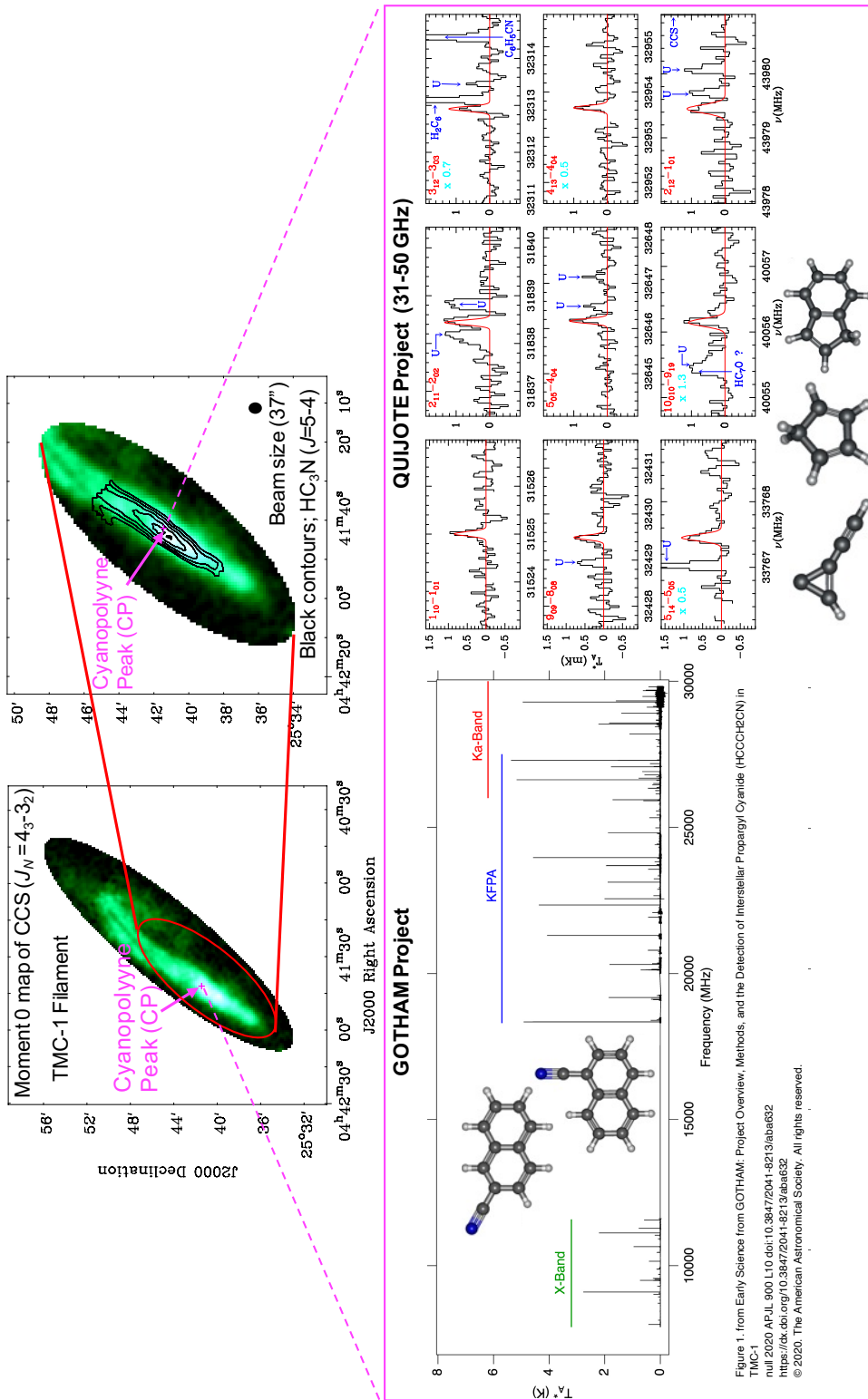


**Fig. 4** Top panels: Moment 0 map of the CCS ( $J_N = 4_3 - 3_2$ ) line overlaid by black contours indicating moment 0 map of the  $HC_3N$  ( $J = 5 - 4$ ) line. These data were obtained with the Nobeyama 45m radio telescope (beam size= $37''$  at 45 GHz). The original data were provided by Dr. Fumitaka Nakamura (NAOJ) and Dr. Kazuhito Dobashi (Tokyo Gakugei University). The magenta cross shows the position of the Cyanopolyyne Peak (TMC-1 CP) observed by the two line survey projects, GOTHAM and QUIJOTE projects. The spectral figures are from [McGuire et al. \(2020\)](#) and [Cernicharo et al. \(2021b\)](#).

One project is GOTHAM (GBT Observations of TMC-1: Hunting Aromatic Molecules<sup>5</sup>) using the Green Bank 100m telescope. This project is a high sensitivity (2 mK) and high velocity resolution ( $0.02 \text{ km s}^{-1}$ ) spectral line survey in the X, K, and Ka bands (see Fig. 4). The beam sizes (FWHM) are  $1.4'$ ,  $32''$ , and  $26.8''$  for the X-Band receiver, KFPA, and Ka-Band (MM-F1) receiver, respectively<sup>6</sup>. They have analyzed spectra using the spectral line stacking and matched filter methods (Loomis et al. 2018b, 2021) utilizing the velocity information derived by Dobashi et al. (2018), and achieved detection of new, rare interstellar molecules.

McGuire et al. (2021) detected two polycyclic aromatic hydrocarbons (PAHs), 1- and 2-cyanonaphthalene, containing two rings of benzene via spectral matched filtering. Some strong lines of 1-cyanonaphthalene can be identified in the smoothed spectra with a 14-kHz resolution. Their molecular structures are shown in Fig. 4. The nitrile bond (-CN) makes the dipole moment larger, thus aiding the detection of benzonitrile (*c*- $\text{C}_6\text{H}_5\text{CN}$ ), the first detected species with a benzene ring at TMC-1 CP (McGuire et al. 2018). Benzonitrile has also been detected in other sources: Serpens 1A, Serpens 1B, Serpens 2, and L1521F (Burkhardt et al. 2021b). Although the detection of pure hydrocarbon rings was considered to be difficult due to their small permanent dipole moments, Burkhardt et al. (2021a) achieved the detection of indene (*c*- $\text{C}_9\text{H}_8$ ). McCarthy et al. (2021) detected 1-cyano-1,3-cyclopentadiene (*c*- $\text{C}_5\text{H}_5\text{CN}$ ), a five-membered ring, and Lee et al. (2021a) detected 2-cyano-1,3-cyclopentadiene, which is an isomer with a little higher energy ( $5 \text{ kJ mol}^{-1}$  or 600 K). Thus, not only molecules with benzene structure but also molecules with five-membered rings with a nitrile bond have been detected. Loomis et al. (2021) reported the detection of  $\text{HC}_{11}\text{N}$ .  $\text{HC}_4\text{NC}$ , an isomer of  $\text{HC}_5\text{N}$ , has been detected by Xue et al. (2020), and soon after Cernicharo et al. (2020a) also reported its detection using the Yebes 40m telescope. Xue et al. (2020) ran chemical simulations with formation pathways of electron recombination reactions of  $\text{HC}_5\text{NH}^+$  and  $\text{HC}_4\text{NCH}^+$ , and reproduced the observed abundance of  $\text{HC}_4\text{NC}$ .

The other project is QUIJOTE (Q-band Ultrasensitive Inspection Journey to the Obscure TMC-1 Environment) line survey using the Yebes 40m telescope. This line survey project covers the frequency range 31.0–50.3 GHz, with beam sizes of  $56''$  and  $31''$  at 31 GHz and 50 GHz, respectively (Fuentetaja et al. 2022a). The frequency resolution is 38.15 kHz, corresponding to  $\sim 0.29 \text{ km s}^{-1}$  at 40 GHz. We note that this velocity resolution is not ideal to observe lines in TMC-1 CP, which have a typical line width of  $\sim 0.5 \text{ km s}^{-1}$ . However, this survey has achieved very high sensitivities of 0.1 – 0.3 mK and various molecules have been successfully detected without resort to stacking analysis.

The QUIJOTE project has reported the detection of many pure hydrocarbons consisting of only carbon and hydrogen: e.g., 1- and 2-ethynyl-1,3-cyclopentadiene (*c*- $\text{C}_5\text{H}_5\text{CCH}$ , Cernicharo et al. 2021d); benzyne (*ortho*- $\text{C}_6\text{H}_4$ , Cernicharo et al. 2021c); *c*- $\text{C}_3\text{HCCH}$ , *c*- $\text{C}_5\text{H}_6$ , *c*- $\text{C}_9\text{H}_8$  (Cernicharo et al. 2021b); fulvenallene (*c*- $\text{C}_5\text{H}_4\text{CCH}_2$ , Cernicharo et al. 2022b); and  $\text{CH}_2\text{CCHC}_4\text{H}$  (Fuentetaja et al. 2022b). The detection of such pure hydrocarbons is astonishing because their dipole moments are very

<sup>5</sup><https://greenbankobservatory.org/science/gbt-surveys/gotham-survey/>

<sup>6</sup><https://www.gb.nrao.edu/scienceDocs/GBTpg.pdf>

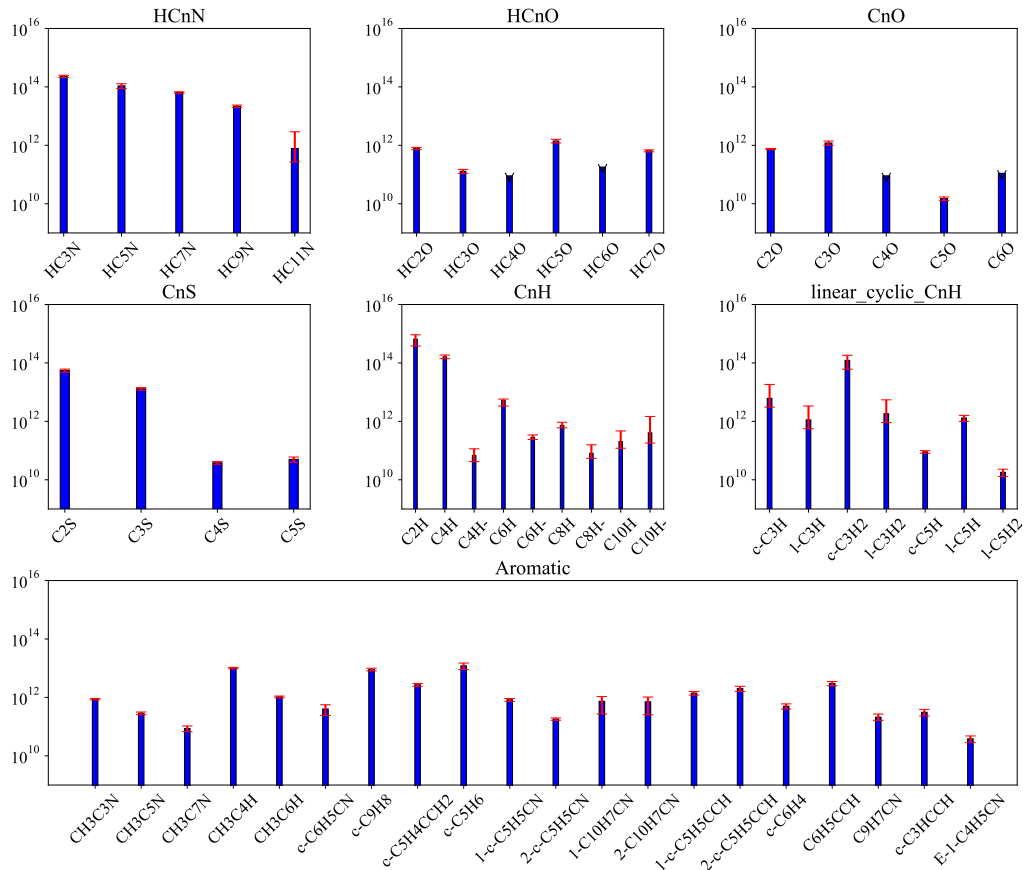


**Fig. 5** Column density variation of carbon chains toward TMC-1 CP.

small. In addition to pure hydrocarbons, the QUIJOTE project has also detected carbon-chain ions: e.g.,  $\text{HC}_3\text{O}^+$  (Cernicharo et al. 2020b);  $\text{HC}_7\text{NH}^+$  (Cabezas et al. 2022c);  $\text{HC}_3\text{S}^+$  (Cernicharo et al. 2021f);  $\text{HCCS}^+$  (Cabezas et al. 2022b);  $\text{C}_5\text{H}^+$  (Cernicharo et al. 2022a). It has also detected five cyano derivatives (*trans*- $\text{CH}_3\text{CHCHCN}$ , *cis*- $\text{CH}_3\text{CHCHCN}$ ,  $\text{CH}_2\text{C}(\text{CH}_3)\text{CN}$ , *gauche*- $\text{CH}_2\text{CHCH}_2\text{CN}$ , *cis*- $\text{CH}_2\text{CHCH}_2\text{CN}$ ; Cernicharo et al. 2022c). The very high sensitivity line survey observations achieved by the QUIJOTE project reveal a wide variety of carbon-chain species. At the same time, these results raise new questions because the abundances of some of the newly detected molecules cannot be explained by chemical models.

Fig. 5 shows column densities of several carbon-chain series at TMC-1 CP (see also Table B2 in Appendix B). We note that several factors could produce artificial (systematic) differences in derived column densities;

1. variation in telescope beam sizes and pointing relative to the source (i.e., leading to different levels of beam dilution)
2. variation of excitation conditions probed by the different transitions
3. variation of analytical methods (e.g., rotational diagram vs. Markov Chain Monte Carlo (MCMC); single-velocity components vs. multi-velocity components)
4. variation of data selection criteria and data quality (e.g., system noise temperatures)

For example, regarding the column densities of cyanopolyynes ( $\text{HC}_{2n+1}\text{N}$ ) obtained by GBT, the column density of  $\text{HC}_9\text{N}$  ( $2.15_{-0.20}^{+0.23} \times 10^{13} \text{ cm}^{-2}$ ; Loomis et al. 2021) is higher than that of  $\text{HC}_7\text{N}$  ( $(1.39 \pm 0.36) \times 10^{13} \text{ cm}^{-2}$ ; Burkhardt et al. 2018), which is an unexpected result. However, we consider that this may be affected by the use of different analytical methods. Column densities smaller than  $\text{HC}_7\text{N}$  have been derived assuming a single velocity component, whereas  $\text{HC}_9\text{N}$  and  $\text{HC}_{11}\text{N}$  have been analyzed with the application of four-velocity components (Loomis et al. 2021). The plotted column densities of  $\text{HC}_9\text{N}$  and  $\text{HC}_{11}\text{N}$  are summations of these four velocity components. This illustrates the need to compare results among different methods carefully. In the following discussion, we will mainly compare carbon-chain species whose column densities have been obtained from the same papers using the same methods in order to avoid such potential systematic uncertainties.

The  $\text{C}_n\text{H}$  series shows an odd-even fluctuation, with the even-numbered species having higher abundances compared to the odd-numbered. The anions have been detected only for the even-numbered members. The neutral/anion abundance ratios are derived to be  $\sim 2386$ , 18, 9, and 0.5 for  $\text{C}_4\text{H}$ ,  $\text{C}_6\text{H}$ ,  $\text{C}_8\text{H}$ , and  $\text{C}_{10}\text{H}$ , respectively. Note that the identification of  $\text{C}_{10}\text{H}$  is tentative (Remijan et al. 2023), and the ratio is just a reference value level. Thus, the longer members have higher relative abundances of anion forms to their neutrals (Table B2 in Appendix B).

The cyclic-to-linear ratios of  $\text{C}_3\text{H}_2$  and  $\text{C}_3\text{H}$  have been discussed (e.g., Loison et al. 2017; Sipilä et al. 2016). Such ratios were derived to be 67 and 5.5 for  $\text{C}_3\text{H}_2$  and  $\text{C}_3\text{H}$  at TMC-1 CP (Loison et al. 2017), and these ratios likely depend on the density. As seen in Fig. 1, these four species are chemically close to each other; electron recombination reactions of  $c/l\text{-C}_3\text{H}_3^+$  could produce these molecules. It is important to fully understand these ratios in various astronomical environments to measure branching ratios of dissociative recombination reactions of their parent hydrocarbon ions (*c.f.*, Fig. 1). The cyclic forms may not be necessarily more abundant than the linear form. In the case of  $\text{C}_5\text{H}$ ,  $l\text{-C}_5\text{H}$  is the most stable isomer, and observations show that  $c\text{-C}_5\text{H}$  is less abundant than  $l\text{-C}_5\text{H}$  by around one order of magnitude (Cabezas et al. 2022a). Thus, the stability of the molecules is likely one of the key factors in determining which isomer(s) is the most abundant. Quantum calculation is essential to investigate the stability. The number of isomers increases as the molecule becomes larger, and sophisticated calculations are necessary (section 5.1.1).

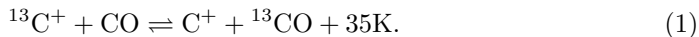
The question of why TMC-1 CP is rich in carbon-chain species may be related to the formation and evolution of the TMC-1 filament. If gravitational collapse is impeded leading to a longer duration starless core phase, then this may allow more time for the growth of longer carbon chains. Magnetic field support is the most likely cause of delayed gravitational collapse. However, precise measurements of magnetic field strengths, e.g., by Zeeman measurements, are difficult to obtain and such information is generally lacking for most starless cores. We note that the extended Q-band (eQ) receiver, recently installed on the Nobeyama 45m radio telescope, will enable improved Zeeman measurements of line of sight magnetic field strengths in starless and star-forming cores with a much shorter observing time (Chiong et al. 2022). Such measurements are needed to study the potential relationships between core dynamics and carbon-chain chemistry.

Another possibility to explain elevated abundances of long carbon chains in TMC-1 is enhanced efficiency of the top-down mechanism, in which large carbon-bearing species such as PAHs are destroyed to form small hydrocarbons. This scenario may be consistent with the detection of molecules including benzene, such as benzonitrile and 1- and 2-cyanonaphthalene. If the enhancement of PAH destruction is due to the global environment, e.g., of Taurus, then one would expect generally elevated abundances of larger carbon-chain species in this region. Revealing the origin of the chemical characteristics of TMC-1 CP, likely requires a better understanding of the chemical heritage from the diffuse ISM to molecular gas conditions across the wider region.

### 3.2 Dilution of $^{13}\text{C}$ species in Starless Cores

It has been found that the  $^{12}\text{C}/^{13}\text{C}$  ratios of carbon-chain species show higher values compared to the local isotopic abundance ratio of about 60 to 70 (Milam et al. 2005). This so called dilution of  $^{13}\text{C}$  species was first discovered in TMC-1 CP, but has since been found in other starless cores.

Variation of the  $^{12}\text{C}/^{13}\text{C}$  ratio of carbon-chain species give further constraints on the processes regulating carbon-chain chemistry in dark clouds. One important cause of  $^{12}\text{C}/^{13}\text{C}$  isotopologue abundance variation is the reaction (e.g., Langer et al. 1984):



The backward reaction is ineffective in cold-temperature conditions ( $\sim 10$  K), so that the abundance of  $^{13}\text{C}^+$  should decrease. Ionic and atomic carbons ( $\text{C}^+$  and  $\text{C}$ ) are the main parent species of carbon-chain molecules and a low abundance of  $^{13}\text{C}^+$  is then expected to result in a deficit of  $^{13}\text{C}$  isotopologues of carbon-chain molecules. Table 2 summarizes the  $^{12}\text{C}/^{13}\text{C}$  ratios of carbon-chain molecules derived in three starless cores: TMC-1 CP; L1521B; and L134N. From Table 2, the following trends can be inferred:

1. Cyanopolyynes ( $\text{HC}_{2n+1}\text{N}$ ) have relatively lower  $^{12}\text{C}/^{13}\text{C}$  ratios compared to the other hydrocarbons. Especially, the  $^{13}\text{C}$  isotopomers of CCH have high values.
2. The  $^{12}\text{C}/^{13}\text{C}$  ratios are different among the dark clouds. The ratios in L134N are relatively low compared to the others.

An explanation for the first point was proposed by Taniguchi et al. (2019b); the high  $^{12}\text{C}/^{13}\text{C}$  ratios of CCH seem to be caused by reactions between hydrocarbons (CCH,  $\text{C}_2\text{H}_2$ , *l,c*- $\text{C}_3\text{H}$ ) and  $\text{C}^+$ . The formed ions will go back to CCH through reactions including electrons and  $\text{H}_2$ . If  $^{13}\text{C}^+$  is diluted by reaction (1), these reactions will produce hydrocarbons with high  $^{12}\text{C}/^{13}\text{C}$  ratios. On the other hand, the  $^{12}\text{C}/^{13}\text{C}$  ratios of cyanopolyynes do not likely change after their formation. The second point may be related to the evolution of the starless cores; TMC-1 CP and L1521B are considered to be chemically younger than L134N (e.g., Dickens et al. 2000).

Currently, the available data are limited, and such studies have been conducted mainly at TMC-1 CP. Thus, it is difficult to reach firm conclusions. Future high-sensitivity survey observations are needed to reveal the detailed mechanisms causing



**Table 2** The  $^{12}\text{C}/^{13}\text{C}$  ratios of carbon-chain molecules in dark clouds

Species	TMC-1 CP	L1521B	L134N
$\text{H}^{13}\text{CCCN}$	$79 \pm 11^{(a)}$	$117 \pm 16^{(b)}$	$61 \pm 9^{(b)}$
$\text{HC}^{13}\text{CCN}$	$75 \pm 10^{(a)}$	$115 \pm 16^{(b)}$	$94 \pm 26^{(b)}$
$\text{HCC}^{13}\text{CN}$	$55 \pm 7^{(a)}$	$76 \pm 6^{(b)}$	$46 \pm 9^{(b)}$
$\text{H}^{13}\text{CCCCCN}$	$98 \pm 14^{(c)}$		
$\text{HC}^{13}\text{CCCCN}$	$101 \pm 14^{(c)}$		
$\text{HCC}^{13}\text{CCCN}$	$95 \pm 12^{(c)}$		
$\text{HCCC}^{13}\text{CCN}$	$93 \pm 13^{(c)}$		
$\text{HCCCC}^{13}\text{CN}$	$85 \pm 11^{(c)}$		
$\text{HC}_7\text{N}$	$73 \pm 21^{(d)}$		
$^{13}\text{CCH}$	$> 250^{(e)}$	$> 271^{(f)}$	$> 142^{(f)}$
$\text{C}^{13}\text{CH}$	$> 170^{(e)}$	$252_{-48}^{+77(f)}$	$101_{-16}^{+24(f)}$
$^{13}\text{CCCCH}$	$141 \pm 15^{(g)}$		
$\text{C}^{13}\text{CCCH}$	$97 \pm 9^{(g)}$		
$\text{CC}^{13}\text{CCH}$	$82 \pm 5^{(g)}$		
$\text{CCC}^{13}\text{CH}$	$118 \pm 8^{(g)}$		
$^{13}\text{CCS}$	$230 \pm 43^{(h)}$		
$\text{C}^{13}\text{CS}$	$54 \pm 2^{(h)}$		
$^{13}\text{CCCS}$	$> 206^{(g)}$		
$\text{C}^{13}\text{CCS}$	$48 \pm 5^{(g)}$		
$\text{CC}^{13}\text{CS}$	$30 - 206^{(g)}$		

Errors indicate the standard deviation. References: (a) [Takano et al. \(1998\)](#), (b) [Taniguchi et al. \(2017a\)](#), (c) [Taniguchi et al. \(2016a\)](#), (d) [Burkhardt et al. \(2018\)](#) (average value), (e) [Sakai et al. \(2010\)](#), (f) [Taniguchi et al. \(2019b\)](#), (g) [Sakai et al. \(2013\)](#), (h) [Sakai et al. \(2007\)](#).

the dilution of  $^{13}\text{C}$  species, which would give information about the chemical relationships among carbon-chain molecules in cold dark clouds. In addition, chemical simulations including the  $^{13}\text{C}$  isotopomers are necessary for an improved quantitative understanding of  $^{13}\text{C}$  species dilution, including its evolution.

### 3.3 Carbon-Chain Species around Low-Mass YSOs

Carbon-chain chemistry around low-mass young stellar objects (YSOs), namely WCCC, has been reviewed in [Sakai & Yamamoto \(2013\)](#), and we do not discuss WCCC in detail. Instead, we summarize observational results published after the review article.

Several survey observations with single-dish telescopes targeting carbon-chain molecules and COMs have been conducted. [Graninger et al. \(2016\)](#) carried out survey observations of  $\text{CH}_3\text{OH}$  and  $\text{C}_4\text{H}$  toward 16 embedded low-mass protostars using the IRAM 30m telescope. A tentative correlation between the gas-phase  $\text{C}_4\text{H}/\text{CH}_3\text{OH}$  abundance ratio and the  $\text{CH}_4/\text{CH}_3\text{OH}$  abundance ratio in ice was found. At the protostellar stage, the gas-phase  $\text{C}_4\text{H}$  is considered to form from  $\text{CH}_4$  sublimated from dust grains (WCCC), whereas the gas-phase  $\text{CH}_3\text{OH}$  is mainly originated from ice mantle (hot corino chemistry). Thus, the suggested tentative correlation between the



gas phase and ice mantle supports the scenario of WCCC; sublimation of  $\text{CH}_4$  is a trigger of carbon-chain formation in lukewarm gas (e.g., [Hassel et al. 2008](#)).

[Higuchi et al. \(2018\)](#) conducted survey observations of two carbon-chain species (CCH and *c*- $\text{C}_3\text{H}_2$ ) and  $\text{CH}_3\text{OH}$  toward 36 Class 0/I protostars in the Perseus molecular cloud using the IRAM 30m and Nobeyama 45m radio telescopes. They found that the column density ratio of CCH/ $\text{CH}_3\text{OH}$  varies by two orders of magnitudes among the target sources, and the majority of the sources show intermediate characters between hot corino and WCCC. In other words, hot corino and WCCC are at opposite ends of a spectrum and both carbon-chain species and COMs are present around most low-mass protostars. In addition, they found a possible trend that sources with higher CCH/ $\text{CH}_3\text{OH}$  ratios are located near cloud edges or in isolated clouds.

However, we need to treat their results carefully because CCH and *c*- $\text{C}_3\text{H}_2$  can be enhanced in photodissociation regions (PDRs) as described in section 3.7. Hence, the observed trend in the CCH/ $\text{CH}_3\text{OH}$  ratio could be a result of PDR chemistry; the ISRF promotes the PDR chemistry at the edge of the molecular cloud rather than WCCC. In addition, CCH is enhanced in outflow cavity walls, as discussed below. Single-dish observations cannot spatially resolve warm envelopes and outflow cavity walls, and thus we cannot distinguish between these components. To investigate the characteristics of WCCC, we should observe large carbon-chain species (e.g.,  $\text{HC}_5\text{N}$ ) that are not predicted to be enhanced in PDRs.

The IRAM Large Program “Astrochemical Surveys At IRAM (ASAI)” is an unbiased line survey from 80 to 272 GHz toward 10 sources with various evolutionary stages. Using the ASAI data, [Lefloch et al. \(2018\)](#) found a difference in environmental conditions between hot corino and WCCC sources: i.e., inside and outside dense filamentary cloud regions, respectively. Their results are likely to be more secure than those of [Higuchi et al. \(2018\)](#) because [Lefloch et al. \(2018\)](#) included long carbon-chain species that cannot be abundant in PDRs due to destruction by the UV radiation.

High-angular-resolution observations with interferometers, such as ALMA and NOEMA, have revealed spatial distributions of carbon-chain molecules around low-mass YSOs. Such observations are essential to distinguish the emission regions of each species (e.g., warm envelopes, outer cold envelopes, cavity walls). [Oya et al. \(2017\)](#) detected both a carbon-chain molecule (CCH) and several COMs toward the low-mass Class 0 protostar L483. They found that the spatial distribution of CCH is different from those of COMs; the CCH emission shows a hole at the protostar position, whereas emission from COMs is concentrated near the protostar. Such emission features are attributed to WCCC and hot corino chemistry, respectively. Their results present an example of the hybrid-type source (c.f., Fig. 9).

[Zhang et al. \(2018\)](#) found that CCH emission traces the outflow cavity with signatures of rotation with respect to the outflow axis toward the NGC 1333 IRAS 4C outflow in the Perseus molecular cloud using ALMA. [Tychoniec et al. \(2021\)](#) analyzed ALMA data set toward 16 protostars and investigated spatial distributions of each molecule. They also found that CCH and *c*- $\text{C}_3\text{H}_2$  trace the cavity wall. This could be explained by the fact that the chemistry of the cavity wall is similar to PDR chemistry. The cavity walls are created by the illuminated by the stellar FUV and X-ray

radiation field, and the PDR-like chemistry dominates cavity walls. The photodissociation of molecules by UV radiation keeps high gas-phase abundances of atomic carbon (C), which is a preferable condition for the formation of hydrocarbons.

Pineda et al. (2020) found a streamer toward the Class 0 YSO IRAS 03292+3039 (or Per-emb-2) in the Perseus star-forming region with NOEMA. Such a streamer may be well traced by carbon-chain molecules such as CCS and HC<sub>3</sub>N, if it is considered to be chemically young. The streamer in this source seems to bring fresh gas from outside of the dense core ( $> 10,500$  au) down to the central protostar where the disk forms. Thus the properties of such streamers are potentially important for the formation and evolution of protoplanetary disks. However, these NOEMA observations did not cover the origin of the streamer. Follow-up single-dish mapping observations of carbon-chain species (HC<sub>3</sub>N, HC<sub>5</sub>N, CCS, and CCH) have revealed the reservoir of the streamer (Taniguchi et al. 2024). The reservoir and streamer are found to be chemically young, and their chemical ages are similar to those of early starless cores. Overall, it can be concluded that a chemically young streamer has the potential to change the chemical composition close to the YSO.

Taking advantage of the characteristics of carbon-chain molecules, we can trace unique features around low-mass YSOs. Rotational-transition lines of carbon-chain molecules are now found to be useful tracers not only in early starless clouds but also around star-forming cores. ALMA Band 1 and the next generation Very Large Array (ngVLA) will cover the 7 mm band or lower frequency bands, which are suitable for observations of carbon-chain molecules, especially longer ones (see Fig. 6). Future observations using such facilities will offer new insights into the carbon-chain chemistry around protostars, including low-, intermediate-, and high-mass systems.

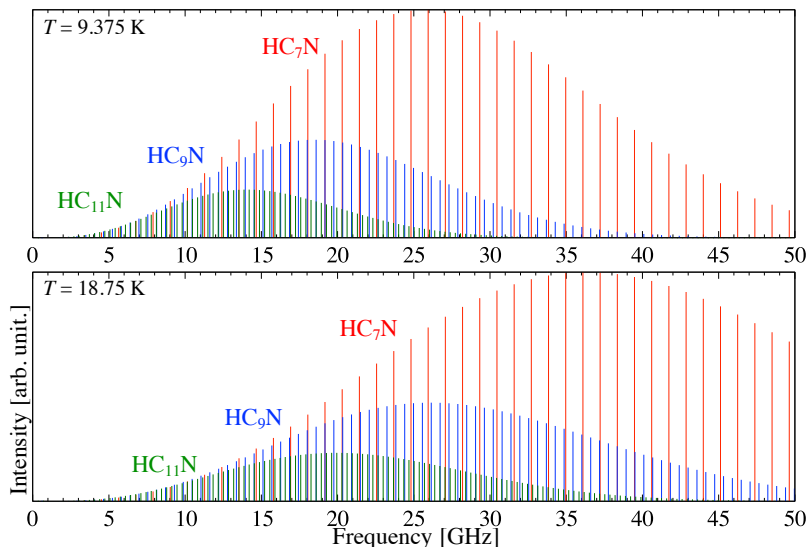


**Fig. 6** Predicted line intensities of long cyanopolynes (red; HC<sub>7</sub>N, blue; HC<sub>9</sub>N, and green; HC<sub>11</sub>N) in the frequency range of 0 – 50 GHz. The upper and lower panels show predictions at temperatures of 9.375 K and 18.75 K, respectively. The data on rest frequency and line intensity are taken from the CDMS database. Longer carbon-chain species show intensity peaks at lower frequencies.

## 3.4 Carbon-Chain Species in High-Mass Star-Forming Regions

### 3.4.1 Chemical Evolutionary Indicators

Carbon-chain molecules classically have been known to be abundant in young starless cores and good chemical evolutionary indicators in low-mass star-forming regions (section 1.2). However, it was unclear whether carbon-chain species can be used as chemical evolutionary indicators in high-mass star-forming regions and behave similarly as in the case of low-mass regions.

Survey observations of several carbon-chain species ( $\text{HC}_3\text{N}$ ,  $\text{HC}_5\text{N}$ ,  $\text{CCS}$ , and  $c\text{-C}_3\text{H}_2$ ) and  $\text{N}_2\text{H}^+$  were carried out using the Nobeyama 45m radio telescope (Taniguchi et al. 2018b, 2019c). Taniguchi et al. (2018b) observed the  $\text{HC}_3\text{N}$  and  $\text{HC}_5\text{N}$  lines in the 42–45 GHz band toward 17 high-mass starless cores (HMSCs) and 35 high-mass protostellar objects (HMPOs), and Taniguchi et al. (2019c) observed  $\text{HC}_3\text{N}$ ,  $\text{N}_2\text{H}^+$ ,  $\text{CCS}$ , and  $c\text{-C}_3\text{H}_2$  in the 81–94 GHz band toward 17 HMSCs and 28 HMPOs. They proposed the column density ratio of  $N(\text{N}_2\text{H}^+)/N(\text{HC}_3\text{N})$  as a chemical evolutionary indicator in high-mass star-forming regions (Fig. 7). This column density ratio decreases as cores evolve from the starless (HMSC) to the protostellar (HMPOs) stage. Sources that were categorized as HMSCs based on the infrared (IR) observations but that are associated with molecular lines of COMs ( $\text{CH}_3\text{OH}$  or  $\text{CH}_3\text{CN}$ ) and/or SiO (plotted as the blue diamond in Fig. 7) tend to fall between HMSCs and HMPOs. These sources are considered to contain early-stage protostars in the dense, dusty cores, which are not easily detected with IR observations. Thus, these sources appear to be at an intermediate evolutionary stage between HMSCs and HMPOs. It is essential to study the physical and chemical features of these sources in detail because they possess information on the initial conditions of high-mass protostars.

The decrease of the  $N(\text{N}_2\text{H}^+)/N(\text{HC}_3\text{N})$  ratio means that  $\text{HC}_3\text{N}$  is efficiently formed and  $\text{N}_2\text{H}^+$  is destroyed, as cores evolve. It is a notable point that the tendency of this column density ratio is opposite to that in low-mass star-forming regions (Suzuki et al. 1992; Benson et al. 1998). This tendency could be explained by higher temperatures and extended warm regions around HMPOs compared to low-mass protostars.  $\text{N}_2\text{H}^+$  is destroyed by a reaction with  $\text{CO}$ , i.e., abundant in the gas phase after being desorbed from dust grains, and  $\text{HC}_3\text{N}$  can be formed by  $\text{CH}_4$  via the WCCC mechanism or via  $\text{C}_2\text{H}_2$  desorbed from dust grains. The desorption of  $\text{CO}$ ,  $\text{CH}_4$ , and  $\text{C}_2\text{H}_2$  from dust grains occurs when temperatures reach around 20 K, 25 K, and 50 K, respectively. In summary, the gas-phase chemical composition is affected by the local heating from young massive protostars, and a chemical evolutionary indicator apparently shows an opposite trend compared to that of the low-mass case. Thus, carbon-chain species likely have the potential to be utilized as chemical evolutionary indicators even for high-mass protostars.

Note that the above observations were conducted using a single-dish telescope and the beam sizes are large ( $\sim 0.5 - 0.9$  pc at 5 kpc, which is a typical distance of high-mass star-forming regions). Hence, higher angular-resolution observations with interferometers will be important to confirm such a chemical evolutionary trend.

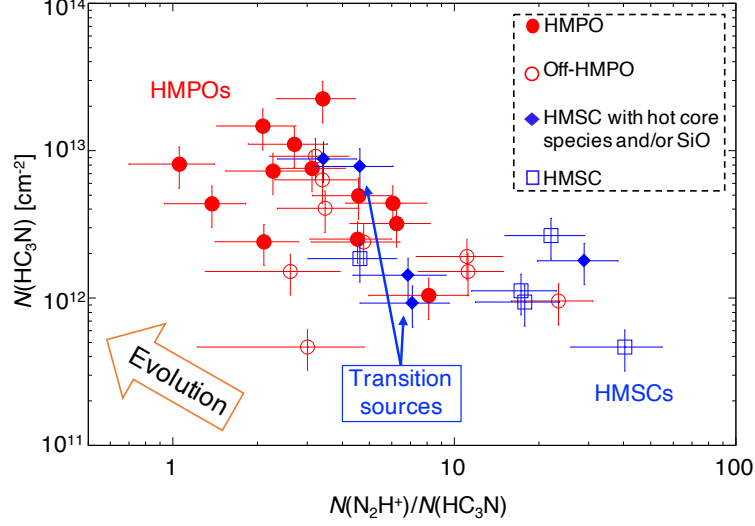


**Fig. 7** A chemical evolutionary indicator in high-mass star-forming regions (Taniguchi et al. 2019c). Off-HMPO means that IRAS-observed positions were not at exact continuum peak positions, but the beam covered the continuum core in the beam edge. Blue diamond plots are sources that were identified as HMSCs based on the IR observations, but which are associated with molecular emission lines of COMs ( $\text{CH}_3\text{OH}$  and/or  $\text{CH}_3\text{CN}$ ) or SiO.

### 3.4.2 Cyanopolyynes around High-Mass Protostars

From the survey observations mentioned in section 3.4.1, the detection rates of  $\text{HC}_3\text{N}$ ,  $\text{HC}_5\text{N}$ ,  $c\text{-C}_3\text{H}_2$ , CCS are derived to be 93%, 50%, 68%, and 46%, respectively, in high-mass star-forming regions (Taniguchi et al. 2018b, 2019c). Law et al. (2018) conducted survey observations toward 16 Class 0/I low-mass protostars with the IRAM 30m telescope and reported that the detection rates of  $\text{HC}_3\text{N}$ ,  $\text{HC}_5\text{N}$ ,  $l\text{-C}_3\text{H}$ ,  $\text{C}_4\text{H}$ , CCS, and  $\text{C}_3\text{S}$  are 75%, 31%, 81%, 88%, 88%, and 38%, respectively. Thus, cyanopolyynes ( $\text{HC}_3\text{N}$  and  $\text{HC}_5\text{N}$ ) show higher detection rates, while CCS is relatively deficient in high-mass star-forming regions compared to low-mass regions. These results imply that carbon-chain chemistry around MYSOs is different from WCCC found around low-mass YSOs.

Taniguchi et al. (2017b) conducted observations of the multi-transition lines of  $\text{HC}_5\text{N}$  using the Green Bank 100m and Nobeyama 45m radio telescopes toward four MYSOs. The derived rotational temperatures are  $\sim 20 - 25$  K, which are similar to the temperature regimes of the WCCC mechanism. However, the derived rotational temperatures are lower limits due to contamination from extended cold components covered by the single-dish telescopes. The MYSO G28.28-0.36 shows a particularly unique chemical character: carbon-chain species are rich, but COMs are deficient (Taniguchi et al. 2018a). This source may be analogous to the WCCC source L1527. These results are suggestive of the chemical diversity around MYSOs, as similar to low-mass cases (hot corino and WCCC).

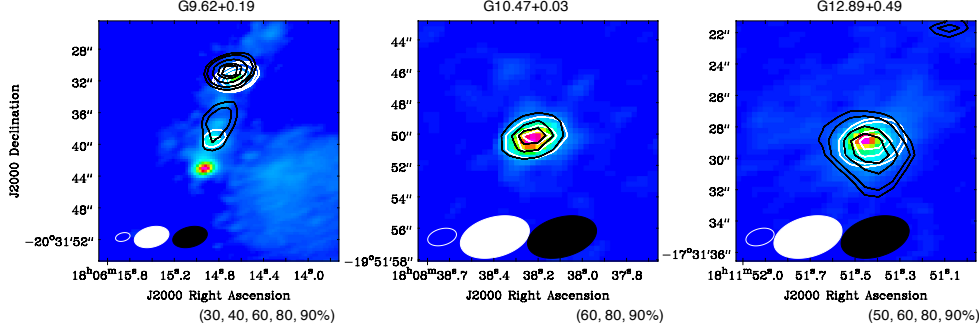


**Fig. 8** Comparison of spatial distributions around MYSOs obtained by ALMA (color scale; continuum image, white contours; the  $\text{CH}_3\text{OH}$  line ( $1_{0,1} - 2_{1,2}$ ,  $v_t = 1$ ;  $E_{\text{up}} = 302.9$  K), black lines; the  $\text{HC}_5\text{N}$  line ( $J = 35 - 34$ ;  $E_{\text{up}} = 80.5$  K). This figure is a modified version of [Taniguchi et al. \(2023\)](#). The contour levels are relative values of the peak intensities, and the contour levels are indicated below each panel. The ellipses at the bottom of each panel indicate the angular resolutions; open one corresponds to the continuum images, and white and black ones correspond to the moment 0 maps of  $\text{CH}_3\text{OH}$  and  $\text{HC}_5\text{N}$ , respectively.

Since the above  $\text{HC}_5\text{N}$  excitation temperatures derived with single-dish data are lower limits due to contamination of cold outer envelopes, it could not be concluded that carbon-chain molecules exist in higher temperature regions around MYSOs compared to the WCCC sources. [Taniguchi et al. \(2021\)](#) derived the  $\text{CCH}/\text{HC}_5\text{N}$  abundance ratios toward three MYSOs and compared the observed ratio with the results of their chemical simulations to constrain temperature regimes where carbon-chain species exist. The  $\text{CCH}/\text{HC}_5\text{N}$  abundance ratio is predicted to decrease as the temperature increases, because  $\text{CCH}$  shows a peak abundance in the gas phase around 30 K, while the gas-phase  $\text{HC}_5\text{N}$  abundance increases as the temperature rises up to  $\sim 100$  K ([Taniguchi et al. 2019a](#)). Details about the chemical simulations are presented in section 4. The observed  $\text{CCH}/\text{HC}_5\text{N}$  abundance ratios toward all of the three MYSOs are  $\sim 15$ , which is much lower than that toward the low-mass WCCC source L1527 ( $625^{+3041}_{-339}$ ). The observed abundance ratios around MYSOs agree with the simulations around 85 K, while the ratio in L1527 matches with the simulations around 35 K. Therefore, carbon-chain species, at least  $\text{HC}_5\text{N}$ , around MYSOs appear to exist in higher temperature regions than the locations where the WCCC mechanism occurs. Such results indicate that carbon-chain chemistry around MYSOs is different from the WCCC mechanism. It is necessary to reveal spatial distributions of carbon-chain molecules around MYSOs to confirm that the carbon-chain chemistry around MYSOs is different from WCCC.

More recently, spatial distributions of the  $\text{HC}_5\text{N}$  line ( $J = 35 - 34$ ;  $E_{\text{up}} = 80.5$  K) around MYSOs have been revealed by ALMA Band 3 data ([Taniguchi et al. 2023](#)). This line has been detected from three sources among five target sources. Fig. 8 shows the comparison of spatial distributions among  $\text{HC}_5\text{N}$ ,  $\text{CH}_3\text{OH}$ , and continuum emission in Band 3 toward the three MYSOs. The  $\text{HC}_5\text{N}$  emission shows single peaks associated with the continuum peaks and is consistent with the emission of the  $\text{CH}_3\text{OH}$  line ( $1_{0,1} - 2_{1,2}$ ,  $v_t = 1$ ;  $E_{\text{up}} = 302.9$  K) which should trace hot core regions with temperatures above 100 K. These results also support the “Hot Carbon-Chain Chemistry (HCCC)”

scenario;  $\text{HC}_5\text{N}$  desorbs from dust grains with temperatures above 100 K and shows gas-phase peak abundances similar to those of COMs.

In summary, carbon-chain molecules are formed even around MYSOs by the HCCC mechanism. Fig. 9 shows a summary of chemical properties found around low-mass and high-mass YSOs, respectively. Currently, a candidate of pure HCCC sources is the MYSO G28.28-0.36, in which COMs are deficient but  $\text{HC}_5\text{N}$  is abundant (Taniguchi et al. 2018a). We note that high angular-resolution observations of COMs toward this MYSO, e.g., with ALMA, are still needed because COMs may be diluted in the large single-dish beams. Only if COMs were found to be deficient in such high resolution data, it could be concluded that MYSO G28.28-0.36 is a pure HCCC source. In addition, to statistically study the chemical diversity around MYSOs, larger source samples observed at high-angular-resolution to trace carbon-chain and COM species are needed.

As seen in Fig. 9, chemical differentiation emerges around both low-mass YSOs and high-mass YSOs. However, at present it is still uncertain (1) what physical factor(s) is important for the chemical differentiation, and (2) whether a common factor(s) dominates the chemical differentiation around low-mass and high-mass YSOs. For instance, temperature, radiation field of energetic photons (e.g., UV photons), and cosmic rays, are likely to be important for causing chemical differentiation (e.g., Fontani et al. 2017; Lefloch et al. 2018; Taniguchi et al. 2019a). It is currently difficult to evaluate quantitatively the relative importance of such physical parameters between low-mass and high-mass YSOs. A study of the carbon-chain chemistry around intermediate-mass YSOs (i.e.,  $2M_\odot < m_* < 8M_\odot$ ), which bridge the gap between the low- and high-mass regimes, may help to solve these open questions.

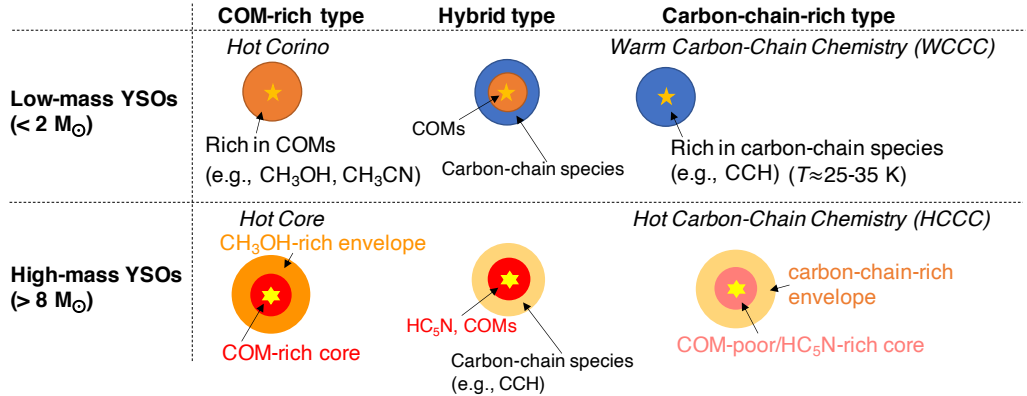


Fig. 9 Chemical properties found around low-mass and high-mass YSO.

### 3.5 Revealing Main Formation Pathways of Carbon-Chain Molecules by <sup>13</sup>C Isotopic Fractionation

Since carbon-chain molecules are unstable even in vacuum chambers on the Earth, it is difficult to conduct laboratory experiments about their reactivity. Consequently, their formation and destruction reactions remain unclear. Instead, the observed <sup>13</sup>C

**Table 3** Main formation mechanisms of HC<sub>3</sub>N and expected <sup>13</sup>C isotopic fractionation

Formation Route	Expected	
	fractionation	Sources
C <sub>2</sub> H <sub>2</sub> + CN → HC <sub>3</sub> N + H	1 : 1 : $x$	TMC-1, L1521B, L1527, G28.28-0.36
CCH + HNC → HC <sub>3</sub> N + H	$y$ : 1 : $z$	L134N
HC <sub>3</sub> NH <sup>+</sup> + e <sup>-</sup> → HC <sub>3</sub> N + H	≈ 1 : 1 : 1	G12.89+0.49, G16.86-2.16

Note “Expected fractionation pattern” means the [H<sup>13</sup>CCCN] : [HC<sup>13</sup>CCN] : [HCC<sup>13</sup>CN] ratio.  $x$ ,  $y$ , and  $z$  are arbitrary values.

isotopic fractionation of carbon-chain molecules, which refers to the relative differences in abundance among the <sup>13</sup>C isotopologues, has been proposed to be a key method for revealing their main formation mechanisms (Takano et al. 1998). In this subsection, we summarize observational results of the <sup>13</sup>C isotopic fractionation of several carbon-chain species toward TMC-1 CP and studies on HC<sub>3</sub>N toward various types of sources, from low-mass starless cores to MYSOs.

The local elemental <sup>12</sup>C/<sup>13</sup>C abundance ratio in the local ISM is around 60–70 (e.g., Milam et al. 2005). Hence, high-sensitivity observations are necessary to detect the <sup>13</sup>C isotopologues of carbon-chain molecules with high enough signal-to-noise (S/N) ratios to compare their abundances. With this constraint, TMC-1 CP is the most promising target source because of the high abundances of carbon-chain molecules (section 3.1). In fact, TMC-1 CP has the largest number of carbon-chain species investigated for <sup>13</sup>C isotopic fractionation: seven species have been studied, HC<sub>3</sub>N (Takano et al. 1998), CCS (Sakai et al. 2007), CCH (Sakai et al. 2010), C<sub>3</sub>S and C<sub>4</sub>H (Sakai et al. 2013), HC<sub>5</sub>N (Taniguchi et al. 2016a), HC<sub>7</sub>N (Burkhardt et al. 2018). Thanks to the advent of new observational facilities, larger molecules can be investigated within reasonable observing times.

Takano et al. (1998) observed the three <sup>13</sup>C isotopologues of HC<sub>3</sub>N (H<sup>13</sup>CCCN, HC<sup>13</sup>CCN, and HCC<sup>13</sup>CN) at TMC-1 CP using the Nobeyama 45m radio telescope. The relative abundance ratios of the three <sup>13</sup>C isotopologues were derived to be 1.0 : 1.0 : 1.4 (±0.2) (1σ) for [H<sup>13</sup>CCCN]:[HC<sup>13</sup>CCN]:[HCC<sup>13</sup>CN]. Table 3 summarizes correspondences of the possible main formation pathway of HC<sub>3</sub>N and its expected <sup>13</sup>C isotopic fractionation (Taniguchi et al. 2017a). Regarding the last one (the electron recombination reaction of HC<sub>3</sub>NH<sup>+</sup>), various formation pathways of the HC<sub>3</sub>NH<sup>+</sup> ion should compete, and then clear <sup>13</sup>C isotopic fractionation would not be seen in HC<sub>3</sub>NH<sup>+</sup>, as well as HC<sub>3</sub>N. The reaction between of “C<sub>2</sub>H<sub>2</sub> + CN → HC<sub>3</sub>N + H” can explain the observed <sup>13</sup>C isotopic fractionation in TMC-1 CP.

At the time five <sup>13</sup>C isotopologues of HC<sub>5</sub>N were detected (Takano et al. 1990), there was no evidence for the <sup>13</sup>C isotopic fractionation due to low S/N ratios. More than 25 years later, Taniguchi et al. (2016a) successfully detected the lines of the five <sup>13</sup>C isotopologues of HC<sub>5</sub>N ( $J = 9 - 8$  and  $16 - 15$  at 23 GHz and 42 GHz bands, respectively) with sufficient S/N ratios of 12–20. The derived abundance ratios among the five <sup>13</sup>C isotopologues of HC<sub>5</sub>N are 1.00 : 0.97 : 1.03 : 1.05 : 1.16 (±0.19) (1σ) for [H<sup>13</sup>CCCCCN] : [HC<sup>13</sup>CCCCN] : [HCC<sup>13</sup>CCCN] : [HCCC<sup>13</sup>CCN] : [HCCCC<sup>13</sup>CN]. Hence, even if the S/N ratios increase, there is no clear difference in abundance among

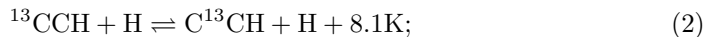


the five  $^{13}\text{C}$  isotopologues of  $\text{HC}_5\text{N}$ , unlike  $\text{HC}_3\text{N}$ . [Taniguchi et al. \(2016a\)](#) proposed that the reactions between hydrocarbon ions ( $\text{C}_5\text{H}_m^+$ ;  $m = 3-5$ ) and nitrogen atoms, followed by electron recombination reactions are the most plausible main formation mechanism of  $\text{HC}_5\text{N}$  at TMC-1 CP. This partly agrees with its general formation route in early starless cores indicated in [Fig. 1](#).

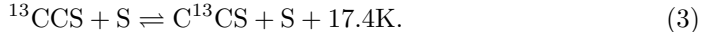
[Burkhardt et al. \(2018\)](#) detected six  $^{13}\text{C}$  isotopologues of  $\text{HC}_7\text{N}$  and five  $^{13}\text{C}$  isotopomers of  $\text{HC}_5\text{N}$  using the Green Bank 100m telescope.  $\text{H}^{13}\text{CC}_6\text{N}$  could not be detected in their observations. They found no significant difference among the  $^{13}\text{C}$  isotopomers of  $\text{HC}_7\text{N}$ , as similar to the case of  $\text{HC}_5\text{N}$ . They concluded that the significant formation route for  $\text{HC}_7\text{N}$  is the reaction of hydrocarbon ions and nitrogen atoms, which is the same conclusion for  $\text{HC}_5\text{N}$  by [Taniguchi et al. \(2016a\)](#).

In addition to cyanopolyynes,  $\text{C}_n\text{S}$  ( $n = 2, 3$ ) and  $\text{C}_{2n}\text{H}$  ( $n = 1, 2$ ) have been studied for  $^{13}\text{C}$  fractionation in TMC-1 CP ([Sakai et al. 2007, 2010, 2013](#)). [Sakai et al. \(2007\)](#) detected the lines of  $^{13}\text{CCS}$  and  $\text{C}^{13}\text{CS}$  ( $J_N = 2_1 - 1_0$ ,  $F = 5/2 - 3/2$ ). The abundance ratio of  $\text{C}^{13}\text{CS}/^{13}\text{CCS}$  was derived to be  $4.2 \pm 2.3$  ( $3\sigma$ ). They proposed that the reaction between CH and CS is the main formation route of CCS in TMC-1 CP. The abundance ratio of  $\text{C}^{13}\text{CH}/^{13}\text{CCH}$  was derived to be  $1.6 \pm 0.4$  ( $3\sigma$ ) ([Sakai et al. 2010](#)). To explain the abundance difference between the two  $^{13}\text{C}$  isotopomers of CCH, [Sakai et al. \(2010\)](#) proposed that the reaction of  $\text{CH} + \text{C}$  is the main formation mechanism of CCH at TMC-1 CP.

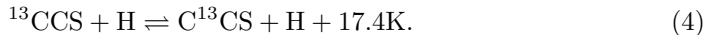
Unlike cyanopolyynes, the  $^{13}\text{C}$  isotopic fractionation of CCS and CCH does not necessarily provide information on their main formation mechanisms. [Furuya et al. \(2011\)](#) ran chemical simulations including  $^{13}\text{C}$  and investigated effects of the isotopomer-exchange reactions. They considered the following two isotopomer-exchange reactions for CCH and CCS, respectively:



and



They also included the following neutral-neutral exchange reaction of CCS to reproduce the observed isotopomer ratio of CCS:



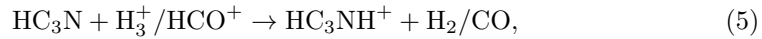
This reaction is regarded as a catalytic reaction by the hydrogen atom. At low temperature conditions ( $T \approx 10$  K),  $\text{C}^{13}\text{CH}$  and  $\text{C}^{13}\text{CS}$  should be more abundant than the other  $^{13}\text{C}$  isotopomers by reactions (2) – (4). Their model results can explain the observed abundance differences between the two  $^{13}\text{C}$  isotopomers of CCH and CCS in TMC-1 CP ([Sakai et al. 2007, 2010](#)). It was found that  $\text{C}^{13}\text{CH}$  is more abundant than  $^{13}\text{CCH}$  in the other starless cores (L1521B and L134N; [Taniguchi et al. 2019b](#)), and such a character may be common for cold dark clouds. Such exchange reactions may contribute to larger species such as  $\text{C}_3\text{S}$  and  $\text{C}_4\text{H}$  ([Sakai et al. 2013](#)). These studies suggest that it is difficult to establish the main formation routes directly from  $^{13}\text{C}$  isotopic fractionation, especially radical-type species. Hence, the main formation routes of CCH and CCS remain uncertain.



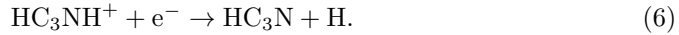
The  $^{13}\text{C}$  isotopic fractionation of  $\text{HC}_3\text{N}$  has been investigated toward various types of sources; low-mass starless cores L1521B and L134N (Taniguchi et al. 2017a), the low-mass YSO L1527 (Taniguchi et al. 2016b; Araki et al. 2016), and three MYSOs (G12.89+0.49 G16.86-2.16, and G28.28-0.36; Taniguchi et al. 2016b, 2021). Table 2 summarizes these results categorized into three types of fractionation patterns.

By comparing the results among the three starless cores (TMC-1 CP, L1521B, L134N), it was found that the  $^{13}\text{C}$  isotopic fractionation in L1521B and TMC-1 CP is similar to each other;  $\text{HCC}^{13}\text{CN}$  is more abundant than the others, and the other two  $^{13}\text{C}$  isotopologues have similar abundances. On the other hand, the results in L134N are different from the other two starless cores; the abundance ratios in L134N are  $1.5 (\pm 0.2) : 1.0 : 2.1 (\pm 0.4)$  ( $1\sigma$ ) for  $[\text{H}^{13}\text{CCCN}]:[\text{HC}^{13}\text{CCN}]:[\text{HCC}^{13}\text{CN}]$ . Based on the classifications (Table 3), the main formation mechanisms of  $\text{HC}_3\text{N}$  are determined as the reactions of  $\text{C}_2\text{H}_2 + \text{CN}$  in L1521B and  $\text{CCH} + \text{HNC}$  in L134N. The  $\text{C}^{13}\text{CH}/^{13}\text{CCH}$  abundance ratio was found to be  $> 1.4$  in L134N (Taniguchi et al. 2019b), which agrees with the abundance ratio of  $1.5 (\pm 0.2) : 1.0$  for  $[\text{H}^{13}\text{CCCN}]:[\text{HC}^{13}\text{CCN}]$ . This is further supporting evidence for the conclusion that the main formation pathway of  $\text{HC}_3\text{N}$  includes CCH in L134N. The difference between L134N and TMC-1CP/L1521B is probably brought about by different HNC/CN abundance ratios ( $\text{HNC}/\text{CN} = 35.6$  and  $54.2$  in TMC-1 CP and L134N, respectively). The HNC/CN abundance ratio depends on the cloud age, and then the main formation mechanism of cyanopolyynes likely changes throughout the cloud evolution.

In the case of star-forming cores (the low-mass YSO L1527 and three MYSOs; G12.89+0.49, G16.86-2.16, G28.28-0.36), L1527 and the MYSO G28.28-0.36 show the same feature as TMC-1 CP. This pattern agrees with the main formation route of the reaction between  $\text{C}_2\text{H}_2$  and CN. This is consistent with the chemical simulations confirming WCCC (Hassel et al. 2008) and formation reactions of cyanopolyynes during the warm-up stage (Taniguchi et al. 2019a). On the other hand, there were no significant differences among the three  $^{13}\text{C}$  isotopologues of  $\text{HC}_3\text{N}$  in the other two MYSOs (G12.89+0.49 and G16.86-2.16). Such results suggest that the main formation route of  $\text{HC}_3\text{N}$  is the electron recombination reaction of the  $\text{HC}_3\text{NH}^+$  ion. The differences among the MYSOs may come from different stellar luminosities or different environments where the target MYSOs were born. For example, strong stellar UV radiation may have changed the initial  $^{13}\text{C}$  isotopic fractionation of  $\text{HC}_3\text{N}$  in G12.89+0.49 and G16.86-2.16, because the following reactions destroy and reform  $\text{HC}_3\text{N}$  in harsh environments (Taniguchi et al. 2019a):



and



Even if  $\text{HC}_3\text{N}$  is mainly formed by the reaction between  $\text{C}_2\text{H}_2$  and CN initially and shows clear  $^{13}\text{C}$  isotopic fractionation, the above reaction cycle could erase the  $^{13}\text{C}$  isotopic fractionation. Another possibility is that the initial main formation route is reaction (6) in G12.89+0.49 and G16.86-2.16 due to strong stellar feedback from other stars which had been formed earlier than the MYSOs G12.89+0.49 and G16.86-2.16.

To solve these questions, we need to increase source samples in various environments and obtain maps of the fractionation.

### 3.6 Carbon-Chain Species in Disks

Before the ALMA era, there were only a few reported detections of carbon-chain species in the protoplanetary disks around T Tauri stars and Herbig Ae stars. [Henning et al. \(2010\)](#) detected CCH from two T Tauri stars, DM Tau and LkCa 15, with the IRAM Plateau de Bure Interferometer (PdBI). The first detection of HC<sub>3</sub>N from protoplanetary disks was achieved using the IRAM 30m telescope and PdBI ([Chapillon et al. 2012](#)). They detected the HC<sub>3</sub>N lines ( $J = 12 - 11$  and  $16 - 15$ ) from protoplanetary disks around two T Tauri stars, GO Tau and LkCa 15, and the Herbig Ae star MWC 480. Studies of disk chemistry have dramatically progressed, thanks to ALMA observations. In this subsection, we summarize studies related to carbon-chain species in protoplanetary disks.

[Qi et al. \(2013\)](#) reported the first detection of *c*-C<sub>3</sub>H<sub>2</sub> in a disk around the Herbig Ae star HD 163296 using the ALMA Science Verification data. Its emission is consistent with the Keplerian rotating disk and traces a ring structure from an inner radius of  $\sim 30$  au to an outer radius of  $\sim 165$  au. The HC<sub>3</sub>N line ( $J = 27 - 26$ ;  $E_{\text{up}} = 165$  K) has been detected from the protoplanetary disk of MWC 480, which is a Herbig Ae star in the Taurus region, using ALMA ([Öberg et al. 2015](#)). Angular resolutions are  $0.4'' - 0.6''$ , corresponding to 50–70 au. The data can spatially resolve the molecular emission, and show a velocity gradient caused by Keplerian rotation of the protoplanetary disk. [Öberg et al. \(2015\)](#) also detected CH<sub>3</sub>CN and H<sup>13</sup>CN in the same observation and found that the abundance ratios among the three species in the protoplanetary disk of MWC 480 are different from those in the solar-type protostellar binary system IRAS 16293-2422. Thus, they suggested that varying conditions among protoplanetary disks can lead to chemical diversity in terms of carbon-chain species.

[Bergner et al. \(2018\)](#) conducted survey observations of CH<sub>3</sub>CN and HC<sub>3</sub>N toward four T Tauri stars (AS 209, IM Lup, LkCa 15, and V4046 Sgr) and two Herbig Ae stars (MWC 480 and HD 163296) with ALMA. Typical angular resolutions are from  $\sim 0.5''$  to  $\sim 1.5''$ . They detected the HC<sub>3</sub>N ( $J = 27 - 26$ ) line from all of their target sources. Besides, the  $J = 31 - 30$  and  $J = 32 - 31$  lines have been detected from MWC 480. The spatial distributions of HC<sub>3</sub>N and CH<sub>3</sub>CN show similarity; compact and typically well within the bounds of the dust continuum. HC<sub>3</sub>N is considered to be formed by only the gas-phase reactions: C<sub>2</sub>H<sub>2</sub> + CN and CCH + HNC (see also Table 3).

The Molecules with ALMA at Planet-forming Scales (MAPS) ALMA Large Program has studied disk chemistry around five target sources (IM Lup, GM Aur, AS 209, HD 163296, and MWC 480) in Bands 3 and 6 ([Öberg et al. 2021](#)). Typical beam sizes are around  $0.3''$  and  $0.1''$  in Band 3 and Band 6, respectively. [Ilee et al. \(2021\)](#) presented the results for HC<sub>3</sub>N, CH<sub>3</sub>CN, and *c*-C<sub>3</sub>H<sub>2</sub>. The HC<sub>3</sub>N and *c*-C<sub>3</sub>H<sub>2</sub> lines have been clearly detected from four of the target sources, with the exception being IM Lup, where only one *c*-C<sub>3</sub>H<sub>2</sub> line has been tentatively detected. The *c*-C<sub>3</sub>H<sub>2</sub> emission shows clear ring-like features in AS 209, HD 163296, and MWC 480, suggestive of an association with the outer dust rings. Two HC<sub>3</sub>N lines ( $J = 11 - 10$  and  $29 - 28$ ) show ring-like distributions in AS 209 and HD 163296, whereas the  $J = 29 - 28$  line

appears centrally peaked in MWC 480. The HC<sub>3</sub>N emission of the  $J = 11 - 10$  line is similarly extended to that of *c*-C<sub>3</sub>H<sub>2</sub>, but the  $J = 29 - 28$  line seems to be more compact. CH<sub>3</sub>CN, on the contrary, appears to have a ring-like feature only in AS 209, while more centrally peaked structures are seen in the other sources. Ilee et al. (2021) demonstrated that the observed HC<sub>3</sub>N emission traces upper layers ( $z/r = 0.1 - 0.4$ ) of the protoplanetary disks compared to that of CH<sub>3</sub>CN ( $z/r \leq 0.1 - 0.2$ ). They also found that the HC<sub>3</sub>N/HCN and CH<sub>3</sub>CN/HCN abundance ratios of the outer regions (50–100 au) in the target disks are consistent with the composition of cometary materials. The warmer disks, HD 163296 and MWC 480, likely have comet formation zones at correspondingly larger radii.

Guzmán et al. (2021) presented distributions of CCH toward the five protoplanetary disks of the MAPS program. They proposed that the CCH emission comes from relatively warmer (20–60 K) layers. In HD 163296, there is a decrease in the column density of CCH and HCN inside of the dust gaps near  $\sim 83$  au, at which a planet has been considered to be located. The similar spatial distributions of CCH and HCN suggest that they are produced by the same chemical processes, and photochemistry is the most probable one.

ALMA observations have revealed the presence of disks around not only T Tauri and Herbig Ae stars, but also around more massive, O-/B-type stars. Csengeri et al. (2018) detected the vibrationally-excited HC<sub>3</sub>N line ( $J = 38 - 37$ ,  $v_7 = 1e$ ) around the O-type star G328.2551-0.5321 (O5–O4 type star) with ALMA. This source is a high-mass protostar in the main accretion phase. Their data have a spatial resolution of around 400 au. The position-velocity (PV) diagram of this HC<sub>3</sub>N vibrationally-excited line is consistent with a Keplerian disk rotation profile, and they proposed that such HC<sub>3</sub>N vibrationally-excited emission could be a new tracer for compact accretion disks around high-mass protostars.

Taniguchi et al. (2022) detected the HC<sub>3</sub>N vibrationally-excited lines ( $J = 24 - 23$ ,  $v_7 = 2, l = 0$  and  $2e$ ) from the hypercompact H<sub>II</sub> (HC H<sub>II</sub>) region G24.47-0.08 A1 using ALMA Band 6 data. Their emission morphologies are largely similar to those of CH<sub>3</sub>CN, which was suggested to trace Keplerian disk rotation around a central mass of  $20 M_{\odot}$  in the previous study of Moscadelli et al. (2021). The column densities of HC<sub>3</sub>N and CH<sub>3</sub>CN were derived using lines of their <sup>13</sup>C isotopologues, and the CH<sub>3</sub>CN/HC<sub>3</sub>N abundance ratios were compared with those in protoplanetary disks around the lower-mass stars obtained by the MAPS program (Ilee et al. 2021). Fig. 10 shows the comparisons of the CH<sub>3</sub>CN/HC<sub>3</sub>N abundance ratios in disks. It is clear that the ratio in the disk around the G24 HC H<sub>II</sub> region is higher than those around the lower-mass stars by more than one order of magnitude.

Such a difference in the CH<sub>3</sub>CN/HC<sub>3</sub>N abundance ratio was explained by the HC<sub>3</sub>N and CH<sub>3</sub>CN chemistry in the disk: efficient thermal sublimation of CH<sub>3</sub>CN from ice mantles and rapid destruction of HC<sub>3</sub>N by the UV photodissociation and/or reactions with ions (H<sup>+</sup>, H<sub>3</sub><sup>+</sup>, HCO<sup>+</sup>). In the protoplanetary disks, CH<sub>3</sub>CN is considered to be efficiently formed by dust-surface reactions: (1) the successive hydrogenation reactions of C<sub>2</sub>N; and (2) a radical-radical reaction between CH<sub>3</sub> and CN (Loomis et al. 2018a). The derived excitation temperature of CH<sub>3</sub>CN in the G24 HC H<sub>II</sub> region ( $T_{\text{ex}} \approx 335$  K) is much higher than its sublimation temperature ( $\sim 95$  K), which

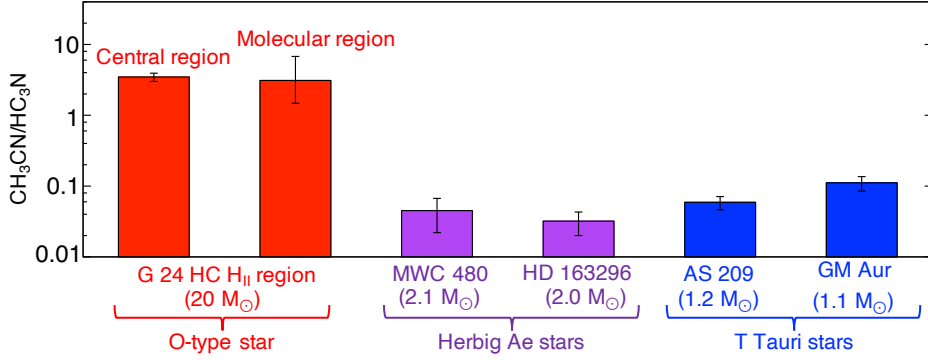


**Fig. 10** Comparison of the  $\text{CH}_3\text{CN}/\text{HC}_3\text{N}$  abundance ratios in disks around various stellar masses, which is modified from Taniguchi et al. (2022). Results of Herbig Ae and T Tauri stars are from Ilee et al. (2021).

suggests that  $\text{CH}_3\text{CN}$  formed on dust surfaces efficiently sublimates by the thermal desorption mechanism. On the other hand, its excitation temperatures around the Herbig Ae and T Tauri stars were derived to be 30–60 K, which is suggestive of the non-thermal desorption mechanisms such as photodesorption (Loomis et al. 2018a; Ilee et al. 2021). This means that  $\text{CH}_3\text{CN}$  sublimation is not efficient in disks around the Herbig Ae and T Tauri stars, leading to low gas-phase abundances of  $\text{CH}_3\text{CN}$ . Both  $\text{HC}_3\text{N}$  and  $\text{CH}_3\text{CN}$  could be destroyed by the UV radiation, and the UV photodissociation rate of  $\text{HC}_3\text{N}$  is higher than that of  $\text{CH}_3\text{CN}$  by a factor of  $\sim 2.4$  (Le Gal et al. 2019). Thus,  $\text{HC}_3\text{N}$  could be more rapidly destroyed by UV photodissociation. In addition,  $\text{HC}_3\text{N}$  is destroyed by reactions with ions, which are expected to be abundant in the  $\text{H}_{\text{II}}$  region. In summary,  $\text{HC}_3\text{N}$  is likely destroyed rapidly in the G24  $\text{HCH}_{\text{II}}$  region.

Until now, there is only one O-type star disk in which the  $\text{CH}_3\text{CN}/\text{HC}_3\text{N}$  abundance ratio has been derived. We need similar data for an increased sample of sources, including T Tauri, Herbig Ae, and O/B type disks, including probing various evolutionary stages, to further test the apparent tentative trends that have been so far revealed. In addition, for such studies of disk structures, especially around the more distant massive protostars, it is important to conduct unbiased line survey observations with high angular resolution.

### 3.7 Carbon-Chain Species in Other Environments

Carbon-chain molecules have been detected not only from star-forming regions in our Galaxy, but also other environments of the ISM. We briefly summarize the carbon-chain species detected in these regions.

Small hydrocarbons have been known to be present in photodissociation regions (PDRs). Cuadrado et al. (2015) observed small hydrocarbons toward the Orion Bar PDR using the IRAM 30m telescope. They detected various small hydrocarbons ( $\text{CCH}$ ,  $\text{C}_4\text{H}$ ,  $c\text{-C}_3\text{H}_2$ ,  $c\text{-C}_3\text{H}$ ,  $\text{C}^{13}\text{CH}$ ,  $^{13}\text{CCH}$ ,  $l\text{-C}_3\text{H}$ , and  $l\text{-H}_2\text{C}_3$ ) and the  $l\text{-C}_3\text{H}^+$  ion. They found that the spatial distributions of  $\text{CCH}$  and  $c\text{-C}_3\text{H}_2$  are similar but do not follow the PAH emission, and suggested that photo-destruction of PAHs is not a necessary requirement for the observed abundances of the smallest hydrocarbons. Instead, the

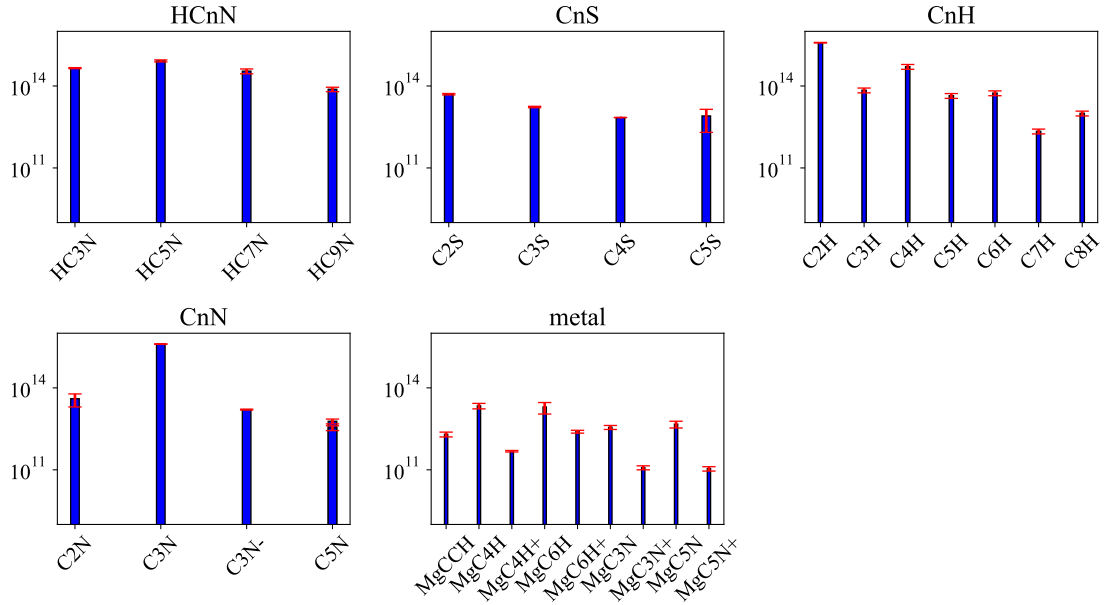


**Fig. 11** Column density variation of carbon chains toward IRC+10216.

gas-phase reactions between  $C^+$  and  $H_2$  produce the small hydrocarbons. [Guzmán et al. \(2015\)](#) observed small hydrocarbons ( $CCH$ ,  $c\text{-}C_3H_2$ ),  $l\text{-}C_3H^+$ , and  $DCO^+$  toward the Horsehead PDR with the PdBI. They demonstrated that top-down chemistry, in which large polyatomic molecules or small carbonaceous grains are photo-destroyed into smaller hydrocarbon molecules or precursors, works in this PDR. Suggestions by these two studies ([Cuadrado et al. 2015](#); [Guzmán et al. 2015](#)) seem in contradiction but may imply that the carbon-chain chemistry in PDRs differs among regions. Thus, further study is needed of carbon-chain chemistry in PDRs.

The envelopes of the carbon-rich Asymptotic Giant Branched (AGB) star IRC+10216 are known as a carbon-chain-rich site. Several carbon-chain molecules have been discovered for the first time in this source in both radio and infrared regimes (see also Table 1). For example, diacetylene ( $C_4H_2$ ) has been detected in mid-infrared observations with the 3m Infrared Telescope Facility (IRTF) from this source ([Fonfría et al. 2018](#)). This molecule is distributed in two populations with different excitation conditions; cold and hot rotational temperatures were derived to be  $47 \pm 7$  K and  $420 \pm 120$  K, respectively. [Pardo et al. \(2022\)](#) conducted deep line survey observations in the Q band with the Yebes 40m telescope and summarized the detected carbon-chain species in this source. The rotational temperatures of the carbon-chain species are around 5–25 K, suggesting that carbon-chain species may exist in different regions. The species detected with the radio telescope exist in colder regions compared to the species detected with the infrared telescope. There remain a lot of unidentified lines (U lines), and future laboratory spectroscopic experiments are necessary for line identifications.

Fig. 11 shows column densities of several carbon-chain series in IRC+10216. Their column densities are provided in Table B3 in Appendix B. As discussed in section 3.1, we can compare column densities straightforwardly if they were derived by the same observing conditions and analytical methods. Otherwise, one needs to carefully assess the original studies and the differences in their methods. In the case of IRC+10216, the spatial distributions of carbon-chain species are not uniform (e.g., Agúndez et al. 2017), and so different beam sizes and beam positions can cause significant differences in the derived column density.

Although column densities of  $C_nH$  were derived by different authors (see Table B3 in Appendix B), a similar zigzag feature as TMC-1 CP (Fig. 5 in section 3.1) can be seen in this series. One of the unique points of its envelope is that metal-bearing carbon-chain species including ions have been discovered. The abundance ratios of  $MgC_4H/MgC_4H^+$  and  $MgC_6H/MgC_6H^+$  are calculated at  $\sim 105$  and  $\sim 20$ , and  $MgC_3N/MgC_3N^+$  and  $MgC_5N/MgC_5N^+$  are  $\sim 1029$  and  $\sim 10$ , respectively. Hence, larger species tend to be in the ionic forms. These ionic forms are considered to be produced by radiative association between  $Mg^+$  and  $C_nH$  or  $C_nN$ , respectively. Longer species of  $C_{2n}H$  and  $C_nN$  show larger dipole moments (see Table 1), which could enhance reactions with the  $Mg^+$  ion. The difference in the radiative association coefficient between  $C_4H$  and  $C_6H$  is one order of magnitude, whereas that between  $C_3N$  and  $C_5N$  is more than three orders of magnitude (Table D.2. in Cernicharo et al. (2023a)), and this seems to be able to explain the observational results. However, Cernicharo et al. (2023a) could not reproduce all of their observed abundances; the modeled column density of  $MgC_3N^+$  was lower than the observed one by a factor of  $\sim 30$ . Experimental data on these radiative association reactions and other formation and destruction reactions are needed to reduce modeling uncertainties to better understand these potential discrepancies. The longer cyanopolyynes may be lower in abundance compared to TMC-1 CP;  $[HC_5N]:[HC_7N]:[HC_9N]$  ratios in IRC+10216 are derived to be  $1:\sim 0.4:\sim 0.09$ , while these ratios in TMC-1 CP are approximately  $1:0.6:0.2$ , respectively. These differences likely reflect different carbon-chain growth mechanisms between starless cores and envelopes around the carbon-rich AGB stars.

The planetary nebula CRL 618, another carbon-chain-rich source, has been studied by radio and infrared observations. Polyacetylenic chains ( $C_4H_2$  and  $C_6H_2$ ) and benzene ( $C_6H_6$ ) have been detected here with the Infrared Space Observatory (ISO) (Cernicharo et al. 2001). The abundances of  $C_4H_2$  and  $C_6H_2$  are lower than that of  $C_2H_2$  by only a factor of 2–4, while benzene is less abundant than acetylene by a factor of  $\sim 40$ . These authors suggested that UV photons from the hot central star and shocks associated with its high-velocity winds affect the chemistry in CRL 618: i.e., the UV photons and shocks drive the polymerization of acetylene and the formation of benzene. These hydrocarbons likely survive in harsh regions compared to star-forming regions. Pardo et al. (2005) observed cyanopolyynes up to  $HC_7N$ , and proposed rapid transformation from small cyanide to longer cyanopolyynes in this source.

Berné & Tielens (2012) investigated formation process of  $C_{60}$  by the infrared observations with *Spitzer* and *Herschel* toward the NGC 7023 reflection nebula. They found that  $C_{60}$  is efficiently formed in cold environments of an interstellar cloud irradiated by

the strong UV radiation field. The most plausible formation route is the photochemical processing of large PAHs.

Carbon-rich AGB stars or planetary nebulae, like IRC+10216 and CRL 618, appear to possess unique carbon-chain chemistry differing from that in star-forming regions and PDRs, and thus be important laboratories to study carbon chemistry, including PAHs and benzene. Future observations with infrared telescopes, such as James Webb Space Telescope (JWST), may give us new insights into carbon chemistry, in particular carbonaceous dust grains, PAHs, and fullerenes. In fact, recent observations with JWST have revealed the presence of dust shells around the Wolf-Rayet binary WR 140, which likely implies an episodic dust formation process (Lau et al. 2022). Using JWST, we can also reveal the spatial distributions of PAHs and fullerenes, as well as dust grains. Similar observations will be able to be applied for C-rich AGB stars or planetary nebulae and reveal the carbon chemistry around these harsh environments. Furthermore, we can investigate relationships among carbon-chain species, hydrocarbons, fullerenes, and carbonaceous dust by a combination of ALMA and JWST. These studies are essential to reveal what forms of carbon are ejected into the ISM and how they are incorporated into future star formation events. This point will be essential to reveal the origin of large carbon-chain molecules and species including benzene rings that have been recently detected at TMC-1 CP (section 3.1).

ALMA observations have detected carbon-chain species in extragalactic sources. The ALMA Comprehensive High-resolution Extragalactic Molecular Inventory (ALCHEMI) large program has conducted line survey observations from 84.2 GHz to 373.2 GHz toward the starburst galaxy NGC 253. Several carbon-chain species (e.g., CCH, *c*-C<sub>3</sub>H<sub>2</sub>, HC<sub>3</sub>N, HC<sub>5</sub>N, HC<sub>7</sub>N, CCS) have been detected from this galaxy (Martín et al. 2021). The detection of more complex carbon-chain species will be reported (Dr. Sergio Martin, ESO/JAO, private comm.). Shimonishi et al. (2020) detected CCH in a hot molecular core in the Large Magellanic Cloud (LMC), and found that the CCH emission traces outflow cavity, as also seen in the low-mass YSOs in our Galaxy (see section 3.3). Such observations toward extragalactic sources with different metallicities will be important for a comprehensive understanding of carbon chemistry in the ISM.

Summaries of this section are as follows:

1. Recent line survey observations toward TMC-1 by the Green Bank 100m and Yebes 40m telescopes discovered various and unexpected carbon-chain molecules. However, abundances of some of them cannot be explained by chemical simulations, meaning that our current knowledge about carbon chemistry in the ISM lacks important processes.
2. Survey observations toward low-mass YSOs revealed that both carbon-chain species and COMs are present around most of the low-mass YSOs. Hot corino and WCCC states are likely to be extreme ends of a continuous distribution.
3. Since carbon-chain molecules trace chemically young gas, their lines can be powerful tracers of streamers, which are important structures to understand star formation and disk evolution.
4. Carbon-chain species are formed around MYSOs. ALMA observations have shown that they exist in hot core regions with temperatures above 100 K. Thus, the



carbon-chain chemistry is not the WCCC mechanism found around low-mass YSOs, but rather indicates the presence of “Hot Carbon-Chain Chemistry (HCCC)”.

5. The vibrationally-excited lines of  $\text{HC}_3\text{N}$  can be used as a disk tracer around massive stars. The disk chemistry around massive stars may be different from that around lower-mass stars (i.e., T Tauri and Herbig Ae stars), although there is the need to increase the source samples to confirm this.
6. Infrared observations toward carbon-rich AGB stars and planetary nebulae have detected polyacetylene chains, benzene, and fullerenes in their envelopes. These sites are unique laboratories to study carbon chemistry which is different from that in star-forming regions.
7. Beyond our Galaxy, several carbon-chain species have also been detected in other galaxies enabled by high-sensitivity ALMA observations.

## 4 Chemical Simulations

Modeling studies of carbon-chain chemistry in starless cores have tried to obtain good agreement with the observed abundances in the dark cloud TMC-1. Recent work has focused on particular species that were newly detected in TMC-1 CP (section 3.1). Here, we review modeling studies covering various types of carbon-chain molecules in dark clouds.

Loison et al. (2014) studied several carbon-chain groups ( $\text{C}_n$ ,  $\text{C}_n\text{H}$ ,  $\text{C}_n\text{H}_2$ ,  $\text{C}_{2n+1}\text{O}$ ,  $\text{C}_n\text{N}$ ,  $\text{HC}_{2n+1}\text{N}$ ,  $\text{C}_{2n}\text{H}^-$ ,  $\text{C}_3\text{N}^-$ ) with gas-grain chemical models including updated reaction rate constants and branching ratios assuming two different C/O ratios (0.7 and 0.95). They added a total of 8 new species and 41 new reactions, and modified 122 rate coefficients taken from the KInetic Database for Astrochemistry (KIDA, kida.uva.2011). Their results clearly show that some carbon-chain molecules depend on the C/O elemental abundance ratio (e.g.,  $\text{C}_n\text{H}$  where  $n = 4, 5, 6, 8$ ). Their models with new parameters can obtain good agreement with the observed abundances in the dark cloud TMC-1 CP, and the models with two C/O ratios (0.7 and 0.95) obtain a similar agreement at different times. Two ages show better agreement between observations and models;  $10^5$  yr and around  $(1 - 2) \times 10^6$  yr. The gas-phase chemistry is dominated at the earlier phase, whereas the grain surface chemistry and gas-grain interaction become more efficient at the later stages because of more frequent collisions between gas-phase particles and dust grains. These authors also compared the modeled results to the observed abundances in another starless core, L134N. Here the models with a C/O ratio of 0.7 are in better agreement with the observed abundances compared to the case with the higher C/O ratio. Ages when the models agree with the observed abundances in L134N best are  $(3 - 5) \times 10^4$  yr and  $\sim 6 \times 10^5$  yr. Large amounts of free C, N, and O are available in the gas phase at the first age, while strong depletion effects are predicted at the later stage. They also suggested that experimental work for the determination of rate constants for the reactions of  $\text{O} + \text{C}_n\text{H}$  and  $\text{N} + \text{C}_n\text{H}$ , especially at low-temperature conditions, is necessary.

The best-fitting ages differ by about one order of magnitude in the two different C/O elemental abundance ratios. These results imply that it is not straightforward to compare chemical ages among starless cores located in different parent molecular



clouds that have different elemental abundances. Thus, we need caution when treating carbon-chain molecules as chemical evolutionary indicators (Suzuki et al. (1992); Benson et al. (1998) and section 3.4.1).

Most recent studies have focused on particular molecules that were newly detected at TMC-1 CP (section 3.1). Classical models for dark clouds consider bottom-up chemistry starting from  $C^+$ , with carbon-chain molecules considered to form mainly by gas-phase reactions (see Fig. 1 in section 1.2). However, such classical views need to be revisited. For example, it has been revealed that both gas-phase and grain-surface formation routes are important for the reproduction of the observed abundance of  $H_2CCCHC_3N$  (Shingledecker et al. 2021). Some molecules detected by the GOTHAM project, especially cyclic molecules, have not been explained by the chemical simulations yet (e.g., *c*- $C_9H_8$ ; Burkhardt et al. 2021a). These results suggest that small rings are formed through the destruction of PAHs or other unknown processes. Our knowledge about connections among different categories (e.g., linear, cyclic, PAHs) likely lacks important processes. Besides, we need to reveal the initial conditions of carbon-bearing species in molecular clouds. Further observations and chemical simulations are necessary to understand carbon-chain chemistry including the newly detected molecules. To achieve this science goal, this is a need to expand such studies to the diffuse ISM and evolved stars, where carbon is ejected into the ISM. This will allow better constraints on the initial chemical composition of star-forming regions and the potential impact on carbon-chain chemistry in starless cores.

Some recent studies with sophisticated chemical simulations focused on the origin of the chemical diversity around YSOs. Aikawa et al. (2020) demonstrated their results with two phases (the static phase and the collapse phase) and a multilayered ice mantle model, and investigated how the WCCC and hot corino chemistry depend on the physical conditions during the static phase. They found:

1. The lower temperatures ( $T \leq 15$  K) during the static phase can produce the WCCC sources more efficiently.
2. The lower visual extinction during the static phase can form  $CH_4$  and carbon-chain molecules become more abundant.
3. A longer static phase is preferable for producing the WCCC sources.
4. It is difficult to produce the prototypical WCCC sources, where carbon-chain species are rich but COMs are deficient. On the contrary, the hot corino sources and hybrid-type sources where both COMs and carbon-chain species are reasonably abundant could be reproduced.

In warm conditions, grain-surface formation and freeze out of  $CH_4$ , which is a key species for WCCC, become less effective. Moreover, the conversion of CO to  $CO_2$  on grain surfaces becomes important, and the gaseous CO abundance decreases. These lead to a low abundance of  $C^+$ , which is formed by the destruction of CO by  $He^+$ . The  $C^+$  ion is another key species for WCCC. Therefore, warm conditions are not suitable for the production of WCCC sources. In the model with a longer static phase,  $CH_4$  accumulates during the static phase, leading to a more favorable condition for WCCC. These results disfavor the scenario of a short timescale of prestellar collapse to explain observed WCCC (Sakai et al. 2008) (see section 2.3).

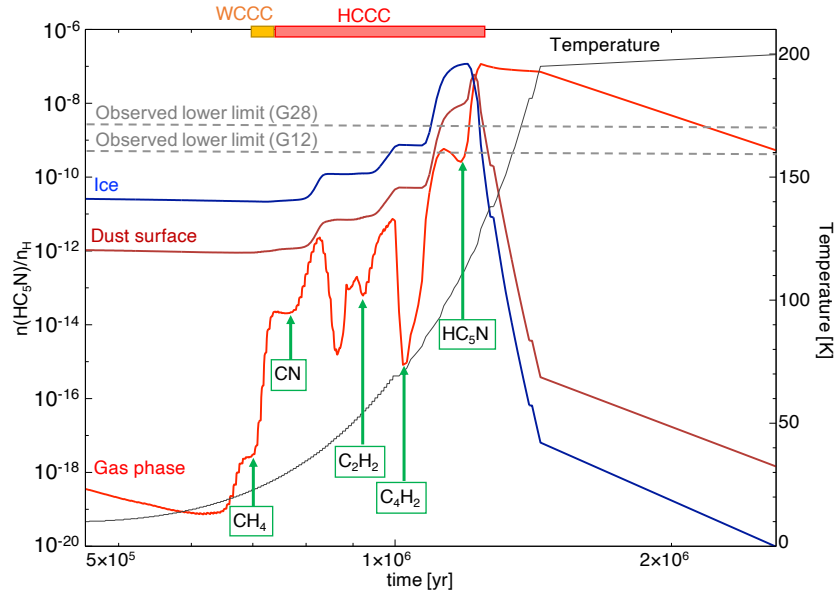


**Fig. 12** The modeled  $\text{HC}_5\text{N}$  abundances in the gas phase (red), dust surface (brown), and ice mantle (blue) during the warm-up and hot-core periods (Taniguchi et al. 2019a). The black line indicates the temperature evolution. Indicated molecules mark the times of efficient sublimation from dust grains. The gray horizontal dashed lines indicate the observed lower limits of the gas-phase  $\text{HC}_5\text{N}$  abundances toward two MYSOs; G12.89+0.49 ( $5 \times 10^{-10}$ ) and G28.28-0.36 ( $2.1 \times 10^{-9}$ ).

Kalvāns (2021) investigated the effects of the UV radiation field and cosmic rays on the formation of WCCC sources. They concluded that WCCC can be caused by exposure of a star-forming core to the interstellar radiation field (ISRF) or just to cosmic rays (with  $\zeta \geq 10^{-16} \text{ s}^{-1}$ ). Such a conclusion agrees with the observational results that hot corino type sources are located inside dense filamentary clouds, while the WCCC sources are located outside such structures (e.g., Lefloch et al. 2018). These two model studies show that various factors, including conditions before the onset of core collapse, are related to carbon-chain chemistry around low-mass YSOs. These factors likely are entangled in most sources.

As with observational studies, chemical simulations focusing on the carbon-chain chemistry around MYSOs are still relatively poorly explored. Taniguchi et al. (2019a) tried to reproduce the observed abundances of  $\text{HC}_5\text{N}$  around the three MYSOs observed with the single-dish telescopes (section 3.4.2) with chemical simulations of hot-core models with a warm-up period. They utilized three different heating timescales ( $t_h$ );  $5 \times 10^4$  yr,  $2 \times 10^5$  yr, and  $1 \times 10^6$  yr, approximating high-mass, intermediate-mass, and low-mass star-formation, respectively (Garrod & Herbst 2006). Fig. 12 shows the model results of  $\text{HC}_5\text{N}$  (gas phase, dust surface, and ice mantle) during the warm-up and hot-core periods with a heating timescale of  $1 \times 10^6$  yr. In Fig. 12, we indicate the lower limits of the gas-phase  $\text{HC}_5\text{N}$  abundance in two MYSOs; G12.89+0.49 and G28.28-0.36 that show the minimum and maximum abundances, respectively (Taniguchi et al. 2017b). The observed abundances derived by single-dish telescopes are considered to be lower limits due to beam dilution. The observed lower limits of  $\text{HC}_5\text{N}$  around the MYSOs can be reproduced when the temperature reaches its sublimation temperature ( $\sim 115$  K) or the hot-core phase ( $T = 200$  K).

These authors also investigated cyanopolyynes chemistry in detail during the warm-up and hot-core periods. Basically, the formation and destruction reactions of  $\text{HC}_3\text{N}$ ,  $\text{HC}_5\text{N}$ , and  $\text{HC}_7\text{N}$  are similar. We give an explanation of  $\text{HC}_5\text{N}$  as an example (Fig. 12). The gas-phase  $\text{HC}_5\text{N}$  abundance (red curves) shows a drastic change with time (or temperature) evolution. During the warm-up period,  $\text{HC}_5\text{N}$  is mainly formed by the reaction between  $\text{C}_4\text{H}_2$  and  $\text{CN}$ . In addition to this, the reaction between  $\text{CCH}$  and  $\text{HC}_3\text{N}$  partly contributes to the  $\text{HC}_5\text{N}$  formation. This reaction ( $\text{CCH} + \text{HC}_3\text{N}$ ) is important around  $t \approx 8.5 \times 10^5$  yr, when the gas-phase  $\text{HC}_3\text{N}$  abundance increases. At that time, the  $\text{HC}_3\text{N}$  production is enhanced by the reaction between  $\text{CCH}$  and  $\text{HNC}$ . We indicate some molecules with green arrows in Fig. 12. These indicate that each molecule directly sublimates from dust grains at these various ages. Methane ( $\text{CH}_4$ ) sublimates from dust grains around 25 K ( $t \approx 7.2 \times 10^5$  yr), and carbon-chain formation starts, namely WCCC. After that,  $\text{CN}$  and  $\text{C}_2\text{H}_2$  sublime from dust grain at  $t = 7.7 \times 10^5$  yr ( $T \approx 31$  K) and  $t = 9.3 \times 10^5$  yr ( $T \approx 55$  K), respectively. The  $\text{C}_4\text{H}_2$  species is formed by the gas-phase reaction of “ $\text{CCH} + \text{C}_2\text{H}_2 \rightarrow \text{C}_4\text{H}_2 + \text{H}$ ”. When the temperature reaches around 73 K ( $t = 1.0 \times 10^6$  yr),  $\text{C}_4\text{H}_2$  directly sublimates from dust grains. The enhancement of the gas-phase abundances of  $\text{CN}$  and  $\text{C}_4\text{H}_2$  boosts the formation of  $\text{HC}_5\text{N}$  in the gas phase.

We can see that the  $\text{HC}_5\text{N}$  abundances in dust surface and ice mantles increase when the gas-phase  $\text{HC}_5\text{N}$  abundance decreases. This means that the  $\text{HC}_5\text{N}$  molecules, which are formed in the gas phase, adsorb onto dust grains and accumulate in ice mantles before the temperature reaches its sublimation temperature ( $T \approx 115$  K, corresponding to  $t = 1.2 \times 10^6$  yr). Taniguchi et al. (2023) have advocated the concept of HCCC (Fig. 3) based on these results.

This chemical simulation is supported by observations of the  $^{13}\text{C}$  isotopic fractionation (c.f., section 3.5) of  $\text{HC}_3\text{N}$  toward the carbon-chain-rich MYSO G28.28-0.36 (Taniguchi et al. 2016b). The proposed main formation pathway of  $\text{HC}_3\text{N}$  is the reaction between  $\text{C}_2\text{H}_2$  and  $\text{CN}$  in this MYSO. This is consistent with the formation process seen in the chemical simulations during the warm-up stage.

Taniguchi et al. (2019a) proposed that longer heating timescales of the warm-up stage ( $t_h$ ) could produce the carbon-chain-rich conditions by comparisons of six modeled results, focusing on cyanopolyynes. In the HCCC mechanism, cyanopolyynes are formed in the gas phase, adsorb onto dust grains, and accumulate in the ice mantle. Their ice-mantle abundances of just-before sublimation determine the gas-phase peak abundances. Thus, longer heating timescales allow cyanopolyynes to accumulate in the ice mantle abundantly, leading to their higher gas-phase abundances in hot core regions. The long heating timescale of the warm-up stage ( $t_h$ ) does not necessarily reflect the timescale of stellar evolution or accretion. It depends on the relationships between the size of the warm region ( $R_{\text{warm}}$ ) and the infall velocity ( $v_{\text{infall}}$ ) as suggested by Aikawa et al. (2008):

$$t_h \propto \frac{R_{\text{warm}}}{v_{\text{infall}}}. \quad (7)$$

If  $R_{\text{warm}}$  becomes larger or  $v_{\text{infall}}$  becomes smaller,  $t_h$  will be longer. The  $R_{\text{warm}}$  and  $v_{\text{infall}}$  values should be related to various physical parameters (e.g., protostellar luminosity, density structure, magnetic field strength). The conditions of  $R_{\text{warm}}$  and

$v_{\text{infall}}$  can be investigated by observations. Combined observations to derive chemical composition and the values of  $R_{\text{warm}}/v_{\text{infall}}$  are needed for a more comprehensive understanding of the chemical evolution and diversity around YSOs.

Although the chemical simulations by [Taniguchi et al. \(2019a\)](#) were able to reproduce the observational results around MYSOs, we need to carefully consider the physical parameters for each MYSO. As shown in [Taniguchi et al. \(2019a\)](#), the cosmic-ray ionization rate is a key parameter for the abundance of cyanopolyynes during the warm-up and hot-core stages. Moreover, different timescales of the warm-up stage affect the  $\text{HC}_5\text{N}$  abundance. Effects from both factors cannot be disentangled easily. The cosmic-ray ionization rate is expected to be higher than the standard value ( $\sim 10^{-17} \text{ s}^{-1}$ ) due to stellar feedback from the MYSO or nearby stars, and then one should potentially vary the cosmic-ray ionization rate for each source. Since  $R_{\text{warm}}$  and  $v_{\text{infall}}$  are observable parameters, we can carry out survey observations of cyanopolyynes toward MYSOs with various  $\frac{R_{\text{warm}}}{v_{\text{infall}}}$  and compare the results with the chemical simulations. Such studies may be able to evaluate the effect of the warm-up stage on the cyanopolyne abundances around MYSOs. In addition, more sophisticated chemical simulations are needed, including a systematic exploration of the relevant parameter space to fully understand the chemical diversity around MYSOs.

More recently, [Lee et al. \(2021b\)](#) demonstrated a machine-learning method. They could reproduce the observed column densities of 87 molecules in TMC-1 within an order of magnitude without prior knowledge about the physical conditions of the source. One of the merits of machine learning is that it can predict the presence of undiscovered species. We can expect further astronomical detections with predictions by machine-learning approaches.

## 5 Theoretical Studies

### 5.1 Role of Quantum Chemical Studies

Quantum chemistry is an indispensable tool to study structures and spectral properties of a given molecule, regardless of laboratory stability, and makes this a necessary component of astrochemical analyses. It is probably the best tool to explore and interpret chemical structures, properties, and, most importantly, detectable spectra of unusual molecules detected in space. In the 1960s and 1970s, when radio telescopes came into action with better sensitivity, many species were identified based on the laboratory data of their rotational spectra. However, there were also many unidentified signatures. Closed shell molecules can be easily handled in the laboratory and generate rotational spectra. The problem arises in the case of radical and charged species because of their highly unstable and reactive nature. Initial detection of  $\text{HCO}^+$  and  $\text{N}_2\text{H}^+$  was in the 1970s and based on quantum chemistry (see [Fortenberry 2015](#), and references therein). Following these, Patrick Thaddeus (Columbia University and then Harvard University) was a part of teams that detected nearly three dozen new molecular species ([McCarthy & Thaddeus 2001](#)). Thaddeus' group standardized the use of quantum chemistry in astrochemical detection.

Several carbon-chain species such  $\text{C}_2\text{H}$ ,  $\text{C}_3\text{N}$ , and  $\text{C}_4\text{H}$  were identified based on SCF (self-consistent field) computation. The usage of quantum chemistry in astrochemistry

became popular and common if species had not been synthesized in a laboratory. Several carbon-chain species, such as  $l\text{-C}_3\text{H}^+$  and  $\text{C}_6\text{H}^-$ , were identified based on the insight of quantum chemistry. This has continued until recent times with the detection of the kentenyl radical ( $\text{HCCO}$ ) towards various dark clouds in 2015. In another example, the detection of  $\text{C}_5\text{N}^-$  in the circumstellar envelope of the carbon-rich star IRC+10216 was based solely on quantum chemical data.

Modern quantum computations consider a lot of improvements with a wide range of quantum mechanical methods, basis sets, especially coupled cluster theory, at the single, double, and perturbative triples [CCSD(T)] level. The CCSD(T) method is exceptionally good at providing molecular structures and rotational constants, which provide reference rotational spectra. The CCSD(T) method is considered the gold standard in quantum chemical calculations to obtain accurate bond energies and molecular properties (e.g., Ramabhadran & Raghavachari 2013; Fortenberry 2015; Barone et al. 2015; Fortenberry 2017). Over the years, many groups have made remarkable contributions to astrochemistry through quantum chemistry for astrochemical detection, understanding of the formation/destruction, and collisional excitation of different interstellar molecules (e.g., groups led by L. Allamandola, C. Bauschlicher, N. Balucani, V. Barone, M. Biczysko, P. Botschwina, R. C. Fortenberry, J. Gauss, J. Kästner, T. J. Lee, J-C Loison, K. Peterson, C. Puzzarini, A. Rimola, H. F. Schaefer, J. Stanton, P. Ugliengo, D. Woon). A comprehensive strategy for treating larger molecules with the required accuracy has been presented by Barone et al. (2015).

### 5.1.1 Ground State and Stability

The ground states of carbon-chain species are crucial because they decide their stability and eventually help us find the true state of the species either in laboratory experiments or in astrophysical environments via a spectral search. Table 1 summarizes the ground state of all the carbon-chain species included in this review article. The ground state, enthalpy of formation, rotational constants, dipole moment, and polarizability of many carbon-chain species can be found in KIDA database (<https://kida.astrochem-tools.org/>) as well as in several works in the literature (e.g., Woon & Herbst 2009; Etim et al. 2016; Etim & Arunan 2017; Bâldea 2019; Etim et al. 2020). For any particular carbon-chain species, the ground state can be found with the help of quantum chemical study.

### 5.1.2 Dipole moment and Polarizability

The dipole moment is an important parameter that decides whether a molecule is polar or non-polar. Non-polar molecules do not have a permanent electric dipole moment and do not show rotational transitions. On the other hand, polar molecules have a permanent electric dipole moment and they show rotational transitions. A higher dipole moment value means a higher intensity of rotational transitions. It is crucial because one can say whether it is detectable or not through their rotational transitions. In addition to the symmetry of molecules, several other factors are important for their detectability in interstellar environments. These factors include the density of spectral lines, the partition functions, and the intrinsic line strengths of the transitions. The dipole moment values of all the carbon-chain species are summarized in Table 1. These

can be measured theoretically with various quantum chemical methods and basis set by inclusion of molecular structures.

The polarizabilities of all carbon-chain species, if available, are summarized in Table 1. The dipole moment and polarizability are crucial for the estimation of ion-neutral reaction rates. Ion-neutral reactions play a crucial role in the ISM, especially in cold dark clouds, for the formation and destruction of various species. For non-polar neutrals, the rate coefficient is given by the so-called Langevin expression:

$$k_L = 2\pi e \sqrt{\frac{\alpha_{\text{pola}}}{\mu}}, \quad (8)$$

where  $e$  is the electronic charge,  $\alpha_{\text{pola}}$  is the polarizability,  $\mu$  is the reduced mass of reactants, and cgs-esu units are utilized so that the units for the rate coefficient are  $\text{cm}^3 \text{s}^{-1}$ . This reaction rate coefficient is independent of the temperature and activation energy, and then the ion-molecule reaction can proceed even in cold molecular clouds ( $T \approx 10 \text{ K}$ ). These lead efficient formation of carbon-chain species in the early molecular cloud stage (section 1.2). For polar-neutral species, trajectory scaling relation is usually used. The best-known formula for the ion-dipolar rate coefficient  $k_D$  in the classical regime and for linear neutrals is the Su-Chesnavich expression (Su & Chesnavich 1982). The Su-Chesnavich formula (see Wakelam et al. (2010); Maergoiz et al. (2009)) is based on the parameter  $x$ , defined by

$$x = \frac{\mu_D}{\sqrt{2\alpha_{\text{pola}}k_B T}}, \quad (9)$$

where  $\mu_D$  is an effective dipole moment of the neutral reactant, which is generally very close to the true dipole moment, and  $k_B$  is the Boltzmann constant. As we can see in Table 1, the dipole moment and polarizability become larger for the longer species among the same series. The parameter  $x$  is proportional to the dipole moment and inversely proportional to the square root of polarizability. Thus, it is important to obtain accurate dipole moment and polarizability by quantum calculation for chemical simulations that reproduce the observed abundances (section 4).

Apart from the estimation of the rate coefficient of ion-neutral reactions, the dipole moment is one of the key parameters to determine the column density of observed species. Accurate estimation of the dipole moments is essential to derive realistic values of column density. For instance, the dipole moment of  $\text{C}_4\text{H}$  was used  $\sim 0.87$  Debye in previous literature, which was the value of mixed states, i.e., ground and excited states. The recent result suggests the dipole moment value is 2.10 Debye, which is 2.4 times larger than the values used before (Oyama et al. 2020). As a result, its column densities have been overestimated by a factor of  $\sim 6$ .

### 5.1.3 Binding Energy of Carbon-Chain Species

A major portion of carbon-chain species is primarily formed in the gas phase (Sections 1.2, 2.3, 2.4). In addition, gas-grain exchange occurs, and many reactions occur on the grain surface. The binding energy (BE) plays a pivotal role in interstellar chemistry,

especially grain surface chemistry, which eventually enriches the gas-phase chemistry. Here, we describe the role of BE in interstellar chemical processes.

Binding energy controls several key processes on the grain surface. In particular, two of these are “desorption” and “diffusion”, which are directly related to the BE of the species. Gas-phase species accrete onto the grain surface depending on their energy barriers with the surfaces. The species may bind to the grain surface via physisorption or chemisorption processes.  $E_{\text{des}}$  expresses the binding energy (or desorption energy) of the species. Species attached to grain surfaces can migrate from one site to another depending on the barrier energy of migration ( $E_{\text{dif}}$ ). This is known as a surface diffusion barrier. The surface diffusion barrier is related to the binding energy of the species following the formula  $E_{\text{dif}} = xE_{\text{des}}$ . Even though  $x$  is a key parameter to describe the mobility of species on grain surfaces, the exact value has not historically been well constrained, broadly ranging from 0.3 to 0.8 (Jin & Garrod 2020). Desorption involves the release of species from the grain surface back into the gas phase. There are various desorption mechanisms, with thermal desorption and non-thermal desorption being the most significant. Both mechanisms directly depend on the binding energy (BE) of the species. Hence, the binding energy is a key parameter in understanding desorption processes and final gas phase abundances of carbon chains in astrochemical models, especially for HCCC (Section 4).

Table A1 in Appendix A summarizes the BE values of all carbon-chain species (if available). Most of the BE values are mainly taken from KIDA (<https://kida.astrochem-tools.org/>). BE estimation of a species heavily depends on the methods and surface used for the calculations (e.g., Penteado et al. 2017; Das et al. 2018; Ferrero et al. 2020; Villadsen et al. 2022; Minissale et al. 2022). The BE values of all carbon-chain species, especially higher-order linear chains, are estimated based on the addition method that are provided in KIDA. In this method, for instance, the BE of HC<sub>7</sub>N is estimated by the addition of binding energies of HC<sub>6</sub>N and C. For such calculations 800 K is usually adopted as the BE of a carbon atom. However, we see a huge difference in BE of a carbon atom between the old value and newly measured ones based on quantum chemical study ( $\geq 10,000$  K; Wakelam et al. 2017; Minissale et al. 2022). Thus, the addition method of BE may lead to large uncertainties in estimating BEs of carbon-chain molecules, especially longer ones. If BE of a carbon atom is  $\geq 10,000$  K is correct, the addition method of BE may not be valid, because long carbon-chain species will have huge BE values. A recent experimental study suggests that the BE of carbon atoms is  $\sim 2900$  K (Tsuge et al. 2023) in shallower binding sites. A lower value ( $< 5000$  K) of carbon atom BE has also been reported in Das et al. (2018). Nonetheless, to overcome this issue, dedicated quantum chemical calculations and/or experiments are required to estimate the BE values of carbon-chain species with higher accuracy. This problem becomes more serious for HCCC (sections 2.4 and 3.4.2). In the HCCC mechanism, cyanopolyynes absorb dust grains during the warm-up stage and evaporate into the gas phase in the hot-core stage. If their estimated BE changes, their sublimation temperatures could change leading to different results in the chemical simulations and an impact on the interpretation of observed abundances.



## 6 Experimental Studies

Experimental studies are essential to measure the rotational, vibrational and electronic spectra of molecules with high resolution and accuracy. They can provide accurate spectra, which are used for their precise identification in data obtained from various radio and infrared telescopes (both ground and space based). Laboratory spectroscopy plays a pivotal role in the detection of molecules in space via such telescopes. Numerous experiments have been conducted over the years to analyze the laboratory spectra of various molecular groups. In this context, we provide a concise overview of experiments focused on carbon-chain species. Cyanopolyynes stand out as one of the most intriguing and significant species in recent decades, primarily due to their profound implications for understanding the physical and chemical properties of star-forming environments and carbon-chain chemistry.

The first carbon-chain molecule, the simplest cyanopolyne  $\text{HC}_3\text{N}$ , was detected with the NRAO 140-foot radio telescope in 1971 based on the laboratory rotational spectra, as documented by [Tyler & Sheridan \(1963\)](#) and [Westenberg & Wilson Jr \(1950\)](#). Subsequently, the detection of  $\text{HC}_5\text{N}$ , the second member of this series, relied on measured rotational spectra in a laboratory setting, as reported by [Alexander et al. \(1976\)](#). Furthermore, the existence of higher-order cyanopolyynes, including  $\text{HC}_7\text{N}$ ,  $\text{HC}_9\text{N}$ , and  $\text{HC}_{11}\text{N}$ , in the ISM was confirmed through various laboratory rotational spectra measurements ([Iida et al. 1991](#); [Travers et al. 1996](#); [McCarthy et al. 2000b](#)). In 1998, Thaddeus and colleagues compiled a comprehensive review of numerous studies focusing on the detection of carbon chains in space, alongside corresponding laboratory investigations ([Thaddeus et al. 1998](#)). Henning and Schnaiter’s 1998 review article delves into both astronomical spectroscopy and laboratory investigations pertaining to cosmic carbon ([Henning & Schnaiter 1998](#)). It specifically explores the diverse structural forms of carbon-containing species and their characterization through experimental studies. Laboratory measurements of the gas-phase electronic spectra of various carbon-chain anions have been conducted and subsequently compared to the diffuse interstellar bands ([Tulej et al. 1998](#)). These comparative analyses yield the initial and persuasive indications of the identity of certain carriers responsible for the diffuse interstellar bands. [McCarthy et al. \(2000a\)](#) conducted a comprehensive laboratory study of the rotational spectra of 11 carbon-chain molecules, encompassing cyanopolyynes, isocyanopolyynes, methylcyanopolyynes, and methylpolyynes.

Laboratory experiments to investigate reactions have been developed too. Experimental investigations of carbon-bearing molecule formation via neutral-neutral reactions are summarized in [Kaiser \(2002\)](#). Subsequently, [Savić \(2004\)](#) discussed the formation of small hydrocarbons and ions that were measured under the interstellar and circumstellar conditions by using ion trap conditions. Laboratory and astronomical identification of the first interstellar anion,  $\text{C}_6\text{H}^-$ , was carried out by [McCarthy et al. \(2006\)](#). In the following year, McCarthy and colleagues measured the rotational spectra of  $\text{C}_4\text{H}^-$  and  $\text{C}_8\text{H}^-$  ([Gupta et al. 2007](#)). The ion chemistry of the ISM has been extensively reviewed, featuring detailed discussions of observations and experimental results in the work of [Snow & Bierbaum \(2008\)](#) and the associated references. Cosmic rays have been utilized to measure the formation of unsaturated hydrocarbons in interstellar ice analogs ([Pilling et al. 2012](#)). This was achieved through irradiation

of a mixture comprising  $\text{H}_2\text{O}$ ,  $\text{NH}_3$ ,  $\text{CO}$  (or  $\text{CO}_2$ ), simple alkanes, and  $\text{CH}_3\text{OH}$ . As a result, various compounds were identified, including hexene, cyclohexene, benzene,  $\text{OCN}^-$ ,  $\text{CO}$ ,  $\text{CO}_2$ , as well as a range of aliphatic and aromatic alkenes and alkynes. In a review article by [Zack & Maier \(2014\)](#), various laboratory spectroscopic techniques for studying carbon species of astrophysical significance, including methods like matrix isolation, cavity ringdown, resonance-enhanced multiphoton ionization, and ion trapping, were presented and discussed in detail. In a recent study, [Gatchell et al. \(2021\)](#) found that during energetic collisions with heavy particles, defective PAHs can form and remain stable in the ISM under thermal equilibrium conditions. These defective PAHs exhibit enhanced reactivity compared to intact or photo-fragmented PAHs, potentially playing a crucial role in interstellar chemistry. Very recently rotational spectra of unsaturated carbon chains such as propadienone, cyanovinylacetylene, and allenylacetylene have been measured in the laboratory ([Melli et al. 2022](#)).

Here we briefly describe a few studies of carbon-chain species, mainly focusing on molecules containing a benzene ring. The first benzene ring ( $\text{C}_6\text{H}_6$ ) and its cyano derivative, benzonitrile (*c*- $\text{C}_6\text{H}_5\text{CN}$ ) were detected toward CRL 618 and TMC-1, respectively, based on their laboratory infrared and rotational spectra (e.g., [McGuire et al. 2018](#)). The most striking and groundbreaking results, the detection of fullerenes ( $\text{C}_{60}$ ,  $\text{C}_{70}$ ) and its protonated form  $\text{C}_{60}^+$ , was also based on their laboratory data (e.g., [Martin et al. 1993](#); [Nemes et al. 1994](#); [Kato et al. 1991](#)). In the 2020s, several PAHs have been identified in the ISM with the aid of their laboratory spectra. For instance, two isomers of cyanonaphthalene ([McGuire et al. 2021](#); [McNaughton et al. 2018](#)), two isomers of ethynyl cyclopentadiene ([McCarthy et al. 2021](#); [Cernicharo et al. 2021d](#); [McCarthy et al. 2020](#)), 2-cyanoindene ([Sita et al. 2022](#)), fulvenallene ([McCarthy et al. 2020](#); [Sakaizumi et al. 1993](#)), ethynyl cyclopropenylidene, cyclopentadiene, and indene ([Cernicharo et al. 2021b](#); [Burkhardt et al. 2021a](#), and references therein). Recently, [Martínez et al. \(2020\)](#) investigated the growth of carbon-containing species from C and  $\text{H}_2$  in conditions analogous of circumstellar envelopes around carbon-rich AGB stars. They found that nanometer-sized carbon particles, pure carbon clusters, and aliphatic carbon species are formed efficiently, whereas aromatics are generated at trace levels and no fullerenes are detected. They also suggested that the formation of aromatic species must occur via other processes, such as the thermal processing of aliphatic material on the surface of dust grains. The astronomical detection of most of the carbon-chain species was based on their laboratory rotational spectra. A more comprehensive list of references to laboratory experiments of rotational, vibrational, and electronic spectra of different molecules can be found in the individual papers reporting their interstellar detection.

## 7 Summary and Open Questions of This Review

### 7.1 Summary

We have reviewed carbon-chain chemistry in the ISM, mainly focusing on recent updates. A summary of our main points is as follows.

1. By the end of 2023, 132 carbon-chain species have been detected in the ISM. This accounts for almost 43% of 305 interstellar molecules detected in the ISM or circumstellar shells. These include various families of carbon-chain species, involving elements of O, N, S, P, and Mg.
2. Two line survey projects toward TMC-1 CP (GOTHAM and QUIJOTE) have recently reported detections of many new carbon-chain species. Abundances of some of these species are not yet reproducible in chemical simulations indicating a need for improved models.
3. In addition to the cold gas conditions of early-phase molecular clouds, carbon-chain formation also occurs around low-, intermediate- and high-mass YSOs. Warm Carbon-Chain Chemistry (WCCC) was found in 2008 around low-mass YSOs, while Hot Carbon-Chain Chemistry (HCCC) has been proposed based on recent observations around high-mass YSOs.
4. Chemical simulations aim to explain conditions forming hot corino and WCCC sources. There are several possible parameters to reproduce the chemical differentiation: e.g., UV radiation field and temperature of the prestellar phase. The most plausible effect is the ISRF rather than the timescale of the prestellar phase.
5. Thanks to high-angular resolution and high-sensitivity observations with ALMA, several carbon-chain species (e.g., CCH, *c*-C<sub>3</sub>H<sub>2</sub>, HC<sub>3</sub>N) have been detected from protoplanetary disks around Herbig Ae and T Tauri stars. Vibrationally-excited lines of HC<sub>3</sub>N have been found to trace disk structures around massive stars.
6. Circumstellar envelopes around carbon-rich AGB stars and planetary nebulae are unique factories of carbon chemistry. Infrared observations have revealed the presence of PAHs and fullerenes in such environments. Recent laboratory experiments investigated chemistry in such regions.
7. Carbon-chain species have been detected even in extragalactic environments, such as the starburst galaxy NGC253 via the ALCHEMI project. In the Large Magellanic Cloud (LMC), CCH emission has been found to trace outflow cavities, as seen in low-mass YSOs in our Galaxy.
8. Theoretical and experimental studies are important for the observational detection of carbon-chain species and for obtaining an understanding of their formation and destruction processes. Developments of these techniques are important to reveal carbon-chain chemistry in various physical conditions in the ISM.
9. Recent new approaches with machine learning will provide us with predictions of possible detectable species in the ISM, which is expected to help accelerate the discoveries of new interstellar molecules.

The presence of carbon-chain species in the ISM has been known since the early 1970s, and many researchers have investigated their features through observations, chemical simulations, laboratory experiments, and quantum calculations. Recent findings raise new questions about carbon-chain chemistry, and it is an exciting time of progress. To solve the newly raised questions, collaborative research involving observations, laboratory experiments, and chemical simulations is crucial.

To understand the carbon-chain chemistry better by observational methods, we need more dedicated low-frequency, high-sensitivity, and high angular resolution observations towards dark clouds, low-, intermediate-, and high-mass YSOs, and other

environments. ALMA Band 1 is now available, and the Square Kilometer Array (SKA) and ngVLA will become available in the near future. Observations using these facilities will be essential to reveal links between ISM physics and carbon-chain chemistry, the origin of chemical differentiation around YSOs, and relationships between WCCC and HCCC. In addition, future observational studies combining infrared data (e.g., from JWST, Thirty Meter Telescope (TMT), European Extremely Large Telescope (E-ELT)) and radio (ALMA, ngVLA, SKA, and future single-dish) telescopes have the potential for breakthrough results. For instance, relationships between PAHs/small dust grains and common carbon-chain species, which can be observed by infrared and radio regimes, respectively, can be studied by such a combination. These studies will help open up the astrochemical field of “the lifecycle of carbon in the ISM”.

## 7.2 Open Key Questions

Recent new discoveries of carbon-chain molecules in the ISM have raised new questions, and we have realized that our knowledge of carbon-chain chemistry is far from complete. We highlight the following open questions:

1. How do large carbon-chain species, which have been found in TMC-1 CP, form? Is there a role for both bottom-up and top-down processes?
2. How are PAHs and fullerenes related to other carbon-chain species in the ISM?
3. In what form is the main carbon reservoir ejected into the ISM **from evolved stars**? How does it propagate into the ISM and become incorporated into molecular clouds where the next-generation of star formation occurs?
4. Which, if any, important formation/destruction processes of carbon-chain species are missing from current chemical models?
5. Can we estimate more accurate branching ratios for different species (e.g., isomers) in electron recombination reactions?
6. How can we obtain accurate binding energy of carbon-chain species?
7. Are there reactions forming and/or destroying carbon-chain species on dust surfaces and within ice mantles?

Answers to these questions likely require combined efforts of multi-wavelength observational, theoretical, and experimental study.

## Appendix A Binding Energies

Table A1 summarizes the binding energies (BE) of carbon-chain species.

**Table A1** Binding energy (BE) of carbon-chain species

Species	BE (K)	Species	BE (K)	Species	BE (K)
C <sub>2</sub>	10000	C <sub>8</sub> N	7200	C <sub>3</sub> O	2750
C <sub>3</sub>	2500	C <sub>9</sub> N	8000	C <sub>5</sub> O	4350
C <sub>4</sub>	3200	C <sub>10</sub> N	8800	C <sub>7</sub> O	5950
C <sub>5</sub>	4000	C <sub>2</sub> H <sub>2</sub>	2587	C <sub>9</sub> O	7550
C <sub>6</sub>	4800	C <sub>2</sub> H <sub>4</sub>	2500	HC <sub>2</sub> O	2400
C <sub>7</sub>	5600	C <sub>2</sub> H <sub>5</sub>	3100	SiC <sub>2</sub>	4300
C <sub>8</sub>	6400	C <sub>2</sub> H <sub>6</sub>	1600	SiC <sub>3</sub>	5100
C <sub>9</sub>	7200	C <sub>4</sub> H <sub>2</sub>	4187	SiC <sub>4</sub>	5900
C <sub>10</sub>	8000	C <sub>5</sub> H <sub>2</sub>	4987		
C <sub>11</sub>	9600	C <sub>6</sub> H <sub>2</sub>	5787		
C <sub>2</sub> H	3000	C <sub>7</sub> H <sub>2</sub>	6587		
<i>l</i> -C <sub>3</sub> H	4000	C <sub>2</sub> P	4300		
<i>c</i> -C <sub>3</sub> H	5200	C <sub>3</sub> P	5900		
C <sub>4</sub> H	3737	C <sub>4</sub> P	7500		
C <sub>5</sub> H	4537	C <sub>2</sub> S	2700		
C <sub>6</sub> H	5337	C <sub>3</sub> S	3500		
C <sub>7</sub> H	6137	C <sub>4</sub> S	4300		
C <sub>8</sub> H	6937	HC <sub>3</sub> N	4580		
<i>c</i> -C <sub>3</sub> H <sub>2</sub>	5900	HC <sub>4</sub> N	5380		
C <sub>2</sub> N	2400	HC <sub>5</sub> N	6180		
C <sub>3</sub> N	3200	HC <sub>6</sub> N	7780		
C <sub>4</sub> N	4000	HC <sub>7</sub> N	7780		
C <sub>5</sub> N	4800	HC <sub>8</sub> N	9380		
C <sub>6</sub> N	5600	HC <sub>9</sub> N	9380		
C <sub>7</sub> N	6400	C <sub>2</sub> O	1950		

Taken from the KIDA (<https://kida.astrochem-tools.org/>), and also see Wakelam et al. (2017), Penteadó et al. (2017), Das et al. (2018).

## Appendix B Observed Column Densities in TMC-1 CP and IRC+10216

Tables B2 and B3 provide information on column densities at TMC-1 CP and IRC+10216. These values are used for Figs.5 and 11 in sections 3.1 and 3.7, respectively.

**Table B2:** Observed column density of carbon chain species toward TMC-1 CP

Species	$N$ (cm $^{-2}$ )	Telescope	Ref.
HC <sub>3</sub> N	$(2.3 \pm 0.2) \times 10^{14}$	RT40m	Cernicharo et al. (2020a)
HC <sub>5</sub> N	$(1.08 \pm 0.2) \times 10^{14}$	RT40m	Cernicharo et al. (2020a)
HC <sub>7</sub> N	$(6.4 \pm 0.4) \times 10^{13}$	RT40m	Cernicharo et al. (2020a)
HC <sub>9</sub> N	$2.15^{+0.23}_{-0.20} \times 10^{13}$	GBT100m	Loomis et al. (2021)
HC <sub>11</sub> N	$7.8^{+21.27}_{-5.08} \times 10^{11}$	GBT100m	Loomis et al. (2021)
C <sub>2</sub> H	$(6.5 \pm 2.7) \times 10^{14}$		Sakai et al. (2010)
C <sub>4</sub> H	$1.62^{+0.25}_{-0.22} \times 10^{14}$	GBT100m	Remijan et al. (2023)
C <sub>4</sub> H <sup>-</sup>	$6.79^{+4.68}_{-2.59} \times 10^{10}$	GBT100m	Remijan et al. (2023)
C <sub>6</sub> H	$5.17^{+0.62}_{-1.83} \times 10^{12}$	GBT100m	Remijan et al. (2023)
C <sub>6</sub> H <sup>-</sup>	$2.84^{+0.58}_{-0.44} \times 10^{11}$	GBT100m	Remijan et al. (2023)
C <sub>8</sub> H	$7.25^{+2.06}_{-1.23} \times 10^{11}$	GBT100m	Remijan et al. (2023)
C <sub>8</sub> H <sup>-</sup>	$8.00^{+7.79}_{-2.59} \times 10^{10}$	GBT100m	Remijan et al. (2023)
C <sub>10</sub> H	$2.02^{+2.68}_{-0.82} \times 10^{11}$	GBT100m	Remijan et al. (2023)
C <sub>10</sub> H <sup>-</sup>	$4.04^{+10.67}_{-2.23} \times 10^{11}$	GBT100m	Remijan et al. (2023)
HC <sub>2</sub> O	$(7.7 \pm 0.7) \times 10^{11}$	RT40m	Cernicharo et al. (2021a)
HC <sub>3</sub> O	$(1.3 \pm 0.2) \times 10^{11}$	RT40m	Cernicharo et al. (2021a)
HC <sub>4</sub> O	$\leq 9.0 \times 10^{10}$	RT40m	Cernicharo et al. (2021a)
HC <sub>5</sub> O	$(1.4 \pm 0.2) \times 10^{12}$	RT40m	Cernicharo et al. (2021a)
HC <sub>6</sub> O	$\leq 1.8 \times 10^{11}$	RT40m	Cernicharo et al. (2021a)
HC <sub>7</sub> O	$(6.5 \pm 0.5) \times 10^{11}$	RT40m	Cernicharo et al. (2021a)
C <sub>2</sub> O	$(7.5 \pm 0.3) \times 10^{11}$	RT40m	Cernicharo et al. (2021a)
C <sub>3</sub> O	$(1.2 \pm 0.2) \times 10^{12}$	RT40m	Cernicharo et al. (2021a)
C <sub>4</sub> O	$\leq 9.0 \times 10^{10}$	RT40m	Cernicharo et al. (2021a)
C <sub>5</sub> O	$(1.5 \pm 0.2) \times 10^{10}$	RT40m	Cernicharo et al. (2021a)
C <sub>6</sub> O	$\leq 1.1 \times 10^{11}$	RT40m	Cernicharo et al. (2021a)
C <sub>2</sub> S	$(5.5 \pm 0.65) \times 10^{13}$	RT40m	Cernicharo et al. (2021f)
C <sub>3</sub> S	$(1.3 \pm 0.13) \times 10^{13}$	RT40m	Cernicharo et al. (2021f)
C <sub>4</sub> S	$(3.8 \pm 0.4) \times 10^{10}$	RT40m	Cernicharo et al. (2021e)
C <sub>5</sub> S	$(5.0 \pm 1.0) \times 10^{10}$	RT40m	Cernicharo et al. (2021e)

CH <sub>3</sub> C <sub>3</sub> N	$(8.66 \pm 0.46) \times 10^{11}$	GBT100m	Siebert et al. (2022)
CH <sub>3</sub> C <sub>5</sub> N	$(2.86 \pm 0.30) \times 10^{11}$	GBT100m	Siebert et al. (2022)
CH <sub>3</sub> C <sub>7</sub> N	$(0.86 \pm 0.19) \times 10^{11}$	GBT100m	Siebert et al. (2022)
CH <sub>3</sub> C <sub>4</sub> H	$(100.8 \pm 5.7) \times 10^{11}$	GBT100m	Siebert et al. (2022)
CH <sub>3</sub> C <sub>6</sub> H	$(10.4 \pm 0.72) \times 10^{11}$	GBT100m	Siebert et al. (2022)
<i>c</i> -C <sub>6</sub> H <sub>5</sub> CN	$(4.0 \pm 1.6) \times 10^{11}$	GBT100m	McGuire et al. (2018)
<i>c</i> -C <sub>9</sub> H <sub>8</sub>	$9.04^{+0.96}_{-0.96} \times 10^{12}$	GBT100m	Sita et al. (2022)
<i>c</i> -C <sub>5</sub> H <sub>4</sub> CCH <sub>2</sub>	$(2.7 \pm 0.3) \times 10^{12}$	RT40m	Cernicharo et al. (2022b)
<i>c</i> -C <sub>5</sub> H <sub>6</sub>	$(1.2 \pm 0.3) \times 10^{13}$	RT40m	Cernicharo et al. (2021d)
1- <i>c</i> -C <sub>5</sub> H <sub>5</sub> CN	$8.27^{+0.9}_{-1.0} \times 10^{11}$	GBT100m	Lee et al. (2021a)
2- <i>c</i> -C <sub>5</sub> H <sub>5</sub> CN	$1.89^{+0.18}_{-0.15} \times 10^{11}$	GBT100m	Lee et al. (2021a)
1-C <sub>10</sub> H <sub>7</sub> CN	$7.35^{+3.33}_{-4.63} \times 10^{11}$	GBT100m	McGuire et al. (2021)
2-C <sub>10</sub> H <sub>7</sub> CN	$7.05^{+3.23}_{-4.50} \times 10^{11}$	GBT100m	McGuire et al. (2021)
1- <i>c</i> -C <sub>5</sub> H <sub>5</sub> CCH	$(1.4 \pm 0.2) \times 10^{12}$	RT40m	Cernicharo et al. (2021d)
2- <i>c</i> -C <sub>5</sub> H <sub>5</sub> CCH	$(2.0 \pm 0.4) \times 10^{12}$	RT40m	Cernicharo et al. (2021d)
<i>c</i> -C <sub>6</sub> H <sub>4</sub>	$(5.0 \pm 1.0) \times 10^{11}$	RT40m	Cernicharo et al. (2021c)
C <sub>6</sub> H <sub>5</sub> CCH	$(3.00 \pm 0.5) \times 10^{12}$	RT40m	Loru et al. (2023)
C <sub>9</sub> H <sub>7</sub> CN	$2.10^{+0.60}_{-0.46} \times 10^{11}$	GBT100m	Sita et al. (2022)
<i>c</i> -C <sub>3</sub> HCCH	$(3.1 \pm 0.8) \times 10^{11}$	RT40m	Cernicharo et al. (2021b)
E-1-C <sub>4</sub> H <sub>5</sub> CN	$3.8^{+1.0}_{-0.91} \times 10^{10}$	GBT100m	Cooke et al. (2023)
<i>c</i> -C <sub>3</sub> H	$6.12^{+12.24}_{-3.06} \times 10^{12}$	IRAM30m	Loison et al. (2017)
<i>l</i> -C <sub>3</sub> H	$1.12^{+2.24}_{-0.56} \times 10^{12}$	IRAM30m	Loison et al. (2017)
<i>c</i> -C <sub>3</sub> H <sub>2</sub>	$(1.22 \pm 0.61) \times 10^{14}$	IRAM30m	Loison et al. (2017)
<i>l</i> -C <sub>3</sub> H <sub>2</sub>	$1.82^{+3.64}_{-0.91} \times 10^{12}$	IRAM30m	Loison et al. (2017)
<i>c</i> -C <sub>5</sub> H	$(9.0 \pm 0.9) \times 10^{10}$	RT40m	Cabezas et al. (2022a)
<i>l</i> -C <sub>5</sub> H	$(1.3 \pm 0.3) \times 10^{12}$	RT40m	Cabezas et al. (2022a)
<i>l</i> -C <sub>5</sub> H <sub>2</sub>	$(1.80 \pm 0.5) \times 10^{10}$	RT40m	Cabezas et al. (2021)

**Acknowledgments.** K.T. is grateful to Professor Eric Herbst (University of Virginia) for leading me to the astrochemical field, working with me, and giving a lot of comments on studies of carbon-chain molecules that are presented in this article. K.T. appreciates Professor Masao Saito (National Astronomical Observatory of Japan) for giving his advice and continuous encouragement. K.T. is supported by JSPS KAKENHI grant No.JP20K14523. P.G acknowledges the support from the Chalmers Initiative of Cosmic Origins Postdoctoral Fellowship. We thank Professor Fumitaka Nakamura (National Astronomical Observatory of Japan) and Professor Kazuhito Dobashi (Tokyo Gakugei University) for providing original data of mapping observations of carbon-chain species toward TMC-1 obtained by the Nobeyama 45m radio telescope. We would also like to thank Dr. Emmanuel E. Etim for his comments and suggestions. J.C.T. acknowledges support from ERC Advanced Grant MSTAR. We appreciate Dr. Ryan Lau for his comments and suggestions.



**Table B3** Column density of observed carbon chain species towards IRC+10216

Species	$N$ ( $\text{cm}^{-2}$ )	Telescope	Ref.
HC <sub>3</sub> N	$(4.5 \pm 0.20) \times 10^{14}$	RT40m	Cernicharo et al. (2020a)
HC <sub>5</sub> N	$(8.3 \pm 0.70) \times 10^{14}$	RT40m	Pardo et al. (2020)
HC <sub>7</sub> N	$(3.5 \pm 0.70) \times 10^{14}$	RT40m	Pardo et al. (2020)
HC <sub>9</sub> N	$(7.6 \pm 1.40) \times 10^{13}$	RT40m	Pardo et al. (2020)
C <sub>2</sub> S	$(5.0 \pm 0.30) \times 10^{13}$	IRAM30m	Agúndez et al. (2014)
C <sub>3</sub> S	$(1.7 \pm 0.10) \times 10^{13}$	IRAM30m	Agúndez et al. (2014)
C <sub>4</sub> S	$< 7.0 \times 10^{12}$	IRAM30m	Agúndez et al. (2014)
C <sub>5</sub> S	$(2 - 14) \times 10^{12}$	IRAM30m	Agúndez et al. (2014)
MgCCH	$(2.0 \pm 0.4) \times 10^{12}$	RT40m	Agúndez et al. (2014)
MgC <sub>4</sub> H	$(2.2 \pm 0.50) \times 10^{13}$	RT40m	Cernicharo et al. (2019)
MgC <sub>6</sub> H	$(2.0 \pm 0.90) \times 10^{13}$	RT40m	Pardo et al. (2021)
MgC <sub>4</sub> H <sup>+</sup>	$(4.8 \pm 0.30) \times 10^{11}$	RT40m	Cernicharo et al. (2023a)
MgC <sub>6</sub> H <sup>+</sup>	$(2.5 \pm 0.30) \times 10^{12}$	RT40m	Cernicharo et al. (2023a)
MgC <sub>3</sub> N	$(3.6 \pm 0.60) \times 10^{12}$	RT40m	Cernicharo et al. (2019)
MgC <sub>5</sub> N	$(4.7 \pm 1.30) \times 10^{12}$	RT40m	Pardo et al. (2021)
MgC <sub>3</sub> N <sup>+</sup>	$(1.2 \pm 0.20) \times 10^{11}$	RT40m	Cernicharo et al. (2023a)
MgC <sub>5</sub> N <sup>+</sup>	$(1.1 \pm 0.20) \times 10^{11}$	RT40m	Cernicharo et al. (2023a)
C <sub>2</sub> H	$(3.84 \pm 0.09) \times 10^{15}$	IRAM30m, Herschel	De Beck et al. (2012)
C <sub>3</sub> H	$(7.0 \pm 1.40) \times 10^{13}$	IRAM30m	Cernicharo et al. (2000)
C <sub>4</sub> H	$(5.1 \pm 1.02) \times 10^{14}$	IRAM30m	Oyama et al. (2020)
C <sub>5</sub> H	$(4.4 \pm 0.88) \times 10^{13}$	IRAM30m	Cernicharo et al. (2000)
C <sub>6</sub> H	$(5.5 \pm 1.10) \times 10^{13}$	IRAM30m	Cernicharo et al. (2000)
C <sub>7</sub> H	$(2.2 \pm 0.44) \times 10^{12}$	IRAM30m	Cernicharo et al. (2000)
C <sub>8</sub> H	$(1.0 \pm 0.20) \times 10^{13}$	IRAM30m	Cernicharo et al. (2000)
C <sub>2</sub> N	$(4.0 \pm 2.00) \times 10^{13}$	ARO12m	Anderson & Ziurys (2014)
C <sub>3</sub> N	$(4.0 \pm 0.10) \times 10^{15}$	ARO12m	Anderson & Ziurys (2014)
C <sub>3</sub> N <sup>-</sup>	$(1.6 \pm 0.60) \times 10^{12}$	IRAM30m	Thaddeus et al. (2008)
C <sub>5</sub> N	$(6.0 \pm 1.20) \times 10^{12}$	IRAM30m	Guélin et al. (1998)
C <sub>5</sub> N <sup>-</sup>	$(3.4 \pm 0.68) \times 10^{12}$	IRAM30m	Cernicharo et al. (2008)

When we cannot obtain errors from the original papers, we indicate 20% errors.

## References

- Adams, N. G., Smith, D., Giles, K., & Herbst, E. 1989, *A&A*, 220, 269
- Agúndez, M., Cabezas, C., Marcelino, N., et al. 2023, *A&A*, 669, L1
- Agúndez, M., Cernicharo, J., & Guélin, M. 2014, *A&A*, 570, A45
- Agúndez, M., Cernicharo, J., & Guélin, M. 2015, *A&A*, 577, L5
- Agúndez, M., Cernicharo, J., Quintana-Lacaci, G., et al. 2017, *A&A*, 601, A4
- Aikawa, Y., Furuya, K., Yamamoto, S., & Sakai, N. 2020, *ApJ*, 897, 110
- Aikawa, Y., Wakelam, V., Garrod, R. T., & Herbst, E. 2008, *ApJ*, 674, 984
- Alexander, A., Kroto, H., & Walton, D. 1976, *Journal of Molecular Spectroscopy*, 62, 175
- Anderson, J. K. & Ziurys, L. M. 2014, *ApJL*, 795, L1
- Apponi, A. J., McCarthy, M. C., Gottlieb, C. A., & Thaddeus, P. 1999, *ApJL*, 516, L103

Araki, M., Takano, S., Sakai, N., et al. 2016, *ApJ*, 833, 291

Avery, L. W., Broten, N. W., MacLeod, J. M., Oka, T., & Kroto, H. W. 1976, *ApJL*, 205, L173

Bâldea, I. 2019, *Advanced Theory and Simulations*, 2, 1900084

Barone, V., Biczysko, M., & Puzzarini, C. 2015, *Accounts of chemical research*, 48, 1413

Benson, P. J., Caselli, P., & Myers, P. C. 1998, *ApJ*, 506, 743

Bergner, J. B., Guzmán, V. G., Öberg, K. I., Loomis, R. A., & Pegues, J. 2018, *ApJ*, 857, 69

Bernath, P. F., Hinkle, K. H., & Keady, J. J. 1989, *Science*, 244, 562

Berné, O. & Tielens, A. G. G. M. 2012, *Proceedings of the National Academy of Science*, 109, 401

Blanksby, S. J., McAnoy, A. M., Dua, S., & Bowie, J. H. 2001, *Monthly Notices of the Royal Astronomical Society*, 328, 89

Botschwina, P. 1987, *Chemical Physics Letters*, 139, 255

Botschwina, P. 1991, *The Journal of Chemical Physics*, 95, 4360

Botschwina, P. 1993, *Journal of physical chemistry*, 99, 6217

Broten, N. W., Oka, T., Avery, L. W., MacLeod, J. M., & Kroto, H. W. 1978, *ApJL*, 223, L105

Brown, R. D., Eastwood, F. W., Elmes, P. S., & Godfrey, P. D. 1983, *Journal of the American Chemical Society*, 105, 6496

Brünken, S., Gupta, H., Gottlieb, C. A., McCarthy, M. C., & Thaddeus, P. 2007, *ApJL*, 664, L43

Burkhardt, A. M., Herbst, E., Kalenskii, S. V., et al. 2018, *Monthly Notices of the Royal Astronomical Society*, 474, 5068

Burkhardt, A. M., Long Kelvin Lee, K., Bryan Changala, P., et al. 2021a, *ApJL*, 913, L18

Burkhardt, A. M., Loomis, R. A., Shingledecker, C. N., et al. 2021b, *Nature Astronomy*, 5, 181

Cabezas, C., Agúndez, M., Fuentetaja, R., et al. 2022a, *A&A*, 663, L2

Cabezas, C., Agúndez, M., Marcelino, N., et al. 2022b, *A&A*, 657, L4

Cabezas, C., Agúndez, M., Marcelino, N., et al. 2022c, *A&A*, 659, L8

Cabezas, C., Pardo, J. R., Agúndez, M., et al. 2023a, *A&A*, 672, L12

Cabezas, C., Tang, J., Agúndez, M., et al. 2023b, *A&A*, 676, L5

Cabezas, C., Tercero, B., Agúndez, M., et al. 2021, *A&A*, 650, L9

Cami, J., Bernard-Salas, J., Peeters, E., & Malek, S. E. 2010, *Science*, 329, 1180

Caminati, W. 1993, *Journal of the Chemical Society, Faraday Transactions*, 89, 4153

Caselli, P. & Ceccarelli, C. 2012, *A&Ar*, 20, 56

Caselli, P., Pineda, J. E., Sipilä, O., et al. 2022, *ApJ*, 929, 13

Cernicharo, J., Agúndez, M., Cabezas, C., et al. 2022a, *A&A*, 657, L16

Cernicharo, J., Agúndez, M., Cabezas, C., et al. 2021a, *A&A*, 656, L21

Cernicharo, J., Agúndez, M., Cabezas, C., et al. 2021b, *A&A*, 649, L15

Cernicharo, J., Agúndez, M., Kaiser, R. I., et al. 2021c, *A&A*, 652, L9

Cernicharo, J., Agúndez, M., Kaiser, R. I., et al. 2021d, *A&A*, 655, L1

Cernicharo, J., Cabezas, C., Agúndez, M., et al. 2021e, *A&A*, 648, L3

- Cernicharo, J., Cabezas, C., Endo, Y., et al. 2021f, *A&A*, 646, L3
- Cernicharo, J., Cabezas, C., Pardo, J. R., et al. 2019, *A&A*, 630, L2
- Cernicharo, J., Cabezas, C., Pardo, J. R., et al. 2023a, *A&A*, 672, L13
- Cernicharo, J., Fuentetaja, R., Agúndez, M., et al. 2022b, *A&A*, 663, L9
- Cernicharo, J., Fuentetaja, R., Cabezas, C., et al. 2022c, *A&A*, 663, L5
- Cernicharo, J., Gottlieb, C. A., Guelin, M., et al. 1991a, *ApJL*, 368, L39
- Cernicharo, J., Gottlieb, C. A., Guelin, M., et al. 1991b, *ApJL*, 368, L43
- Cernicharo, J. & Guelin, M. 1996, *A&A*, 309, L27
- Cernicharo, J., Guélin, M., Agúndez, M., et al. 2007, *A&A*, 467, L37
- Cernicharo, J., Guélin, M., Agúndez, M., McCarthy, M. C., & Thaddeus, P. 2008, *ApJL*, 688, L83
- Cernicharo, J., Guélin, M., & Kahane, C. 2000, *Astronomy and Astrophysics Supplement Series*, 142, 181
- Cernicharo, J., Guélin, M., & Pardo, J. R. 2004, *ApJL*, 615, L145
- Cernicharo, J., Heras, A. M., Tielens, A. G. G. M., et al. 2001, *ApJL*, 546, L123
- Cernicharo, J., Kahane, C., Gomez-Gonzalez, J., & Guelin, M. 1986, *A&A*, 164, L1
- Cernicharo, J., Marcelino, N., Agúndez, M., et al. 2020a, *A&A*, 642, L8
- Cernicharo, J., Marcelino, N., Agúndez, M., et al. 2020b, *A&A*, 642, L17
- Cernicharo, J., Marcelino, N., Pardo, J. R., et al. 2020c, *A&A*, 641, L9
- Cernicharo, J., Pardo, J. R., Cabezas, C., et al. 2023b, *A&A*, 670, L19
- Chantzios, J., Rivilla, V. M., Vasyunin, A., et al. 2020, *A&A*, 633, A54
- Chapillon, E., Dutrey, A., Guilloteau, S., et al. 2012, *ApJ*, 756, 58
- Chiong, C.-C., Nakamura, F., Nishimura, A., et al. 2022, in *Society of Photo-Optical Instrumentation Engineers (SPIE) Conference Series*, Vol. 12190, Millimeter, Submillimeter, and Far-Infrared Detectors and Instrumentation for Astronomy XI, ed. J. Zmuidzinas & J.-R. Gao, 121900M
- Choe, J. C. 2021, *ApJ*, 914, 136
- Compagnon, I., Antoine, R., Broyer, M., et al. 2001, *Phys. Rev. A*, 64, 025201
- Cooke, I. R., Xue, C., Changala, P. B., et al. 2023, *ApJ*, 948, 133
- Cordiner, M. A., Charnley, S. B., Kisiel, Z., McGuire, B. A., & Kuan, Y. J. 2017, *ApJ*, 850, 187
- Cox, A. P., Ewart, I. C., & Stigliani, W. M. 1975, *Journal of the Chemical Society, Faraday Transactions 2: Molecular and Chemical Physics*, 71, 504
- Crawford, T. D., Stanton, J. F., Saeh, J. C., & Schaefer, H. F. 1999, *Journal of the American Chemical Society*, 121, 1902
- Csengeri, T., Bontemps, S., Wyrowski, F., et al. 2018, *A&A*, 617, A89
- Cuadrado, S., Goicoechea, J. R., Pilleri, P., et al. 2015, *A&A*, 575, A82
- Dalgarno, A. 2008, *The Annual Review of Astronomy and Astrophysics*, 46, 1
- Das, A., Sil, M., Gorai, P., Chakrabarti, S. i. K., & Loison, J. C. 2018, *ApJs*, 237, 9
- De Beck, E., Lombaert, R., Agúndez, M., et al. 2012, *A&A*, 539, A108
- Dickens, J. E., Irvine, W. M., Snell, R. L., et al. 2000, *ApJ*, 542, 870
- Dobashi, K., Shimoikura, T., Nakamura, F., et al. 2018, *ApJ*, 864, 82
- Dobashi, K., Shimoikura, T., Ochiai, T., et al. 2019, *ApJ*, 879, 88
- Etim, E. E. & Arunan, E. 2017, *APSS*, 362, 4
- Etim, E. E., Gorai, P., Das, A., Chakrabarti, S. K., & Arunan, E. 2016, *ApJ*, 832, 144

- Etim, E. E., Gorai, P., Ghosh, R., & Das, A. 2020, *Spectrochimica Acta Part A: Molecular Spectroscopy*, 230, 118011
- Ewing, D. 1989, *Journal of the American Chemical Society*, 111, 8809
- Fatima, M., Müller, H. S. P., Zingsheim, O., et al. 2023, *A&A*, 680, A25
- Ferrero, S., Zamirri, L., Ceccarelli, C., et al. 2020, *ApJ*, 904, 11
- Foing, B. H. & Ehrenfreund, P. 1994, *nat*, 369, 296
- Fonfría, J. P., Agúndez, M., Cernicharo, J., Richter, M. J., & Lacy, J. H. 2018, *ApJ*, 852, 80
- Fontani, F., Ceccarelli, C., Favre, C., et al. 2017, *A&A*, 605, A57
- Fortenberry, R. C. 2015, *Journal of Physical Chemistry A*, 119, 9941
- Fortenberry, R. C. 2017, *International Journal of Quantum Chemistry*, 117, 81
- Frisch, M. J., Trucks, G. W., Schlegel, H. B., et al. 2013, *Gaussian 09 Revision D.01*, gaussian Inc. Wallingford CT
- Fuentetaja, R., Agúndez, M., Cabezas, C., et al. 2022a, *A&A*, 667, L4
- Fuentetaja, R., Cabezas, C., Agúndez, M., et al. 2022b, *A&A*, 663, L3
- Furuya, K., Aikawa, Y., Sakai, N., & Yamamoto, S. 2011, *ApJ*, 731, 38
- Garrod, R. T. & Herbst, E. 2006, *A&A*, 457, 927
- Gatchell, M., Ameixa, J., Ji, M., et al. 2021, *Nature Communications*, 12, 6646
- Ghiasi, R. & Monnajemi, M. 2006, *Journal of the Korean Chemical Society*, 50, 281
- Gordon, V. D., McCarthy, M., Apponi, A., & Thaddeus, P. 2002, *ApJs*, 138, 297
- Graedel, T. E., Langer, W. D., & Frerking, M. A. 1982, *ApJs*, 48, 321
- Graninger, D. M., Wilkins, O. H., & Öberg, K. I. 2016, *ApJ*, 819, 140
- Guelin, M. & Cernicharo, J. 1991, *A&A*, 244, L21
- Guelin, M., Cernicharo, J., Travers, M. J., et al. 1997, *A&A*, 317, L1
- Guelin, M., Green, S., & Thaddeus, P. 1978, *ApJL*, 224, L27
- Guelin, M., Neininger, N., & Cernicharo, J. 1998, *A&A*, 335, L1
- Guelin, M. & Thaddeus, P. 1977, *ApJL*, 212, L81
- Gupta, H., Brünken, S., Tamassia, F., et al. 2007, *The Astrophysical Journal*, 655, L57
- Guzmán, V. V., Bergner, J. B., Law, C. J., et al. 2021, *ApJs*, 257, 6
- Guzmán, V. V., Pety, J., Goicoechea, J. R., et al. 2015, *ApJL*, 800, L33
- Halfen, D. T., Clouthier, D. J., & Ziurys, L. M. 2008, *ApJL*, 677, L101
- Hassel, G. E., Herbst, E., & Garrod, R. T. 2008, *ApJ*, 681, 1385
- Henning, T. & Schnaiter, M. 1998, *Earth, Moon, and Planets*, 80, 179
- Henning, T., Semenov, D., Guilloteau, S., et al. 2010, *ApJ*, 714, 1511
- Herbst, E. 1983, *ApJs*, 53, 41
- Herbst, E., Adams, N. G., & Smith, D. 1983, *ApJ*, 269, 329
- Herbst, E., Smith, D., & Adams, N. G. 1984, *A&A*, 138, L13
- Herbst, E. & van Dishoeck, E. F. 2009, *The Annual Review of Astronomy and Astrophysics*, 47, 427
- Higuchi, A. E., Sakai, N., Watanabe, Y., et al. 2018, *ApJs*, 236, 52
- Hinkle, K. W., Keady, J. J., & Bernath, P. F. 1988, *Science*, 241, 1319
- Hirano, T., Nakagawa, N., Murakami, A., & Nomura, O. 1989, *Chemical Physics Letters*, 162, 89
- Hollenbach, D. & Salpeter, E. E. 1971, *ApJ*, 163, 155
- Hollis, J. M., Remijan, A. J., Jewell, P. R., & Lovas, F. J. 2006, *ApJ*, 642, 933

- Iida, M., Ohshima, Y., & Endo, Y. 1991, *The Astrophysical Journal*, 371, L45
- Ilee, J. D., Walsh, C., Booth, A. S., et al. 2021, *ApJs*, 257, 9
- Jensen, S. S., Jørgensen, J. K., Kristensen, L. E., et al. 2019, *A&A*, 631, A25
- Jin, M. & Garrod, R. T. 2020, *ApJS*, 249, 26
- Jørgensen, J. K., Belloche, A., & Garrod, R. T. 2020, *The Annual Review of Astronomy and Astrophysics*, 58, 727
- Kaifu, N., Ohishi, M., Kawaguchi, K., et al. 2004, *PASJ*, 56, 69
- Kaifu, N., Suzuki, H., Ohishi, M., et al. 1987, *ApJL*, 317, L111
- Kaiser, R. I. 2002, *Chemical Reviews*, 102, 1309
- Kalvāns, J. 2021, *ApJ*, 910, 54
- Kato, T., Kodama, T., Shida, T., et al. 1991, *Chemical Physics Letters*, 180, 446
- Kawaguchi, K., Kasai, Y., Ishikawa, S.-I., et al. 1994, *ApJL*, 420, L95
- Kawaguchi, K., Takano, S., Ohishi, M., et al. 1992, *ApJL*, 396, L49
- Keto, E. & Caselli, P. 2010, *MNRAS*, 402, 1625
- Kong, S., Tan, J. C., Caselli, P., et al. 2016, *ApJ*, 821, 94
- Könyves, V., André, P., Men'shchikov, A., et al. 2015, *A&A*, 584, A91
- Kraka, E. & Cremer, D. 1993, *Chemical Physics Letters*, 216, 333
- Kroto, H. W., Kirby, C., Walton, D. R. M., et al. 1978, *ApJs*, 219, L133
- Langer, W. D., Graedel, T. E., Frerking, M. A., & Armentrout, P. B. 1984, *ApJ*, 277, 581
- Langer, W. D., Velusamy, T., Kuiper, T. B. H., et al. 1997, *ApJL*, 480, L63
- Lau, R. M., Hankins, M. J., Han, Y., et al. 2022, *Nature Astronomy*, 6, 1308
- Laurie, V. W. 1956, *The Journal of Chemical Physics*, 24, 635
- Law, C. J., Öberg, K. I., Bergner, J. B., & Graninger, D. 2018, *ApJ*, 863, 88
- Le Gal, R., Brady, M. T., Öberg, K. I., Roueff, E., & Le Petit, F. 2019, *ApJ*, 886, 86
- Lee, K. L. K., Changala, P. B., Loomis, R. A., et al. 2021a, *ApJL*, 910, L2
- Lee, K. L. K., Patterson, J., Burkhardt, A. M., et al. 2021b, *ApJL*, 917, L6
- Lefloch, B., Bachiller, R., Ceccarelli, C., et al. 2018, *Monthly Notices of the Royal Astronomical Society*, 477, 4792
- Li, A. 2020, *Nature Astronomy*, 4, 339
- Loison, J.-C., Agúndez, M., Wakelam, V., et al. 2017, *MNRAS*, 470, 4075
- Loison, J.-C., Wakelam, V., Hickson, K. M., Bergeat, A., & Mereau, R. 2014, *Monthly Notices of the Royal Astronomical Society*, 437, 930
- Loomis, R. A., Burkhardt, A. M., Shingledecker, C. N., et al. 2021, *Nature Astronomy*, 5, 188
- Loomis, R. A., Cleeves, L. I., Öberg, K. I., et al. 2018a, *ApJ*, 859, 131
- Loomis, R. A., Öberg, K. I., Andrews, S. M., et al. 2018b, *The Astronomical Journal*, 155, 182
- Loru, D., Cabezas, C., Cernicharo, J., Schnell, M., & Steber, A. L. 2023, *A&A*, 677, A166
- Maergoiz, A. I., Nikitin, E. E., & Troe, J. 2009, *International Journal of Mass Spectrometry*, 280, 42
- Marcelino, N., Agúndez, M., Tercero, B., et al. 2020, *A&A*, 643, L6
- Martin, M. C., Koller, D., & Mihaly, L. 1993, *Phys. Rev. B*, 47, 14607
- Martín, S., Mangum, J. G., Harada, N., et al. 2021, *A&A*, 656, A46

- Martínez, L., Santoro, G., Merino, P., et al. 2020, *Nature Astronomy*, 4, 97
- Matthews, H. E., Friberg, P., & Irvine, W. M. 1985, *ApJ*, 290, 609
- Matthews, H. E., Irvine, W. M., Friberg, P., Brown, R. D., & Godfrey, P. D. 1984, *nat*, 310, 125
- McCarthy, M., Chen, W., Travers, M., & Thaddeus, P. 2000a, *The Astrophysical Journal Supplement Series*, 129, 611
- McCarthy, M., Levine, E., Apponi, A., & Thaddeus, P. 2000b, *Journal of Molecular Spectroscopy*, 203, 75
- McCarthy, M. C., Gottlieb, C. A., Gupta, H., & Thaddeus, P. 2006, *ApJL*, 652, L141
- McCarthy, M. C., Lee, K. L. K., Carroll, P. B., et al. 2020, *Journal of Physical Chemistry A*, 124, 5170
- McCarthy, M. C., Lee, K. L. K., Loomis, R. A., et al. 2021, *Nature Astronomy*, 5, 176
- McCarthy, M. C. & Thaddeus, P. 2001, *Chemical society reviews*, 30, 177
- McGuire, B. A. 2022, *ApJs*, 259, 30
- McGuire, B. A., Burkhardt, A. M., Kalenskii, S., et al. 2018, *Science*, 359, 202
- McGuire, B. A., Burkhardt, A. M., Loomis, R. A., et al. 2020, *ApJL*, 900, L10
- McGuire, B. A., Burkhardt, A. M., Shingledecker, C. N., et al. 2017, *ApJL*, 843, L28
- McGuire, B. A., Loomis, R. A., Burkhardt, A. M., et al. 2021, *Science*, 371, 1265
- McNaughton, D., Jahn, M. K., Travers, M. J., et al. 2018, *Monthly Notices of the Royal Astronomical Society*, 476, 5268
- Melli, A., Melosso, M., Bizzocchi, L., et al. 2022, *The Journal of Physical Chemistry A*, 126, 6210
- Milam, S. N., Savage, C., Brewster, M. A., Ziurys, L. M., & Wyckoff, S. 2005, *ApJ*, 634, 1126
- Minissale, M., Aikawa, Y., Bergin, E., et al. 2022, *ACS Earth and Space Chemistry*, 6, 597
- Mohamed, S., McCarthy, M., Cooksy, A., Hinton, C., & Thaddeus, P. 2005, *The Journal of chemical physics*, 123, 234301
- Morris, M., Turner, B. E., Palmer, P., & Zuckerman, B. 1976, *ApJ*, 205, 82
- Moscadelli, L., Cesaroni, R., Beltrán, M. T., & Rivilla, V. M. 2021, *A&A*, 650, A142
- Nakamura, F., Kamenno, S., Kusune, T., et al. 2019, *PASJ*, 71, 117
- Nakamura, F., Ogawa, H., Yonekura, Y., et al. 2015, *PASJ*, 67, 117
- Nemes, L., Ram, R. S., Bernath, P. F., et al. 1994, *Chemical Physics Letters*, 218, 295
- Nguyen, T. L., Mebel, A. M., Lin, S. H., & Kaiser, R. I. 2001, *Journal of Physical Chemistry A*, 105, 11549
- Öberg, K. I. & Bergin, E. A. 2021, *Physics Reports*, 893, 1
- Öberg, K. I., Guzmán, V. V., Furuya, K., et al. 2015, *nat*, 520, 198
- Öberg, K. I., Guzmán, V. V., Walsh, C., et al. 2021, *ApJs*, 257, 1
- Ohishi, M., Kaifu, N., Kawaguchi, K., et al. 1989a, *ApJL*, 345, L83
- Ohishi, M., Kaifu, N., Kawaguchi, K., et al. 1989b, *ApJL*, 345, L83
- Ohishi, M., Suzuki, H., Ishikawa, S.-I., et al. 1991, *ApJL*, 380, L39
- Oya, Y., Sakai, N., Watanabe, Y., et al. 2017, *ApJ*, 837, 174
- Oyama, T., Ozaki, H., Sumiyoshi, Y., et al. 2020, *ApJ*, 890, 39
- Pardo, J. R., Bermúdez, C., Cabezas, C., et al. 2020, *A&A*, 640, L13
- Pardo, J. R., Cabezas, C., Fonfría, J. P., et al. 2021, *A&A*, 652, L13

- Pardo, J. R., Cernicharo, J., & Goicoechea, J. R. 2005, *ApJ*, 628, 275
- Pardo, J. R., Cernicharo, J., Tercero, B., et al. 2022, *A&A*, 658, A39
- Pascoli, G. & Lavendy, H. 1998, *International Journal of Mass Spectrometry*, 181, 11
- Penteado, E. M., Walsh, C., & Cuppen, H. M. 2017, *ApJ*, 844, 71
- Pety, J., Gratier, P., Guzmán, V., et al. 2012, *A&A*, 548, A68
- Pety, J., Teyssier, D., Fossé, D., et al. 2005, *A&A*, 435, 885
- Pilling, S., Andrade, D., Da Silveira, E., et al. 2012, *Monthly Notices of the Royal Astronomical Society*, 423, 2209
- Pineda, J. E., Segura-Cox, D., Caselli, P., et al. 2020, *Nature Astronomy*, 4, 1158
- Prasad, S. S. & Huntress, W. T., J. 1980a, *ApJs*, 43, 1
- Prasad, S. S. & Huntress, W. T., J. 1980b, *ApJ*, 239, 151
- Puzzarini, C. 2008, *Chemical Physics*, 346, 45
- Qi, C., Öberg, K. I., Wilner, D. J., & Rosenfeld, K. A. 2013, *ApJL*, 765, L14
- Ramabhadran, R. O. & Raghavachari, K. 2013, *Journal of chemical theory and computation*, 9, 3986
- Remijan, A., Scolati, H. N., Burkhardt, A. M., et al. 2023, *ApJL*, 944, L45
- Remijan, A. J., Hollis, J. M., Lovas, F. J., et al. 2007, *ApJL*, 664, L47
- Remijan, A. J., Hollis, J. M., Snyder, L. E., Jewell, P. R., & Lovas, F. J. 2006, *ApJL*, 643, L37
- Ridgway, S. T., Hall, D. N. B., Wojslaw, R. S., Kleinmann, S. G., & Weinberger, D. A. 1976, *Nature*, 264, 345
- Roueff, E., Felenbok, P., Black, J. H., & Gry, C. 2002, *A&A*, 384, 629
- Saito, S., Kawaguchi, K., Yamamoto, S., et al. 1987, *ApJL*, 317, L115
- Sakai, N., Ikeda, M., Morita, M., et al. 2007, *ApJ*, 663, 1174
- Sakai, N., Sakai, T., Hirota, T., Burton, M., & Yamamoto, S. 2009, *ApJ*, 697, 769
- Sakai, N., Sakai, T., Hirota, T., & Yamamoto, S. 2008, *ApJ*, 672, 371
- Sakai, N., Saruwatari, O., Sakai, T., Takano, S., & Yamamoto, S. 2010, *A&A*, 512, A31
- Sakai, N., Takano, S., Sakai, T., et al. 2013, *Journal of Physical Chemistry A*, 117, 9831
- Sakai, N. & Yamamoto, S. 2013, *Chemical Reviews*, 113, 8981
- Sakaizumi, T., Katoh, F., Ohashi, O., & Yamaguchi, I. 1993, *Journal of Molecular Spectroscopy*, 159, 112
- Sakaizumi, T., Kikuchi, H., Ohashi, O., & Yamaguchi, I. 1987, *Bulletin of the Chemical Society of Japan*, 60, 3903
- Savić, I. 2004
- Shimonishi, T., Das, A., Sakai, N., et al. 2020, *ApJ*, 891, 164
- Shingledecker, C. N., Lee, K. L. K., Wandishin, J. T., et al. 2021, *A&A*, 652, L12
- Siebert, M. A., Lee, K. L. K., Remijan, A. J., et al. 2022, *ApJ*, 924, 21
- Sipilä, O., Spezzano, S., & Caselli, P. 2016, *A&A*, 591, L1
- Sita, M. L., Changala, P. B., Xue, C., et al. 2022, *ApJL*, 938, L12
- Snow, T. P. & Bierbaum, V. M. 2008, *Annu. Rev. Anal. Chem.*, 1, 229
- Snyder, L. E., Hollis, J. M., Jewell, P. R., Lovas, F. J., & Remijan, A. 2006, *ApJ*, 647, 412
- Souza, S. P. & Lutz, B. L. 1977, *ApJL*, 216, L49
- Spezzano, S., Bizzocchi, L., Caselli, P., Harju, J., & Brünken, S. 2016, *A&A*, 592, L11



Spezzano, S., Caselli, P., Pineda, J. E., et al. 2020, *A&A*, 643, A60

Su, T. & Chesnavich, W. J. 1982, *Journal of Chemical Physics*, 76, 5183

Suzuki, H. 1983, *ApJ*, 272, 579

Suzuki, H., Ohishi, M., Kaifu, N., Ishikawa, S.-I., & Kasuga, T. 1986, *PASJ*, 38, 911

Suzuki, H., Yamamoto, S., Ohishi, M., et al. 1992, *ApJ*, 392, 551

Takano, S., Masuda, A., Hirahara, Y., et al. 1998, *A&A*, 329, 1156

Takano, S., Suzuki, H., Ohishi, M., et al. 1990, *ApJL*, 361, L15

Taniguchi, K., E Pineda, J., Caselli, P., et al. 2024, arXiv e-prints, arXiv:2402.19099

Taniguchi, K., Herbst, E., Caselli, P., et al. 2019a, *ApJ*, 881, 57

Taniguchi, K., Herbst, E., Majumdar, L., et al. 2021, *ApJ*, 908, 100

Taniguchi, K., Herbst, E., Ozeki, H., & Saito, M. 2019b, *ApJ*, 884, 167

Taniguchi, K., Majumdar, L., Caselli, P., et al. 2023, *ApJs*, 267, 4

Taniguchi, K., Ozeki, H., & Saito, M. 2017a, *ApJ*, 846, 46

Taniguchi, K., Ozeki, H., Saito, M., et al. 2016a, *ApJ*, 817, 147

Taniguchi, K., Saito, M., Hirota, T., et al. 2017b, *ApJ*, 844, 68

Taniguchi, K., Saito, M., Majumdar, L., et al. 2018a, *ApJ*, 866, 150

Taniguchi, K., Saito, M., & Ozeki, H. 2016b, *ApJ*, 830, 106

Taniguchi, K., Saito, M., Sridharan, T. K., & Minamidani, T. 2018b, *ApJ*, 854, 133

Taniguchi, K., Saito, M., Sridharan, T. K., & Minamidani, T. 2019c, *ApJ*, 872, 154

Taniguchi, K., Tanaka, K. E. I., Zhang, Y., et al. 2022, *ApJ*, 931, 99

Thaddeus, P., Cummins, S. E., & Linke, R. A. 1984, *ApJL*, 283, L45

Thaddeus, P., Gottlieb, C. A., Gupta, H., et al. 2008, *ApJ*, 677, 1132

Thaddeus, P., Gottlieb, C. A., Hjalmarsen, A., et al. 1985a, *ApJL*, 294, L49

Thaddeus, P., McCarthy, M., Travers, M., Gottlieb, C., & Chen, W. 1998, *Faraday Discussions*, 109, 121

Thaddeus, P., Vrtilik, J. M., & Gottlieb, C. A. 1985b, *ApJL*, 299, L63

Travers, M., McCarthy, M., Kalmus, P., Gottlieb, C., & Thaddeus, P. 1996, *The Astrophysical Journal*, 469, L65

Travers, M. J., McCarthy, M. C., Gottlieb, C. A., & Thaddeus, P. 1997, *ApJL*, 483, L135

Tsuge, M., Molpeceres, G., Aikawa, Y., & Watanabe, N. 2023, *Nature Astronomy*, 1

Tucker, K. D., Kutner, M. L., & Thaddeus, P. 1974, *ApJL*, 193, L115

Tulej, M., Kirkwood, D., Pachkov, M., & Maier, J. 1998, *The Astrophysical Journal*, 506, L69

Turner, B. E. 1971, *ApJL*, 163, L35

Tychoniec, L., van Dishoeck, E. F., van't Hoff, M. L. R., et al. 2021, *A&A*, 655, A65

Tyler, J. K. & Sheridan, J. 1963, *Transactions of the Faraday Society*, 59, 2661

Villadsen, T., Ligterink, N. F. W., & Andersen, M. 2022, *A&A*, 666, A45

Wakelam, V., Loison, J. C., Mereau, R., & Ruaud, M. 2017, *Molecular Astrophysics*, 6, 22

Wakelam, V., Smith, I. W. M., Herbst, E., et al. 2010, *Space Science Review*, 156, 13

Walsh, C., Harada, N., Herbst, E., & Millar, T. J. 2009, *ApJ*, 700, 752

Wang, S., Li, J., Guo, X., Jiang, L., & Zhang, J. 2009, *Journal of Molecular Structure: THEOCHEM*, 900, 118

Watanabe, N. & Kouchi, A. 2002, *ApJL*, 571, L173

- Welty, D. E., Howk, J. C., Lehner, N., & Black, J. H. 2013, *Monthly Notices of the Royal Astronomical Society*, 428, 1107
- Westenberg, A. & Wilson Jr, E. B. 1950, *Journal of the American Chemical Society*, 72, 199
- Winnewisser, G. & Walmsley, C. M. 1978, *A&A*, 70, L37
- Wohlfart, K., Schnell, M., Grabow, J.-U., & Küpper, J. 2008, *Journal of Molecular Spectroscopy*, 247, 119
- Woon, D. E. 1996, *ApJ*, 456, 602
- Woon, D. E. & Herbst, E. 2009, *ApJs*, 185, 273
- Xue, C., Willis, E. R., Loomis, R. A., et al. 2020, *ApJL*, 900, L9
- Yamamoto, S., Saito, S., Kawaguchi, K., et al. 1987, *ApJL*, 317, L119
- Zack, L. N. & Maier, J. P. 2014, *Chemical Society Reviews*, 43, 4602
- Zhang, Y., Higuchi, A. E., Sakai, N., et al. 2018, *ApJ*, 864, 76